Design and Preparation of Micropatterns to Control Cell Functions

Xinlong Wang

August 2016

Design and Preparation of Micropatterns to Control Cell Functions

Xinlong Wang

Doctoral Program in Materials Science and Engineering

Submitted to the Graduate School of
Pure and Applied Sciences
in Partial Fulfillment of the Requirements
for the Degree of Doctor of Philosophy in
Engineering

at the
University of Tsukuba

Content

List of abbreviations

AFM	Atomic force microscope
ALP	Alkaline phosphatase
ASCs	Adult stem cells
AuNPs	Gold nanoparticles
BMP	Bone morphogenetic protein
BSP	Bone sialoprotein
DMEM	Dulbecco's modified eagle medium
EGF	Epidermal growth factor
ESCs	Embryonic stem cells
FABP4	Fatty acid binding protein 4
FBS	Fetal bovine serum
FGF2	Fibroblast growth factor 2
GAG	Glycosaminoglycan
HA	Hyaluronic acid
hESCs	Human embryonic stem cells
HSCs	Hematopoietic stem cells
iPSCs	Induced pluripotent stem cells
LIF	Leukemia inhibitory factor
LPL	Lipoprotein lipase
mESCs	Mouse embryonic stem cells
MSCs	Mesenchymal stem cells
MuSCs	Muscle stem cells
NMR	Nuclear magnetic resonance
NSCs	Neural stem cells
OCN	Osteocalcin
OPN	Osteopontin
PAAc	Poly(acrylic acid)
PBS	Phosphate buffer saline
PDMS	Poly(dimethyl siloxane)
PEG	Poly(ethylene glycol)
PPARγ2	Peroxisome proliferator-activated receptor γ2
PVA	Poly(vinyl alcohol)
RT-PCR	Real-time polymerase chain reaction
RUNX2	Runt-related gene 2
TBS	Tris-buffered saline
TCPS	Tissue culture polystyrene
TGF-β	Transforming growth factor-β
UV	Ultraviolet
YAP	Yes-associated protein

Chapter 1

General introduction

1.1 Cells for tissue engineering

Tissue and organ damage caused by diseases or other injuries is a major problem in health care [1]. Traditional treatments using drugs, transplantation, surgical repair, artificial prostheses and medical devices have limitations for truly recovery of the functional tissues or organs. Started by Langer and Vacanti, tissue engineering appeared as an alternative or complementary treatment for tissue and organ damage with great promise [2]. Three key components involved in tissue engineering are cells, scaffolds and growth factors (Figure 1.1). Cells as one of the major components play critical roles in formation of tissue and organ. The cell source for tissue engineering can be generally divided into two categories: somatic cells and stem cells.

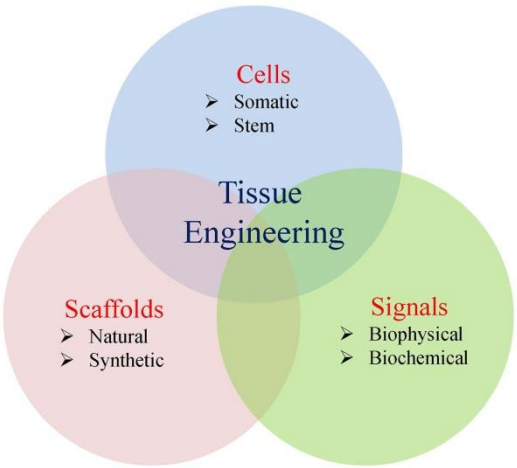

Figure 1.1 Brief illustration of tissue engineering.

1.1.1 Somatic cells

In general, any cell other than a gamete, germ cell, gametocyte or undifferentiated stem cell belongs to somatic cells. They are frequently used for skin, vascular, and cartilage regeneration. Some of them are even applied for clinical applications. Human fibroblasts were cultured on a micronized acellular

dermal matrix microcarrier and applied for skin regeneration [3]. The newborn human dermal fibroblasts from foreskins were used to produce artificial skin approved by FDA [4]. Chondrocyte sheets obtained from superimposing of monolayer sheets were used for cartilage repair [5,6]. Endothelial progenitor cells were used for vascular regeneration in many studies [7-9]. Although some types of somatic cells can be used for tissue regeneration, majority of differentiated and progenitor cells are difficult to acquire or expand under current technologies which limited their application. In order to solve the problem, stem cells become an attractive cell source for tissue engineering.

1.1.2 Stem cells

Stem cells are defined as the unspecialized cells that can perpetuate themselves through self-renewal and to generate highly differentiated descendant with specific function [10,11]. The most attractive features of stem cells are multipotency and self-renewal (Figure 1.2). These features make them versatile and promising cell source for regenerative medicine and tissue engineering. The stem cells can be generally divided into three categories: embryonic stem cells (ESCs), induced pluripotent stem cells (iPSCs) and adult stem cells (ASCs). The ESCs are pluripotent stem cells derived from inner cell mass of blastocysts [12]. They are reported to have the potential to differentiate into all cell types in the body and were supposed to be a useful cell source for tissue engineering. However, the risk of tumor formation became the major concern of the clinical application of ESCs [13]. Meanwhile, since the generation of ESCs destructs the blastocysts, ethical concern is always accompanied with the use of ESCs. Furthermore, it has not been feasible to establish the patient-specific ESCs cell line because ESCs can only generate from the embryos. iPSCs are a new type of pluripotent stem cells generated directly from adult cells [14,15]. A set of transcriptional genes (originally Oct4, Sox2, cMyc and Klf4) were introduced into adult cell to reprogram them into pluripotent. The iPSCs hold great promise for tissue engineering and regenerative medicine. They have same capacity to differentiate into all cell types as the ESCs but without ethical concern. And the patient-specific iPSCs cell lines can be acquired which overcomes the immune problem. However, the use of iPSCs still has to face the risk of tumor formation since the cMyc and Klf4 are oncogenic and the use of virus vectors may also trigger the oncogenes. Meanwhile, current reprogramming procedures are extremely slow and inefficient.

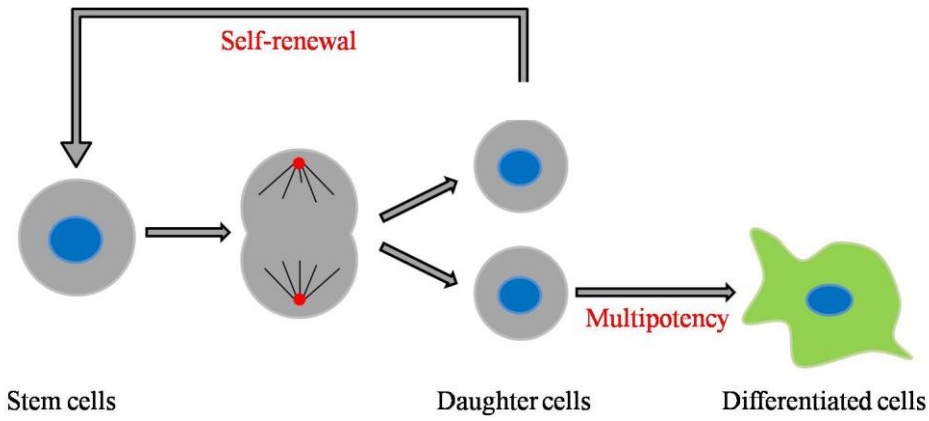

Figure 1.2 The stem cell features.

The ASCs are tissue-specific stem cells that multiply through cell division to replenish certain type of dying cells and regenerate damage tissues. The ASCs include various types of cells such as mesenchymal

stem cells (MSCs), hematopoietic stem cells (HSCs), neural stem cells (NSCs) and so on. Among them, MSCs attract plenty of interests due to their easy availability and high potential for regeneration of bone, cartilage and many other tissues. They can be harvested in many tissues such as bone marrow, adipose tissue, dental pulp and are capable to differentiate into osteoblasts, adipocytes, chondrocytes, myoblasts and tenocytes [16]. They were even reported to differentiate into cell types other than mesenchymal tissues [17]. Therefore, the MSCs are ideal cell source for tissue engineering.

1.1.2.1 Self-renewal of mesenchymal stem cells

Self-renewal refers to the asymmetrically or symmetrically division of stem cells with the maintenance of developmental potential [18]. It is a very important and useful property of stem cells and is not simple cell proliferation. During self-renewal, at least one of the daughter cells needs to inherit the developmental potential similar to the mother stem cell. Self-renewal is not a unique property of stem cells but also shared by some restricted progenitor and differentiated cells. Meanwhile, the cancer cells also have the capacity to self-renew. Therefore, understanding the self-renewal of stem cells would contribute to not only tissue regeneration but also for cancer therapy.

Self-renewal is a very complex process involving networks that balance proto-oncogenes, gate-keeping tumor suppressors and care-taking tumor suppressors. Polycomb group genes have been indicated to maintain stem cell fate by suppressing the initiation of differentiation programs [19]. Wnt, Notch and BMP signaling pathways were also proved to instruct stem cells [20]. Besides genetic pathways, stemness of cells can also be confirmed by expression of surface markers. According to the criteria, MSCs should express CD73, CD90, CD105, and lack expression of CD11b or CD14, CD19 or CD79α, CD34, CD45 and HLA-DR surface molecules [21]. There are also some other widely accepted surface molecules which can be used to identify MSCs. CD44 has been reported to be the receptor of hyaluronan and expressed on MSCs [22]. CD106 is involved in the interaction between MSCs and T lymphocyte, and it is supposed to be the marker representing the immature, multipotent MSCs [23,24]. Positive expression of STRO-1 has been found on a subpopulation of MSCs derived from bone marrow which had the capacity for osteogenic differentiation [25].

Recent studies about self-renewal mainly focused on the maintenance of multipotency of stem cells. *In vivo*, the majority of stem cells are quiescent under homeostasis, but capable to undergo activation upon stimulation [26]. This quiescent state contributes to stem cell maintenance. ESCs kept their undifferentiated state and maintained their full differentiation capacity when being encapsulated in a hyaluronic acid hydrogel [27]. And ESCs retained their undifferentiated state on nanopatterned polydimethylsiloxane (PDMS) substrate, but randomly differentiated on flat plastic culture dishes [28]. Skeletal muscle stem cells (MuSCs) retained their stemness when being cultured on soft hydrogels which have similar elasticity as nature muscle, and repaired damaged muscle while being transplanted into mice [29]. As to MSCs, previous studies have proved that soft hydrogel could be an alternative for maintenance of stem cell phenotype. When MSCs were seeded on 250-Pa soft hydrogel, they halted progression and became quiescent, but exhibited capability to differentiate into adipocytes or osteoblasts in presence of chemical or mechanical stimuli [30]. MSCs cultured within a composite collagen-pullulan hydrogel expressed significantly higher level of Oct4, Sox2 and Klf4 which are associated with self-renewal and multipotency compared to MSCs in standard cell culture [31]. And the nanopatterned surfaces can affect the self-renewal of stem cells. The 120 nm pits in a square array with center-center spacing of 300 nm maintained MSCs phenotype and multipotency above eight weeks *in vitro* culture [32]. Meanwhile, micropatterned surfaces were also reported to influence

self-renewal of MSCs. Cells with small size were more quiescent than those with large size and kept the potential to osteogenic and adipogenic differentiation [33].

1.1.2.2 Differentiation of mesenchymal stem cells

The MSCs are able to differentiate into osteocytes, adipocytes, chondrocytes, stormal cells, myoblasts and tenocytes depending on the culture conditions [34-45]. Among the various differentiation potential, the osteogenic and adipogenic differentiation are most widely studied and supposed to make great contributions to tissue engineering. To induce the osteogenic differentiation, MSCs are usually cultured with DMEM medium supplemented with 10% FBS, 1000 mg/L glucose, 584 mg/L glutamine, 100 μg/mL streptomycin, 100 U/mL penicillin, 50 mg/L ascorbic acid, 0.1mM nonessential amino acids, 100 nM dexamethasone and 10 mM β-glycerophosphate disodium salt hydrate [46]. The osteogenic differentiated cells can be characterized using various methods. The staining of alkaline phosphatase (ALP), Alizarin Red S and Von Kossa can be used to judge the mineralized matrix [47-49]. Immunofluorescence staining of matrix proteins osteopontin (OPN) and osteocalcin (OCN) can also be used to evaluate the osteogenic differentiation of MSCs [50]. Certainly, the osteogenic differentiation related gene expression (RUNX2, BMP2, ALP, etc.) measured by polymerase chain reaction (PCR) is also helpful. To induce the adipogenic differentiation, MSCs are usually cultured with DMEM medium supplemented 10% FBS, 4500 mg/L glucose, 584 mg/L glutamine, 100 μg/mL streptomycin, 100 U/mL penicillin, 0.4 mM proline, 50 mg/L ascorbic acid, 0.1 mM nonessential amino acids, 1 μM dexamethasone, 10 μg/mL insulin, 0.5 mM methylisobutylxanthine and 100 μM indomethacin [16]. Fat droplets which can be stained using Oil Red O and Niel Red are good markers for adipogenic differentiation of MSCs [51]. The expression level of maker genes such as peroxisome proliferator-activated receptor γ2 (PPARγ2), fatty acid binding protein 4 (FABP4) and lipoprotein lipase (LPL) are used to evaluate the adipogenic differentiation [52-56].

1.2 Stem cell fate determination regulated by microenvironment

There are plenty of obstacles need to be overcome in order to promote the clinical application of stem cells. The most urgent problem is to reliably determine stem cell fate. It is always challenging because there are many complex influence factors regulated by cell microenvironment. Cell microenvironment (cell niche) refers to the microenvironment where the cells are found [57]. It is very important especially for stem cell fate determination no matter under *in vivo* or *in vitro* conditions. During development, various niche factors affected the gene expression of stem cells to induce either self-renewal or differentiation of stem cells [58-60]. *In vivo*, stem cell niches maintain the cells in a quiescent state, but after tissue injury, the surrounding microenvironment activates signals to stem cells to either promote self-renew or differentiation to form new tissues. Several factors are important to regulate stem cell characteristics within the niche such as soluble or tethered factors, cell-cell interactions between stem cells, as well as interactions between stem cells and neighboring differentiated cells, ECM components and physical morphogens (Figure 1.3) [61]. During *in vitro* culture, the cell culture substrates or other biomaterials need to be taken into account as they become part of the cell microenvironment. The cells firstly contact to the substrate and depending on the properties of the contacting surface, the cell adhesion, spreading, migration, proliferation, differentiation and even apoptosis can be triggered. In one word, these external stimuli from cell microenvironment regulated internal signals that determine stem cell fate.

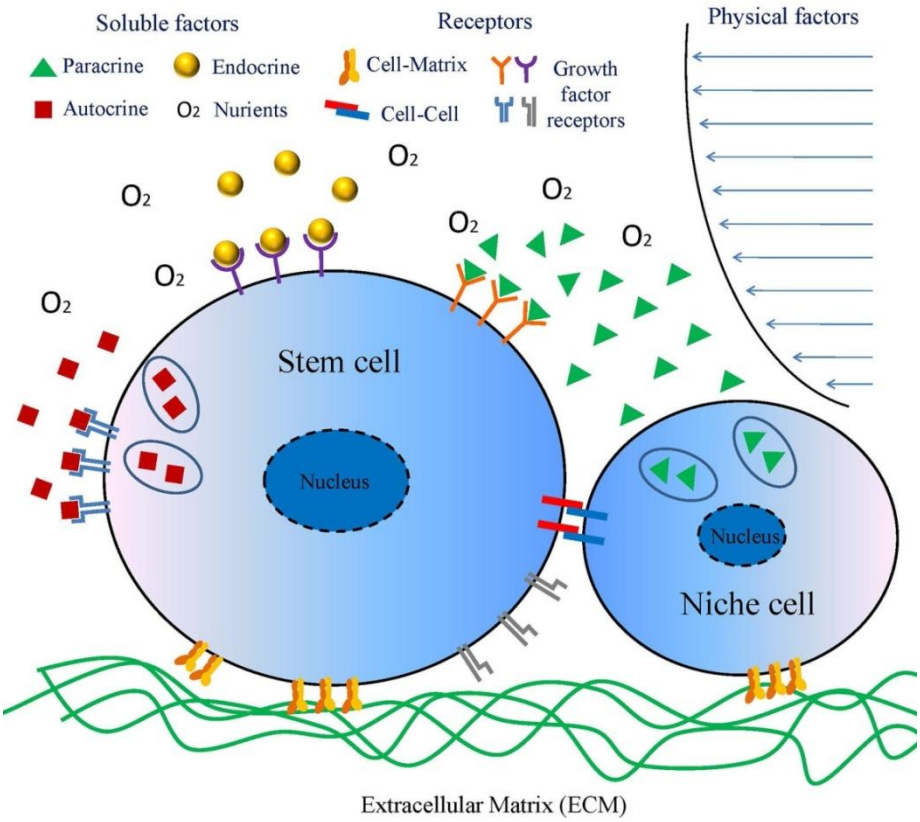

Figure 1.3 Cell microenvironment mainly refers to the soluble factors, neighboring cells, extracellular matrix (ECM) and the physical morphogens that play critical roles in cell fate determination.

1.2.1 Soluble factors

The soluble factors are composed of the soluble oxygen, nutrients, cytokines, growth factors and proteins supplemented in cell microenvironment and play important roles in regulating cell behaviors. Meanwhile, these soluble factors can also be tethered to the ECM in order to alter their local concentration and stability. Previous studies reported that the synovial fluid from patients with rheumatoid arthritis (RA-SF) containing transforming growth factor-beta1 (TGF-β1) induced the myogenic differentiation of adipose-derived mesenchymal stem cells [62]. Immunodepletion of TGF-β1 from RA-SF inhibited the expression of α-smooth muscle actin (α-SMA) indicating that TGF-β1 played critical role in RA-SF-induced myogenic differentiation of MSCs. And TGF-β were also shown to be involved in self-renewal of stem cells [63,64]. Meanwhile, the TGF-β3 can be immobilized onto scaffold and hydrogel to induce the chondrogenic differentiation of MSCs [65,66]. Fibroblast growth factors (FGF) are important in neurogenic differentiation of stem cells. In presence of FGF-2, ESCs formed numerous progenitor cells with neural-like structures and can differentiated into neurons and astrocytes after transplantation into mouse brain [67]. And nanofibers tethered with FGF-2 were able to support proliferation and colony formation of ESCs [68]. Interestingly, the epidermal growth factors (EGF) were also reported to regulate neurogenic differentiation of stem cells. Induced by EGF, partial MSCs differentiated into neuron-like cells *in vitro* [69]. And both the soluble or tethered EGF was reported to induce the osteogenic and adipogenic differentiation of stem cells [70,71]. The leukemia inhibitory factor (LIF) secreted by fibroblast is essential for *in vitro* expansion of ESCs no matter

supplemented in medium or immobilized on culture substrate [72,73]. The self-renewal rate of ESCs decreased in absence of LIF.

Besides the growth factors, small molecules as one of the components of soluble factors are also involved in stem cell fate determination. The oxygen tension was shown to be related with the differentiation of stem cells. Hypoxia condition (low concentration of oxygen) facilitated the neurogenic differentiation of ESCs and chondrogenic differentiation of MSCs [74,75]. Dexamethasone (Dex) known as a steroid drug was reported to influence stem cell differentiation. Low concentration (10-100 nM) promoted the osteogenic differentiation of MSCs, while high concentration (1 μM) induced adipogenic differentiation [46,16]. Recently, the extracellular vesicles (e.g. exosomes) released from cells attracted lots of interests. The extracellular vesicles are composed of various soluble factors and the synergistic influence of sets of soluble factors can be investigated. The exosomes released from skeletal muscle cells were able to induce the myogenic differentiation of adipose-derived stem cells [76]. And proosteogenic exosomes induced the osteogenic differentiation of MSCs and could be tethered to ECM to have long-term effect [77].

1.2.2 Extracellular matrix

The extracellular matix (ECM) refers to the extracellular molecules that provide the structural and biochemical support for cells [78]. The ECM are secreted by the cell in the matrix and composed of two major classes of macromolecules: glycosaminoglycans and fibrous proteins. The glycosaminoglycans usually covalently link to proteins and form the proteoglycan that provide the gel-like environment that protect cells from mechanical stress while permitting the exchange of the nutrients and metabolisms. The fibrous proteins participate in the construction of the ECM and mediate cell migration and other cell behaviors.

The ECM has important roles in cell fate determination. Several methods have been developed to acquire the multiple components of ECM such as tissue decellularization, cell-derived ECM and chemical coating of ECM. A decellularized heart with preserved ECM and vascular architecture was prepared by coronary perfusion with detergent [79]. The decellularized heart was seeded with cardiac and epithelial cells and incubated in a bioreactor that mimics cardiac physiology. After 28 d culture, a functional artificial heart was obtained. Similarly, artificial liver, kidney and cartilage could be obtained using decellularized method [80-82]. Cell-derived ECM can also used as culture substrate for regulation of stem cell functions. For instance, the osteogenic differentiated MSCs-derived ECM facilitated the osteogenic differentiation of MSCs [83]. And a series of stepwise ECM derived from different stage of osteogenic, adipogenic and chondrogenic differentiated MSCs were developed to simulate the dynamic change of ECM during tissue formation [84-86]. Coating of ECM molecules provides the simple method to investigate the influence of certain types of ECM component on stem cell functions. Using an ECM microarray platform, five types of ECM molecules (collagen I, III, IV, laminin and fibronectin) were arranged into 32 different combinations to induce the differentiation of ESCs [87].

The researches mentioned above were mainly focused on the influence of biochemical composition on stem cell fate determination. Since the ECM also provide the structural and mechanical support for cells, their biophysical properties were also important for stem cells. Recently, the topographical features of ECM were reported to influence the adhesion, migration, self-renewal and differentiation of stem cells. Increasing in surface roughness (ranging from 3.5 nm to 80 nm) enhanced the neural stem cell adhesion and spreading and promoted their differentiation into neuron cells [88]. The periodic grooved surfaces enhanced the cell adhesion and guided cell orientation which facilitated the myogenic and neurogenic differentiation of stem cell [89,90]. Depending on the arrangements of 120 nm diameter and 100 nm deep nanopits, MSCs

underwent self-renewal and osteogenic differentiation, respectively [91,92]. Another widely studied biophysical property of ECM was the elasticity. As previous report, stem cells would differentiate into various cell types depending on the elasticity of ECM. The MSCs underwent neurogenic, myogenic and osteogenic differentiation on soft (0.1–1 kPa), middle (8-17 kPa) and stiff (25-40 kPa) matrix, respectively [93]. While in another study, PVA/HA hydrogel with gradient stiffness was prepared to study the influence of stiffness gradient on differentiation of MSCs. The results showed that the MSCs underwent neurogenic, myogenic, chondrogenic and osteogenic differentiation on matrix with stiffness of 20 kPa, 40 kPa, 80 kPa and 190 kPa, respectively [94]. According to those researches, MSCs would differentiate into neuron or other soft tissues when cultured on ECM with low stiffness, while differentiate into bone and other hard tissues when cultured on ECM with high stiffness. But depending on the ECM component, the required to undergo same differentiation might be different indicating a strong correlation between ECM chemistry and mechanics to regulation stem cell functions.

1.2.3 Cell-cell interactions

In multicellular tissues, cells may cling to one another through several types of junctions including anchoring junctions, occluding junctions, channel-forming junctions and signal-relaying junctions. The anchoring junctions and occluding junctions provide the spatial and geometrical constraints of cells. The channel-forming junctions and signal-relaying junctions have important roles in signal transmission because they allowed the exchange of signal molecules and other metabolism. Direct interactions between stem cells and supporting cells modulate stem cell retention and regulation. *In vivo*, endothelial cells (EC) stabilization via MSCs interactions is known to facilitate the maturation of blood vessels impacting many physiologic systems, from tumors to engineered tissues [95]. And direct cell-cell interactions between neural stem cells and their niche cells maintained the quiescent state of the stem cells [96]. Additionally, human ESCs have to aggregate into clusters for their survival and self-renewal indicating that the cell-cell interactions between stem cells themselves are also important factors for stem cell fate determination [97].

In vitro, the most commonly used method for investigating the influence of cell-cell interaction on relevant cell properties is straightforward cell-cell contact. By changing the cell seeding density, the cell position can be modulated to control the degree of cell signaling. Cortical stem cells differentiated into neurons, astrocytes and oligodendrocytes with strong cell-cell interactions, and differentiated into smooth muscle cells with weak cell-cell interactions [98]. More precisely controlled cell-cell interactions could be achieved using micropattened surfaces. Semi-quantitative analysis of the cell-cell interactions showed that the osteogenic and chondrogenic differentiation potential of MSCs enhanced with the increase of cell-cell interactions [99-102].

1.2.4 Physical morphogens

During development, tissues are always suffering various physical stresses such as compression, stretch, shear flow and electrical stimuli and so on. And these physical morphogens are necessary for regulation of cell functions and even tissue formation [103]. Applying compressive force (2 g/cm^2) to human pluripotent stem cell line C2C12 enhanced their osteogenic and chondrogenic differentiation while suppressed the adipogenic differentiation [104]. Compression could also promote the osteogenic differentiation of MSCs and inhibit the adipogenic differentiation of adipose-derived stem cells [105,106]. Static stretch force leaded to MSCs alignment along the pre-stretched direction and promoted the myogenic

differentiation [107]. And stimulated by cyclic stretching force, MSCs were reported to differentiate into osteoblast and cardiomyocyte [108,109]. Shear fluid mimics the shear force generated by blood flow and can be used to investigate the tissue morphogenesis during *in vivo* condition. Many studies reported that shear flow affected the cell alignment and cell fate determination [110-113]. The physical stimuli especially these mechanical forces participated in regulation of cell functions through mechanotransduction pathway. The mechanical signal can affect the enzyme protein activity which biochemically regulate cell functions, or directly transferred to nucleus through cytoskeleton architecture [114-116].

1.3 Micropatterning for Stem cell fate determination

As mentioned above, cell microenvironment plays pivotal role in stem cell fate determination. Therefore, technologies to simulate the microenvironment are necessary and essential for tissue engineering and regenerative medicine. Micropatterned cell culture substrates are one of the useful biomaterials which mimic cell microenvironment to control cell morphogenesis and functions [117]. Conventional cell culture using uniform substrates lacks the control of cell morphology which is important for cell function manipulation. In contrary, micropatterned cells had controlled and stable morphology which enabled the investigation of the influence of subcellular components (e.g. cytoskeleton) on cell functions. Therefore, micropatterning is an important technique for design and engineering of biomaterials to mimic *in vivo* microenvironment [118].

1.3.1 Cell micropatterning methods

Micropatterning of single and multiple cells has promoted the development of biosensors, microarrays, and biomaterials for cell function manipulation [119,120]. Several micropatterning techniques have been developed to precisely control the cell morphologies such as photolithography, soft lithography, photoimmobilization, laser/plasma ablation, stencil-assisted patterning, and robotic printing.

1.3.1.1 Photolithography

Photolithography was initially used for fabrication of electronic microcircuits in semiconductor industry. Lately, it was explored to be applied in biomaterials engineering and used as a dominant method for micropatterning of inorganic substrate such as silicon wafer, glass and metal. In the photolithography process, the geometric features on a mask were transferred onto the target substrate using UV illumination (Figure 1.4). The target substrate is usually coated with photoresist material. The positive photoresist will become soluble in developing solution, while the negative one became insoluble in developing solution. Then the surface is covered by a quartz mask with designed microfeatures and exposed to UV illumination. After initial development, the photoresist micropattern is obtained. In the following step, biomolecules (e.g. fibronectin) are allowed to adhere on to the surface. After photoresist lift-off, the biomolecules micropatterned surface is prepared. Various micropatterns have been prepared for cell biology study using the photolithography method. For instance, the hydrophobic heptadecafluoro-1,1,2,2-tetrahydrodecyl-trichlorosilane self-assembled monolayers were micropatterned onto a silicon oxide adhesion layer at single cell level [121]. And the micropatterns can support the osteoblast networks for more than 2 weeks. Although photolithography is a good method for micropatterning, there are still some limitations of this method. Clean

room and other expensive facilities are needed which are not easily available for biologists. Additionally, organic solvent used for development is toxic and the residual is harmful to cells and may denature the biomolecules.

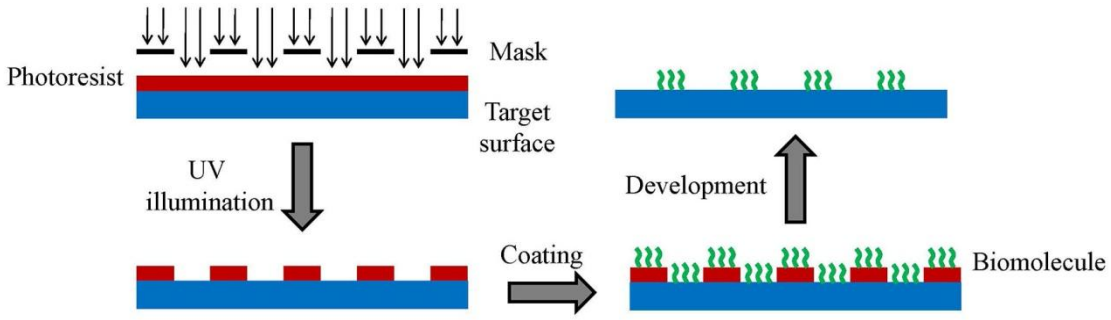

Figure 1.4 Typical photolithography micropatterning process

1.3.1.2 Soft lithography

Soft lithography refers to a set of techniques used to create micropatterns using a soft elastomeric stamp developed by Whitesides and colleagues [122,123]. This method can provide feature size in several hundreds nanometer scale. Two most typical micropatterns methods are microcontact printing and microfluidic patterning [124,125].

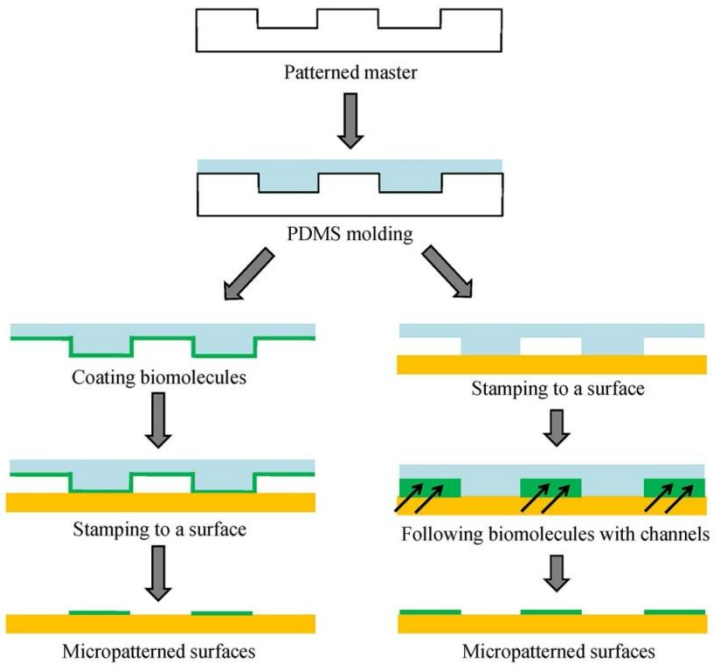

Figure 1.5 Schematic procedure for microcontact printing (left) and microfluidic patterning (right).

An elastomeric stamp is necessary for the patterning processes. The poly(dimethyl)-siloxane (PDMS) stamp is used in most cases. Other alternative materials such as poly-olefin-plastomers (POP) and agarose were also reported to be used as stamp for soft lithography micropatterning [126,127]. Depending on the methods, the stamp may be used in different ways. For instance, in a microcontact printing process, the stamp firstly will be immersed in biomolecule solution to allow the attachment of interest biomolecules. And then the stamp will contact with a substrate under a pressure in order to transfer the biomolecules onto the

substrate to obtain the micropatterned surfaces (Figure 1.5). While in a microfluidic patterning process, the cast PDMS stamp will directly contact with the substrate and then the biomolecule solution will flow through the microchannels between the PDMS stamp and substrate until the micropatterns form. Soft lithography has become a widely used method for cell micropatterning with low cost. And some other derived methods include micromolding in capillaries, microtransfer molding, replica molding and solvent-assisted micromolding [122,128-130]. However, several shortcomings need to be considered for application of this method. The elastomeric stamps are easily deformed and may cause the distortion of the micropatterns. And it is not suitable for patterning on soft substrate. This method is not appropriate for multiple molecule (more than two) patterning. And the ligand density usually cannot be precisely controlled using soft lithography.

1.3.1.3 Photoimmobilization

Photo-reactive molecules can be immobilized onto a substrate to generate the micropatterns for manipulation of cell morphology. In a general process, photo-reactive polymers will be firstly coated onto the substrate and irradiated upon UV or laser irradiation under a photomask with various microfeatures. After development, the micropatterned surfaces can be acquired (Figure 1.6). Different photo-reactive polymers including photo-reactive poly(ethylene glycol) (PEG), photo-reactive polyallylamine (PAAm) and photo-reactive poly(acrylic acid) (PAAc) were prepared for the micropatterning process [131]. This is a simple and robust method to prepare the micropatterned surfaces. Majority of the organic cell culture substrates can be used for micropatterning. Meanwhile, the chemical bonded micropatterns are suitable for long-term cell culture. Furthermore, the surface properties (wettability, static electric charge, etc.) can be tuned by using various photo-reactive polymers.

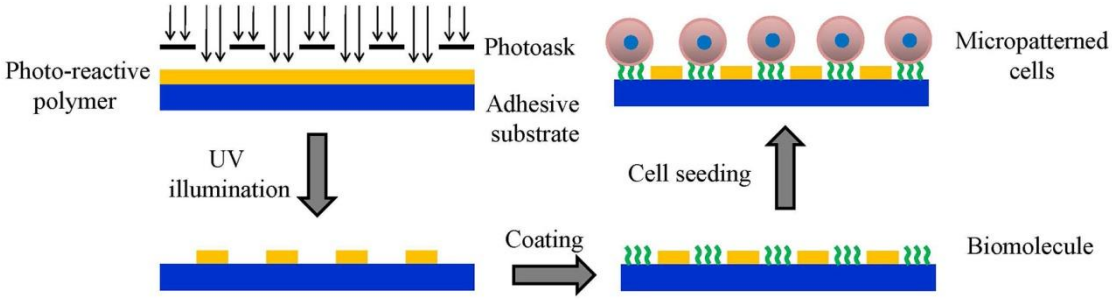

Figure 1.6 Schematic processes for photoimmobilization patterning.

1.3.1.4 Other micropatterning methods

Other typical micropatterning methods include laser/plasma ablation, stencil-assisted patterning and robotic printing. Laser or plasma with huge energy can be used to directly generate micro- or nano-features on substrate [132]. This method has high resolution (several nm) but also high cost in both time and money. Therefore, it is not appropriate for large scale preparation of micropatterns. A stencil has similar function as a mask but with through-holes of designed geometries. Compact the stencil with the substrate enabled the locally modification of the substrate through the holes while kept the region outside the holes unmodified. Then peeling off the stencil, and the micropatternd surface can be acquired. This method is adequate for coculture of two cell types. After putting the stencil on cell-adhesive substrate, first cell seeding will be performed without any modification of the substrate. The first type of cells will attach onto the substrate through the holes. Then, the unattached cells will be removed and the stencil will be peeled off. A second

cell seeding of different types of cells will allow the cells attach onto the remaining cell adhesive region on the substrate. Therefore, the coculture of two types of cells can be achieved [133]. Robotic printing has two types of printing techniques including contact and non-contact printing. Contact printing directly delivers the biomolecule solution with a tiny needle [134]. This method may destroy the substrate mechanically. Non-contact printing using a glass capillary as the needle and attached with piezoelectric fitting to contract the capillary selectively print the biomolecule onto the substrate [135]. This method can avoid the damage caused by direct contact of needle and substrate, but the processing time will increase a lot.

1.3.2 Application of micropatterning in biological field

Micropatterning technology is becoming increasingly popular in biomedical research, since it can provide many biophysical cues which can be highly controlled by designing different pattern geometries. During past decades, many studies have been done to explore the influence of cell microenvironments on cell functions by using micropatterns. Naturally, the microenvironment firstly affects cell adhesion and spreading through regulation of focal adhesions (FAs) formation. The cell adhesion and spreading state further determines the cytoskeleton architecture and the establishment of cell polarity. All these properties regulate the gene expression of cells through different pathways and finally affected the proliferation and differentiation of stem cells.

1.3.2.1 Cell adhesion on micropatterned surfaces

Cell adhesion to extracellular matrix (ECM) plays an important role in many cell behaviors including the migration, proliferation and apoptosis [136]. When cell contact with the ECM, initial cell adhesion onto a ECM is dominated by the binding of integrin receptors to the extracellular matrix (ECM) molecules (fibronectin, vitronectin, laminin, etc.). Activated integrin receptors cluster together with a complex of structure proteins (talin, vinculin, etc.) to form the FAs. The FAs are tightly associated with cytoskeleton and stabilized by actin-myosin contractility. In return, the reinforced FAs affect the assembly of cytoskeleton which determines cell shape. The generated intracellular force can be applied onto the underlying substrate through the cytoskeleton and FAs, and can mediate many cell behaviors such as migration, proliferation and differentiation. Until now, integrin-based cell adhesion and cadherin-dependent cell adhesion have been studied by using micropatterns.

Integrins are transmembrane receptors that attach the cytoskeleton to the ECM. Its formation and maturation was reported to be correlated with the cell size which can be controlled by micropatterns [137]. And a correlation between the tyrosine kinase signaling with FAs and the cell size also existed. At single molecule level, the clustering of the intergrins was regulated by the distance between the adhesion spots [138]. When the distance is larger than 73 nm, aberrant FAs formation can be observed and the cell adhesion and spreading is limited. When the distance is smaller than 58 nm, intergrins cluster together and effective cell adhesion and spreading will be observed.

Cadherins are another class of thransmembrane proteins that play important roles in cell adhesion and cell-cell interactions. Recently, it was reported that the cadherin-based adhesion network is mechanosensitve [139]. The cadherins are coated onto the elastic polyacrylamide hydrogels with different stiffness. And cells cultured on stiff substrates form cadherin clusters and the intracellular tension is higher indicating the the cadherin-based adhesion is involved in the mechanotransduction pathway. Future studies should focus on generation of co-patterning of integrin and cadherin to reconstruct physiological adhesive

microenvironment.

1.3.2.2 Cell polarity regulated by micropatterned surfaces

Cell polarity refers to the spatial organization of cellular components. The cytoskeleton structure can be manipulated by the micropatterns and the oriented cytoskeleton will guide the formation of cell polarity. Micropatterns with various shapes can force cells to spread non-adhesive areas over which cells form reinforced actin bundles and enhance the RhoA pathway which affects the cytoskeleton force distribution [140]. Annular micropatterns are used to investigate the cell migration. Cells located at inside and outside of a donut micropattern showed different migration speed. The inside cells spread homogeneously, while the outside cells formed leader and follower cells during migration [141]. The intracellular organization including the positioning of Golgi apparatus, centrosome and nucleus of cells is also dependent on their adhesive geometries. Therefore, the anisotropic micropatterns can be used to direct surface polarity and intracellular organization of cells [142]. Also cell division is orientated relative to the microenvironment geometry. A localized reduction in cell adhesion prevents spindle pole positioning toward this region. By contrast, a localized increase in cell adhesion attracts spindle poles [143].

1.3.2.3 Stem cell differentiation on micropatterned surfaces

Cell morphogenesis regulated by the micropatterns not only affects cytoskeleton structures, but also determines the cell fate such as proliferation and differentiation. Spreading area, shapes and aspect ratio as the biophysical cues which can change the cell contraction were confirmed to influence the differentiation of stem cells as summarized in Figure 1.7 based on previous studies [144-151].

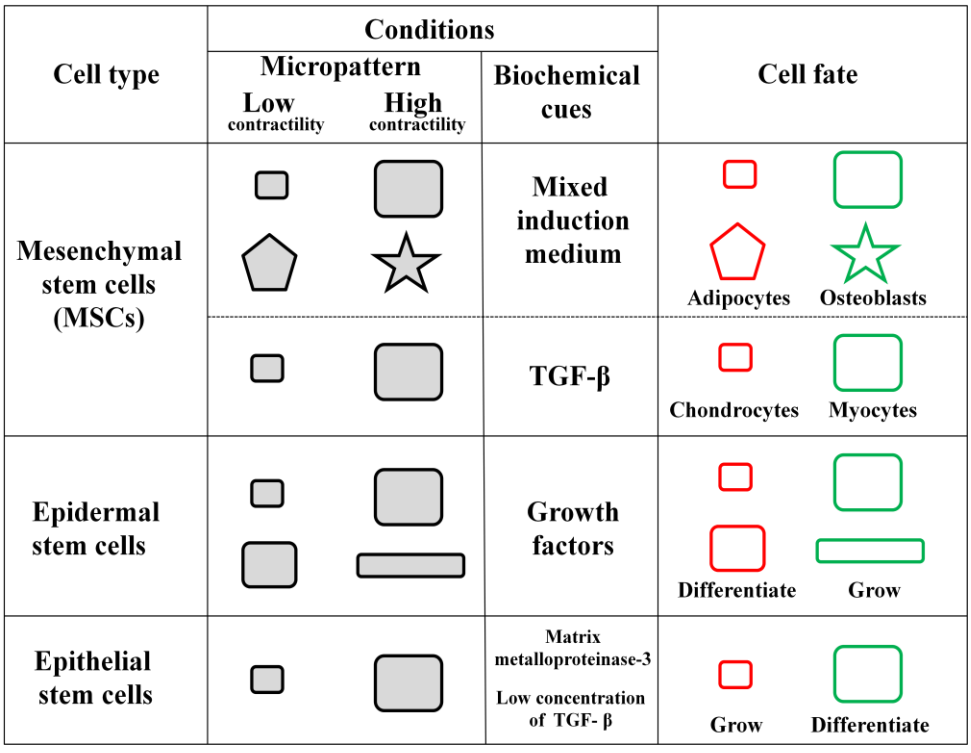

Figure 1.7 Cell fate determination regulated by micropatterned surfaces. The proliferation and differentiation of cells are dependent on both cell type and ECM micropatterned geometries.

1.4 Motivation, objectives and outline

1.4.1Motivation

Stem cells are promising cell source for tissue engineering and regenerative medicine due to their inherent multi-potency and self-renewal properties. However, the unspecific differentiation and loss of stemness during cell culture limit the clinical application of the stem cells. *In vivo*, the majority of stem cells are quiescent under homeostasis, but capable to undergo activation upon stimulation. The stem cell fate was mainly determined by their microenvironment including soluble and tethered factors, extracellular matrix (ECM), neighboring cells and physical morphogens. Strategies to mimic the microenvironment are needed for manipulation of stem cell functions.

Conventional efforts using soluble factors, ECM components, cell coculture and physical stimuli are mainly performed on uniform substrates. This is suitable for analysis of entire cell population at multiple cell level. However, the morphology and cytoskeleton architecture of individual cells cannot be controlled. In contrary, micropatterning technology can provide relative stable and reproducible cell morphology and cytoskeleton assembly. Therefore, micropatterning should be a useful tool for the investigation and manipulation of cell functions at single cell level. Commonly used micropatterning techniques include photolithography, contact printing, laser/plasma based etching and so on. These methods have some limitations in high cost and complex fabricating processes. Simple and robust micropatterning technology is highly required for practical application. In this study, a simple micropatterning method will be developed to prepare various micropatterns with stable micropatten structures during long period of cell culture.

The micropatterns have been widely used for manipulation of cell functions. They can be used to regulate cell migration, cell polarity, cell proliferation and cell differentiation. But some issues are still elusive. For example, the influence of cell morphology on maintenance of cell stemness, cell nanomechanics, cell/nanomaterials interactionsand the independent influence of cell adhesion and spreading on stem cell differentiation remain unclear. Therefore, in this research the micropatterns will be used for cell culture to elucidate the effects of cell size and geometry on the stemness maintenance of stem cells, cell nanomechanics, cell/nanomaterials interactions and the independent influence of cell adhesion and spreading on stem cell differentiation.

1.4.2 Objectives and outline

In this study, photo-reactive PVA was synthesized and used for micropatterning of TCPS surfaces by UV photolithography. A few types of photomasks were designed to control the size and geometry of micropatterns. The micropatterns were used for culture of a few cell types to disclose the influence of cell morphogenesis on cell functions. The details are outlines as follows.

Chapter 2 describes the influence of cell size, shape and aspect ratio on maintenance of multipotency of stem cells. The detailed preparation processes of the micropatterns were described in this chapter. The prepared micropatterns were characterized using phase-contrast microscope and AFM scanning. The regulation of cell morphogenesis by micropatterns was confirmed according to phase-contrast fluorescence images of the attached cells. The multipotency of MSCs on micropatterns was evaluated by the expression level of surface markers. The cytoskeleton assembly, cell mechanical state and nuclear activity

were analyzed to reveal the possible mechanism.

Chapter 3 describes the nanomechanical properties of MSCs, NHOst and MG-63 cells on micropatterns with various sizes. Cell elasticity was firstly evaluated from approach process during AFM nanoindentation. The cytoskeleton architecture of the micropatterned cells was stained to disclose the relationship between cell elasticity and their cytoskeleton structure. Non-specific adhesion between cell membrane and AFM tip was evaluated from retract process. The membrane roughness and phosphoezrin expression were investigated to reveal the influence of cell size and type on cell non-specific adhesion. A transfer contact assay was developed to check the influence of cell adhesion on cell migration.

Chapter 4 describes the cellular uptake of AuNPs influenced by cell morphogenesis. The AuNPs were synthesized using the Turkevich method and conjugated with FITC labeled PEG-SH. The NPs were characterized using SEM, TEM, DLS and fluorescence spectra. Cell morphology and membrane tension were evaluated by fluorescence staining and AFM nanoindentation. Cellular uptake of AuNPs was detected using confocal microscope.

Chapter 5 describes the independent influence of cell adhesion area and spreading area on osteogenic and adipogenic differentiation of MSCs. Ten types of isotropical micropatterns that were composed of 2 μm microdots were prepared to precisely control the adhesion area and spreading area of MSCs. The focal adhesion formation of micropattened cells was analyzed via vinculin staining. Myosin and F-actin were stained to check the cytoskeleton assembly of micropatterned cells. Mechanotransduction was evaluated using AFM and YAP/TAZ staining. Osteogenic differentiation and adipogenic differentiation were analyzed by ALP staining and Oil Red O staining, respectively.

Chapter 6 gives the concluding remarks and suggests the future prospects

1.5 References

[1] Persidis A. Biotechnology 2000. Nature Biotechnology. 1999;17:1239.

[2] Langer R, Vacanti J. Tissue engineering. Science. 1993;260:920-6.

[3] Zhang X, Deng Z, Wang H, Yang Z, Guo W, Li Y, et al. Expansion and delivery of human fibroblasts on micronized acellular dermal matrix for skin regeneration. Biomaterials. 2009;30:2666-74.

[4] FDA OKS ARTIFICIAL SKIN. http://www.wired.com/2001/02/fda-oks-artificial-skin/

[5] Ebihara G, Sato M, Yamato M, Mitani G, Kutsuna T, Nagai T, et al. Cartilage repair in transplanted scaffold-free chondrocyte sheets using a minipig model. Biomaterials. 2012;33:3846-51.

[6] Mitani G, Sato M, Lee JI, Kaneshiro N, Ishihara M, Ota N, et al. The properties of bioengineered chondrocyte sheets for cartilage regeneration. BMC Biotechnology. 2009;9:17.

[7] Kalka C, Masuda H, Takahashi T, Kalka-Moll WM, Silver M, Kearney M, et al. Transplantation of ex vivo expanded endothelial progenitor cells for therapeutic neovascularization. Proceedings of the National Academy of Sciences. 2000;97:3422-7.

[8] Werner N, Kosiol S, Schiegl T, Ahlers P, Walenta K, Link A, et al. Circulating endothelial progenitor cells and cardiovascular outcomes. New England Journal of Medicine. 2005;353:999-1007.

[9] Zhang M, Rehman J, Malik AB. Endothelial progenitor cells and vascular repair. Current Opinion in Hematology. 2014;21:224-8.

[10] Reya T, Morrison SJ, Clarke MF, Weissman IL. Stem cells, cancer, and cancer stem cells. Nature. 2001;414:105-11.

[11] Lutolf MP, Gilbert PM, Blau HM. Designing materials to direct stem-cell fate. Nature.

2009;462:433-41.
[12] Thomson JA, Itskovitz-Eldor J, Shapiro SS, Waknitz MA, Swiergiel JJ, Marshall VS, et al. Embryonic stem cell lines derived from human blastocysts. Science. 1998;282:1145-7.
[13] Knoepfler PS. Deconstructing stem cell tumorigenicity: a roadmap to safe regenerative medicine. Stem Cells. 2009;27:1050-6.
[14] Takahashi K, Yamanaka S. Induction of pluripotent stem cells from mouse embryonic and adult fibroblast cultures by defined factors. Cell. 2006;126:663-76.
[15] Takahashi K, Tanabe K, Ohnuki M, Narita M, Ichisaka T, Tomoda K, et al. Induction of pluripotent stem cells from adult human fibroblasts by defined factors. Cell. 2007;131:861-72.
[16] Pittenger MF, Mackay AM, Beck SC, Jaiswal RK, Douglas R, Mosca JD, et al. Multilineage potential of adult human mesenchymal stem cells. Science. 1999;284:143-7.
[17] Jiang Y, Jahagirdar BN, Reinhardt RL, Schwartz RE, Keene CD, Ortiz-Gonzalez XR, et al. Pluripotency of mesenchymal stem cells derived from adult marrow. Nature. 2002;418:41-9.
[18] Shenghui H, Nakada D, Morrison SJ. Mechanisms of stem cell self-renewal. Annual Review of Cell and Developmental. 2009;25:377-406.
[19] Boyer LA, Plath K, Zeitlinger J, Brambrink T, Medeiros LA, Lee TI, et al. Polycomb complexes repress developmental regulators in murine embryonic stem cells. Nature. 2006;441:349-53.
[20] Blanpain C, Horsley V, Fuchs E. Epithelial stem cells: turning over new leaves. Cell. 2007;128:445-58.
[21] Dominici M, Le Blanc K, Mueller I, Slaper-Cortenbach I, Marini F, Krause D, et al. Minimal criteria for defining multipotent mesenchymal stromal cells. The International Society for Cellular Therapy position statement. Cytotherapy. 2006;8:315-7.
[22] Zhu H, Mitsuhashi N, Klein A, Barsky LW, Weinberg K, Barr ML, et al. The role of the hyaluronan receptor CD44 in mesenchymal stem cell migration in the extracellular matrix. Stem Cells. 2006;24:928-35.
[23] Majumdar MK, Keane-Moore M, Buyaner D, Hardy WB, Moorman MA, McIntosh KR, et al. Characterization and functionality of cell surface molecules on human mesenchymal stem cells. Journal of Biomedical Science. 2003;10:228-41.
[24] Boxall SA, Jones E. Markers for characterization of bone marrow multipotential stromal cells. Stem Cells International. 2012;2012.
[25] Docheva D, Haasters F, Schieker M. Mesenchymal stem cells and their cell surface receptors. Current Rheumatology Reviews. 2008;4:155-60.
[26] Osawa M, Egawa G, Mak S-S, Moriyama M, Freter R, Yonetani S, et al. Molecular characterization of melanocyte stem cells in their niche. Development. 2005;132:5589-99.
[27] Gerecht S, Burdick JA, Ferreira LS, Townsend SA, Langer R, Vunjak-Novakovic G. Hyaluronic acid hydrogel for controlled self-renewal and differentiation of human embryonic stem cells. Proceedings of the National Academy of Sciences. 2007;104:11298-303.
[28] Jeon K, Oh H-J, Lim H, Kim J-H, Lee DH, Lee E-R, et al. Self-renewal of embryonic stem cells through culture on nanopattern polydimethylsiloxane substrate. Biomaterials. 2012;33:5206-20.
[29] Gilbert PM, Havenstrite KL, Magnusson KE, Sacco A, Leonardi NA, Kraft P, et al. Substrate elasticity regulates skeletal muscle stem cell self-renewal in culture. Science. 2010;329:1078-81.
[30] Winer JP, Janmey PA, McCormick ME, Funaki M. Bone marrow-derived human mesenchymal stem cells become quiescent on soft substrates but remain responsive to chemical or mechanical stimuli. Tissue Engineering Part A. 2008;15:147-54.
[31] Rustad KC, Wong VW, Sorkin M, Glotzbach JP, Major MR, Rajadas J, et al. Enhancement of mesenchymal stem cell angiogenic capacity and stemness by a biomimetic hydrogel scaffold. Biomaterials.

2012;33:80-90.
[32] McMurray RJ, Gadegaard N, Tsimbouri PM, Burgess KV, McNamara LE, Tare R, et al. Nanoscale surfaces for the long-term maintenance of mesenchymal stem cell phenotype and multipotency. Nature Materials. 2011;10:637-44.
[33] Zhang D, Kilian KA. The effect of mesenchymal stem cell shape on the maintenance of multipotency. Biomaterials. 2013;34:3962-9.
[34] Mauney JR, Kirker‐Head C, Abrahamson L, Gronowicz G, Volloch V, Kaplan DL. Matrix‐mediated retention of *in vitro* osteogenic differentiation potential and *in vivo* bone‐forming capacity by human adult bone marrow‐derived mesenchymal stem cells during ex vivo expansion. Journal of Biomedical Materials Research Part A. 2006;79:464-75.
[35] Ohgushi H, Kotobuki N, Funaoka H, Machida H, Hirose M, Tanaka Y, et al. Tissue engineered ceramic artificial joint—ex vivo osteogenic differentiation of patient mesenchymal cells on total ankle joints for treatment of osteoarthritis. Biomaterials. 2005;26:4654-61.
[36] Choi YS, Park S-N, Suh H. Adipose tissue engineering using mesenchymal stem cells attached to injectable PLGA spheres. Biomaterials. 2005;26:5855-63.
[37] Neubauer M, Hacker M, Bauer-Kreisel P, Weiser B, Fischbach C, Schulz MB, et al. Adipose tissue engineering based on mesenchymal stem cells and basic fibroblast growth factor *in vitro*. Tissue Engineering. 2005;11:1840-51.
[38] Alhadlaq A, Tang M, Mao JJ. Engineered adipose tissue from human mesenchymal stem cells maintains predefined shape and dimension: implications in soft tissue augmentation and reconstruction. Tissue Engineering. 2005;11:556-66.
[39] Cui JH, Park K, Park SR, Min B-H. Effects of low-intensity ultrasound on chondrogenic differentiation of mesenchymal stem cells embedded in polyglycolic acid: an *in vivo* study. Tissue Engineering. 2006;12:75-82.
[40] Hofmann S, Knecht S, Langer R, Kaplan DL, Vunjak-Novakovic G, Merkle HP, et al. Cartilage-like tissue engineering using silk scaffolds and mesenchymal stem cells. Tissue Engineering. 2006;12:2729-38.
[41] Galmiche MC, Koteliansky VE, Briere J, Herve P, Charbord P. Stromal cells from human long-term marrow cultures are mesenchymal cells that differentiate following a vascular smooth muscle differentiation pathway. Blood. 1993;82:66-76.
[42] Gang EJ, Jeong JA, Hong SH, Hwang SH, Kim SW, Yang IH, et al. Skeletal myogenic differentiation of mesenchymal stem cells isolated from human umbilical cord blood. Stem Cells. 2004;22:617-24.
[43] Tian H, Bharadwaj S, Liu Y, Ma H, Ma PX, Atala A, et al. Myogenic differentiation of human bone marrow mesenchymal stem cells on a 3D nano fibrous scaffold for bladder tissue engineering. Biomaterials. 2010;31:870-7.
[44] Gang EJ, Bosnakovski D, Simsek T, To K, Perlingeiro RC. Pax3 activation promotes the differentiation of mesenchymal stem cells toward the myogenic lineage. Experimental Cell Research. 2008;314:1721-33.
[45] Nöth U, Schupp K, Heymer A, Kall S, Jakob F, Schütze N, et al. Anterior cruciate ligament constructs fabricated from human mesenchymal stem cells in a collagen type I hydrogel. Cytotherapy. 2005;7:447-55.
[46] Jaiswal N, Haynesworth SE, Caplan AI, Bruder SP. Osteogenic differentiation of purified, culture‐expanded human mesenchymal stem cells *in vitro*. Journal of Cellular Biochemistry. 1997;64:295-312.
[47] Kotobuki N, Ioku K, Kawagoe D, Fujimori H, Goto S, Ohgushi H. Observation of osteogenic differentiation cascade of living mesenchymal stem cells on transparent hydroxyapatite ceramics. Biomaterials. 2005;26:779-85.

[48] Penney D, Powers J, Frank M, Willis C, Churukian C. Analysis and testing of biological stains--the biological stain commission procedures. Biotechnic & Histochemistry. 2002;77:237-75.
[49] Drury R. Theory and practice of histotechnology. Journal of Clinical Pathology. 1981;34:1406.
[50] Dalby MJ, Gadegaard N, Tare R, Andar A, Riehle MO, Herzyk P, et al. The control of human mesenchymal cell differentiation using nanoscale symmetry and disorder. Nature Materials. 2007;6:997-1003.
[51] Song W, Lu H, Kawazoe N, Chen G. Adipogenic differentiation of individual mesenchymal stem cell on different geometric micropatterns. Langmuir. 2011;27:6155-62.
[52] Wahli W, Braissant O, Desvergne B. Peroxisome proliferator activated receptors: transcriptional regulators of adipogenesis, lipid metabolism and more…. Chemistry & Biology. 1995;2:261-6.
[53] Schoonjans K, Staels B, Auwerx J. The peroxisome proliferator activated receptors (PPARS) and their effects on lipid metabolism and adipocyte differentiation. Biochimica et Biophysica Acta (BBA)-Lipids and Lipid Metabolism. 1996;1302:93-109.
[54] Hietanen E, Greenwood M. A comparison of lipoprotein lipase activity and adipocyte differentiation in growing male rats. Journal of Lipid Research. 1977;18:480-90.
[55] Park JS, Chu JS, Tsou AD, Diop R, Tang Z, Wang A, et al. The effect of matrix stiffness on the differentiation of mesenchymal stem cells in response to TGF-β. Biomaterials. 2011;32:3921-30.
[56] Mauney JR, Volloch V, Kaplan DL. Matrix-mediated retention of adipogenic differentiation potential by human adult bone marrow-derived mesenchymal stem cells during ex vivo expansion. Biomaterials. 2005;26:6167-75.
[57] Discher DE, Mooney DJ, Zandstra PW. Growth factors, matrices, and forces combine and control stem cells. Science. 2009;324:1673-7.
[58] Watt FM, Hogan BL. Out of Eden: stem cells and their niches. Science. 2000;287:1427.
[59] Fuchs E, Tumbar T, Guasch G. Socializing with the neighbors: stem cells and their niche. Cell. 2004;116:769-78.
[60] Reilly GC, Engler AJ. Intrinsic extracellular matrix properties regulate stem cell differentiation. Journal of Biomechanics. 2010;43:55-62.
[61] Vunjak-Novakovic G, Scadden DT. Biomimetic platforms for human stem cell research. Cell Stem Cell. 2011;8:252-61.
[62] Song HY, Kim MY, Kim KH, Lee IH, Shin SH, Lee JS, et al. Synovial fluid of patients with rheumatoid arthritis induces α-smooth muscle actin in human adipose tissue-derived mesenchymal stem cells through a TGF-β1-dependent mechanism. Experimental & Molecular Medicine. 2010;42:565-73.
[63] Liu S-P, Lin C-H, Lin S-J, Fu R-H, Huang Y-C, Chen S-Y, et al. Electrospun Polyacrylonitrile-Based Nanofibers Maintain Embryonic Stem Cell Stemness via TGF-Beta Signaling. Journal of Biomedical Nanotechnology. 2016;12:732-42.
[64] Watabe T, Miyazono K. Roles of TGF-β family signaling in stem cell renewal and differentiation. Cell Research. 2009;19:103-15.
[65] Park JS, Woo DG, Yang HN, Lim HJ, Chung H-M, Park K-H. Heparin-bound transforming growth factor-β3 enhances neocartilage formation by rabbit mesenchymal stem cells. Transplantation. 2008;85:589-96.
[66] Park K, Cho KJ, Kim JJ, Kim IH, Han DK. Functional PLGA scaffolds for chondrogenesis of bone-marrow-derived mesenchymal stem cells. Macromolecular Bioscience. 2009;9:221-9.
[67] Zhang S-C, Wernig M, Duncan ID, Brüstle O, Thomson JA. *In vitro* differentiation of transplantable neural precursors from human embryonic stem cells. Nature Biotechnology. 2001;19:1129-33.

[68] Nur-E-Kamal A, Ahmed I, Kamal J, Babu AN, Schindler M, Meiners S. Covalently attached FGF-2 to three-dimensional polyamide nanofibrillar surfaces demonstrates enhanced biological stability and activity. Molecular and Cellular Biochemistry. 2008;309:157-66.
[69] Jin W, Xing Y-q, Yang A-h. Epidermal growth factor promotes the differentiation of stem cells derived from human umbilical cord blood into neuron-like cells via taurine induction *in vitro*. In Vitro Cellular & Developmental Biology-Animal. 2009;45:321-7.
[70] Del Angel-Mosqueda C, Gutiérrez-Puente Y, López-Lozano AP, Romero-Zavaleta RE, Mendiola-Jiménez A, Medina-De la Garza CE, et al. Epidermal growth factor enhances osteogenic differentiation of dental pulp stem cells *in vitro*. Head & Face Medicine. 2015;11:29.
[71] Rodrigues M, Blair H, Stockdale L, Griffith L, Wells A. Surface Tethered Epidermal Growth Factor Protects Proliferating and Differentiating Multipotential Stromal Cells from FasL-Induced Apoptosis. Stem Cells. 2013;31:104-16.
[72] Sasaki N, Shinomi M, Hirano K, Ui-Tei K, Nishihara S. LacdiNAc (GalNAcβ1-4GlcNAc) Contributes to Self-Renewal of Mouse Embryonic Stem Cells by Regulating Leukemia Inhibitory Factor/STAT3 Signaling. Stem Cells. 2011;29:641-50.
[73] Cetinkaya G, Türkoğlu H, Arat S, Odaman H, Onur MA, Gümüşderelioğlu M, et al. LIF-immobilized nonwoven polyester fabrics for cultivation of murine embryonic stem cells. Journal of Biomedical Materials Research Part A. 2007;81:911-9.
[74] Binh NH, Aoki H, Takamatsu M, Hatano Y, Hirata A, Tomita H, et al. Time-sensitive effects of hypoxia on differentiation of neural stem cells derived from mouse embryonic stem cells *in vitro*. Neurological Research. 2014;36:804-13.
[75] Cao B, Li Z, Peng R, Ding J. Effects of cell–cell contact and oxygen tension on chondrogenic differentiation of stem cells. Biomaterials. 2015;64:21-32.
[76] Choi JS, Yoon HI, Lee KS, Choi YC, Yang SH, Kim I-S, et al. Exosomes from differentiating human skeletal muscle cells trigger myogenesis of stem cells and provide biochemical cues for skeletal muscle regeneration. Journal of Controlled Release. 2016;222:107-15.
[77] Narayanan R, Huang C-C, Ravindran S. Hijacking the Cellular Mail: Exosome Mediated Differentiation of Mesenchymal Stem Cells. Stem Cells International. 2016;2016.
[78] Michel G, Tonon T, Scornet D, Cock JM, Kloareg B. The cell wall polysaccharide metabolism of the brown alga Ectocarpus siliculosus. Insights into the evolution of extracellular matrix polysaccharides in Eukaryotes. New Phytologist. 2010;188:82-97.
[79] Ott HC, Matthiesen TS, Goh S-K, Black LD, Kren SM, Netoff TI, et al. Perfusion-decellularized matrix: using nature's platform to engineer a bioartificial heart. Nature Medicine. 2008;14:213-21.
[80] Uygun BE, Soto-Gutierrez A, Yagi H, Izamis M-L, Guzzardi MA, Shulman C, et al. Organ reengineering through development of a transplantable recellularized liver graft using decellularized liver matrix. Nature Medicine. 2010;16:814-20.
[81] Song JJ, Guyette JP, Gilpin SE, Gonzalez G, Vacanti JP, Ott HC. Regeneration and experimental orthotopic transplantation of a bioengineered kidney. Nature Medicine. 2013;19:646-51.
[82] Schwarz S, Koerber L, Elsaesser AF, Goldberg-Bockhorn E, Seitz AM, Dürselen L, et al. Decellularized cartilage matrix as a novel biomatrix for cartilage tissue-engineering applications. Tissue Engineering Part A. 2012;18:2195-209.
[83] Datta N, Pham QP, Sharma U, Sikavitsas VI, Jansen JA, Mikos AG. *In vitro* generated extracellular matrix and fluid shear stress synergistically enhance 3D osteoblastic differentiation. Proceedings of the National Academy of Sciences of the United States of America. 2006;103:2488-93.

[84] Hoshiba T, Kawazoe N, Chen G. The balance of osteogenic and adipogenic differentiation in human mesenchymal stem cells by matrices that mimic stepwise tissue development. Biomaterials. 2012;33:2025-31.
[85] Hoshiba T, Kawazoe N, Tateishi T, Chen G. Development of extracellular matrices mimicking stepwise adipogenesis of mesenchymal stem cells. Advanced Materials. 2010;22:3042-7.
[86] Cai R, Nakamoto T, Kawazoe N, Chen G. Influence of stepwise chondrogenesis-mimicking 3D extracellular matrix on chondrogenic differentiation of mesenchymal stem cells. Biomaterials. 2015;52:199-207.
[87] Flaim CJ, Chien S, Bhatia SN. An extracellular matrix microarray for probing cellular differentiation. Nature Methods. 2005;2:119-25.
[88] Blumenthal NR, Hermanson O, Heimrich B, Shastri VP. Stochastic nanoroughness modulates neuron–astrocyte interactions and function via mechanosensing cation channels. Proceedings of the National Academy of Sciences. 2014;111:16124-9.
[89] Wang P-Y, Li W-T, Yu J, Tsai W-B. Modulation of osteogenic, adipogenic and myogenic differentiation of mesenchymal stem cells by submicron grooved topography. Journal of Materials Science: Materials in Medicine. 2012;23:3015-28.
[90] Yang K, Jung K, Ko E, Kim J, Park KI, Kim J, et al. Nanotopographical manipulation of focal adhesion formation for enhanced differentiation of human neural stem cells. ACS Applied Materials & Interfaces. 2013;5:10529-40.
[91] Dalby MJ, Gadegaard N, Tare R, Andar A, Riehle MO, Herzyk P, et al. The control of human mesenchymal cell differentiation using nanoscale symmetry and disorder. Nature Materials. 2007;6:997-1003.
[92] McMurray RJ, Gadegaard N, Tsimbouri PM, Burgess KV, McNamara LE, Tare R, et al. Nanosclae surface for the long-term maintenance of mesenchymal stem cell phenotype and multipotency. Nature Materials. 2011;10:637-44.
[93] Engler AJ, Sen S, Sweeney HL, Discher DE. Matrix elasticity directs stem cell lineage specification. Cell. 2006;126:677-89.
[94] Oh SH, An DB, Kim TH, Lee JH. Wide-range stiffness gradient PVA/HA hydrogel to investigate stem cell differentiation behavior. Acta Biomaterialia. 2016;35:23-31.
[95] Eng G, Lee BW, Parsa H, Chin CD, Schneider J, Linkov G, et al. Assembly of complex cell microenvironments using geometrically docked hydrogel shapes. Proceedings of the National Academy of Sciences. 2013;110:4551-6.
[96] Ottone C, Krusche B, Whitby A, Clements M, Quadrato G, Pitulescu ME, et al. Direct cell–cell contact with the vascular niche maintains quiescent neural stem cells. Nature Cell Biology. 2014;16:1045-56.
[97] Ludwig TE, Bergendahl V, Levenstein ME, Yu J, Probasco MD, Thomson JA. Feeder-independent culture of human embryonic stem cells. Nature Methods. 2006;3:637-46.
[98] Tsai RY, McKay RD. Cell contact regulates fate choice by cortical stem cells. The Journal of Neuroscience. 2000;20:3725-35.
[99] Song W, Lu H, Kawazoe N, Chen G. Gradient patterning and differentiation of mesenchymal stem cells on micropatterned polymer surface. Journal of Bioactive and Compatible Polymers. 2011;26:242-56.
[100] Wang X, Song W, Kawazoe N, Chen G. The osteogenic differentiation of mesenchymal stem cells by controlled cell–cell interaction on micropatterned surfaces. Journal of Biomedical Materials Research Part A. 2013;101:3388-95.
[101] Tang J, Peng R, Ding J. The regulation of stem cell differentiation by cell-cell contact on

micropatterned material surfaces. Biomaterials. 2010;31:2470-6.
[102] Cao B, Li Z, Peng R, Ding J. Effects of cell-cell contact and oxygen tension on chondrogenic differentiation of stem cells. Biomaterials. 2015,64:21-32.
[103] Childs PG, Boyle CA, Pemberton GD, Nikukar H, Curtis AS, Henriquez FL, et al. Use of nanoscale mechanical stimulation for control and manipulation of cell behaviour. Acta Biomaterialia. 2016,34:159-168.
[104] Yanagisawa M, Suzuki N, Mitsui N, Koyama Y, Otsuka K, Shimizu N. Effects of compressive force on the differentiation of pluripotent mesenchymal cells. Life Sciences. 2007;81:405-12.
[105] Ode A, Kurtz A, Schmidt-Bleek K, Schrade P, Kolar P, Buttgereit F, et al. CD73 and CD29 concurrently mediate the mechanically induced decrease of migratory capacity of mesenchymal stromal cells. European Cells and Materials. 2011;22:26-42.
[106] Li G, Fu N, Yang X, Li M, Ba K, Wei X, et al. Mechanical compressive force inhibits adipogenesis of adipose stem cells. Cell Proliferation. 2013;46:586-94.
[107] Liu C, Baek S, Kim J, Vasko E, Pyne R, Chan C. Effect of static pre-stretch induced surface anisotropy on orientation of mesenchymal stem cells. Cellular and Molecular Bioengineering. 2014;7:106-21.
[108] Huang CH, Chen MH, Young TH, Jeng JH, Chen YJ. Interactive effects of mechanical stretching and extracellular matrix proteins on initiating osteogenic differentiation of human mesenchymal stem cells. Journal of Cellular Biochemistry. 2009;108:1263-73.
[109] Guo Y. Effects of mechanical stimulus on mesenchymal stem cells differentiation toward cardiomyocytes. Asian Biomedicine (Research Reviews and News). 2011:655.
[110] Nakayama KH, Surya VV, Gole M, Walker T, Yang W, Lai E, et al. Nanoscale patterning of extracellular matrix alters endothelial function under shear stress. Nano Letters. 2015.
[111] Franco CA, Jones ML, Bernabeu MO, Vion A-C, Barbacena P, Fan J, et al. Non-canonical Wnt signalling modulates the endothelial shear stress flow sensor in vascular remodelling. Elife. 2016;5:e07727.
[112] Sonam S, Sathe SR, Yim EK, Sheetz MP, Lim CT. Cell contractility arising from topography and shear flow determines human mesenchymal stem cell fate. Scientific Reports. 2016;6.
[113] Liu Y-S, Liu Y-A, Huang C-J, Yen M-H, Tseng C-T, Chien S, et al. Mechanosensitive TRPM7 mediates shear stress and modulates osteogenic differentiation of mesenchymal stromal cells through Osterix pathway. Scientific Reports. 2015;5.
[114] Vogel V, Sheetz M. Local force and geometry sensing regulate cell functions. Nature Reviews Molecular Cell Biology. 2006;7:265-75.
[115] Wozniak MA, Chen CS. Mechanotransduction in development: a growing role for contractility. Nature Reviews Molecular Cell Biology. 2009;10:34-43.
[116] Wang N, Tytell JD, Ingber DE. Mechanotransduction at a distance: mechanically coupling the extracellular matrix with the nucleus. Nature Reviews Molecular Cell Biology. 2009;10:75-82.
[117] Théry M. Micropatterning as a tool to decipher cell morphogenesis and functions. Journal of Cell Science. 2010;123:4201-13.
[118] Nakanishi J, Takarada T, Yamaguchi K, Maeda M. Recent advances in cell micropatterning techniques for bioanalytical and biomedical sciences. Analytical Sciences. 2008;24:67-72.
[119] Falconnet D, Csucs G, Grandin HM, Textor M. Surface engineering approaches to micropattern surfaces for cell-based assays. Biomaterials. 2006;27:3044-63.
[120] Yap F, Zhang Y. Protein and cell micropatterning and its integration with micro/nanoparticles assembly. Biosensors and Bioelectronics. 2007;22:775-88.
[121] Jing G, Wang Y, Zhou T, Perry SF, Grimes MT, Tatic-Lucic S. Cell patterning using molecular vapor deposition of self-assembled monolayers and lift-off technique. Acta Biomaterialia. 2011;7:1094-103.

[122] Xia Y, Whitesides GM. Soft lithography. Annual Review of Materials Science. 1998;28:153-84.
[123] Kane RS, Takayama S, Ostuni E, Ingber DE, Whitesides GM. Patterning proteins and cells using soft lithography. Biomaterials. 1999;20:2363-76.
[124] Kumar A, Whitesides GM. Features of gold having micrometer to centimeter dimensions can be formed through a combination of stamping with an elastomeric stamp and an alkanethiol ‘‘ink’’followed by chemical etching. Applied Physics Letters. 1993;63:2002-4.
[125] Delamarche E, Bernard A, Schmid H, Bietsch A, Michel B, Biebuyck H. Microfluidic networks for chemical patterning of substrates: design and application to bioassays. Journal of the American Chemical Society. 1998;120:500-8.
[126] Csucs G, Künzler T, Feldman K, Robin F, Spencer ND. Microcontact printing of macromolecules with submicrometer resolution by means of polyolefin stamps. Langmuir. 2003;19:6104-9.
[127] Mayer M, Yang J, Gitlin I, Gracias DH, Whitesides GM. Micropatterned agarose gels for stamping arrays of proteins and gradients of proteins. Proteomics. 2004;4:2366-76.
[128] Trau M, Yao N, Kim E, Xia Y, Whitesides G, Aksay I. Microscopic patterning of orientated mesoscopic silica through guided growth. Nature. 1997;390:674-6.
[129] Zhao X-M, Smith SP, Waldman SJ, Whitesides GM, Prentiss M. Demonstration of waveguide couplers fabricated using microtransfer molding. Applied Physics Letters. 1997;71:1017-9.
[130] Rogers JA, Bao Z, Dhar L. Fabrication of patterned electroluminescent polymers that emit in geometries with feature sizes into the submicron range. Applied Physics Letters. 1998;73:294-6.
[131] Guo L, Kawazoe N, Fan Y, Ito Y, Tanaka J, Tateishi T, et al. Chondrogenic differentiation of human mesenchymal stem cells on photoreactive polymer-modified surfaces. Biomaterials. 2008;29:23-32.
[132] Goessl A, Bowen-Pope DF, Hoffman AS. Control of shape and size of vascular smooth muscle cells *in vitro* by plasma lithography. Journal of Biomedical Materials Research. 2001;57:15-24.
[133] Tourovskaia A, Barber T, Wickes BT, Hirdes D, Grin B, Castner DG, et al. Micropatterns of chemisorbed cell adhesion-repellent films using oxygen plasma etching and elastomeric masks. Langmuir. 2003;19:4754-64.
[134] Wagner P, Kim R. Protein biochips: an emerging tool for proteomics research. Current Drug Discovery. 2002:23-8.
[135] Lemieux B, Aharoni A, Schena M. Overview of DNA chip technology. Molecular Breeding. 1998;4:277-89.
[136] Schwartz MA, Ginsberg MH. Networks and crosstalk: integrin signalling spreads. Nature Cell Biology. 2002;4:E65-E8.
[137] Chen CS, Alonso JL, Ostuni E, Whitesides GM, Ingber DE. Cell shape provides global control of focal adhesion assembly. Biochemical and Biophysical Research Cmmunications. 2003;307:355-61.
[138] Arnold M, Cavalcanti-Adam EA, Glass R, Blümmel J, Eck W, Kantlehner M, et al. Activation of integrin function by nanopatterned adhesive interfaces. ChemPhysChem. 2004;5:383-8.
[139] Ladoux B, Anon E, Lambert M, Rabodzey A, Hersen P, Buguin A, et al. Strength dependence of cadherin-mediated adhesions. Biophysical Journal. 2010;98:534-42.
[140] Thery M, Pepin A, Dressaire E, Chen Y, Bornens M. Cell distribution of stress fibres in response to the geometry of the adhesive environment. Cell Motility and the Cytoskeleton. 2006;63:341-55.
[141] Rolli CG, Nakayama H, Yamaguchi K, Spatz JP, Kemkemer R, Nakanishi J. Switchable adhesive substrates: Revealing geometry dependence in collective cell behavior. Biomaterials. 2012;33:2409-18.
[142] Théry M, Racine V, Piel M, Pépin A, Dimitrov A, Chen Y, et al. Anisotropy of cell adhesive microenvironment governs cell internal organization and orientation of polarity. Proceedings of the National

Academy of Sciences. 2006;103:19771-6.
[143] Thery M, Jimenez-Dalmaroni A, Racine V, Bornens M, Jülicher F. Experimental and theoretical study of mitotic spindle orientation. Nature. 2007;447:493-6.
[144] Thakar RG, Cheng Q, Patel S, Chu J, Nasir M, Liepmann D, et al. Cell-shape regulation of smooth muscle cell proliferation. Biophysical Journal. 2009;96:3423-32.
[145] Kurpinski K, Chu J, Hashi C, Li S. Anisotropic mechanosensing by mesenchymal stem cells. Proceedings of the National Academy of Sciences. 2006;103:16095-100.
[146] McBeath R, Pirone DM, Nelson CM, Bhadriraju K, Chen CS. Cell shape, cytoskeletal tension, and RhoA regulate stem cell lineage commitment. Developmental Cell. 2004;6:483-95.
[147] Kilian KA, Bugarija B, Lahn BT, Mrksich M. Geometric cues for directing the differentiation of mesenchymal stem cells. Proceedings of the National Academy of Sciences. 2010;107:4872-7.
[148] Gao L, McBeath R, Chen CS. Stem cell shape regulates a chondrogenic versus myogenic fate through Rac1 and N cadherin. Stem Cells. 2010;28:564-72.
[149] Connelly JT, Gautrot JE, Trappmann B, Tan DW-M, Donati G, Huck WT, et al. Actin and serum response factor transduce physical cues from the microenvironment to regulate epidermal stem cell fate decisions. Nature cell Biology. 2010;12:711-8.
[150] Nelson CM, Khauv D, Bissell MJ, Radisky DC. Change in cell shape is required for matrix metalloproteinase-induced epithelial-mesenchymal transition of mammary epithelial cells. Journal of Cellular Biochemistry. 2008;105:25-33.
[151] Gomez EW, Chen QK, Gjorevski N, Nelson CM. Tissue geometry patterns epithelial–mesenchymal transition via intercellular mechanotransduction. Journal of Cellular Biochemistry. 2010;110:44-51.

Chapter 2

Stemness variation of human mesenchymal stem cells by micropatterns

2.1 Summary

In this chapter, a method to prepare precisely controlled micropattern structures was developed by using photo-reactive poly(vinyl alcohol). The micropatterns were designed to have different size, shape and aspect ratio. The micropatterns were used for culture of human bone marrow-derived mesenchymal stem cells at single cell level to investigate how the micropatterns affect the functions of stem cells. The morphogenic features of stem cells were regulated by the micropatterns. The stem cells in the micropatterns showed different properties of cell quiescence, stemness and nanomechanics. The cells with small spreading area and low aspect ratio were more quiescent and softer than their large and elongated counterpart, and they showed higher potential to maintain the multipotency of stem cells. The stemness of stem cells could be controlled by the micropattern structures. The results provided very useful information for stem cell research and regenerative medicine.

2.2 Introduction

Stem cells have attracted tremendous attention in tissue engineering and regenerative medicine because of their pluripotency in differentiation to different cell types. Mesencymal stem cells (MSCs) are one of the most commonly used stem cells due to their easy availability, high expansion efficiency and multilineage differentiation [1-4]. Multipotency and self-renewal are the essential characters of stem cells [5]. *In vivo*, the majority of stem cells are quiescent under homeostasis, but capable to undergo activation upon stimulation [6]. The quiescent state contributes to stem cell maintenance. Stem cells may lose their pluripotency during *in vitro* expansion culture which limits their application in clinical use [7]. Motivation to maintain the stemness of stem cells during expansion culture has initiated plenty of researches to disclose details of interaction between stem cells and biomaterials [8-13]. Biomaterials can provide various physiochemical and biological cues to interact with stem cells and therefore impact significant influence on stem cells functions. For instance, micropatterns which enabled the geometrical and mechanical control of

cell morphogenesis have been extensively used to regulate stem cell survival, proliferation and differentiation [14]. However, the influence of spreading area, aspect ratio and geometry of cells on the stemness of stem cells remains unclear. Thus in this study, different micropatterns were prepared to control the spreading area, geometry and aspect ratio of single stem cells and disclosed the influences of these physical cues on the maintenance of stemness of MSCs.

2.3 Materials and methods

2.3.1 Materials

The chemicals and reagents were purchased from Sigma Aldrich unless otherwise noted. Polystyrene tissue culture flasks and dishes were purchased form BD Falcon. MSCGM medium were purchased from Lonza. Human MSCs were obtained from Osiris Therapeutics, Inc. (Columbia, MA) at passage 2. BrdU labeling reagent and the secondary antibodies used for immunofluorescence staining were purchased from Invitrogen TM (Grand Island, NY). 4′,6-diamidino-2-phenylindole (DAPI) mounting medium was purchased from Vector Laboratories, Inc (Burlingame, CA). The primary antibodies mouse anti-CD44s, mouse anti-CD45, mouse anti-CD106 and mouse anti-STRO-1 were purchase from R&D Systems (Abingdon, OX). Rabbit anti-CD11b and rabbit anti-CD73 were purchased from Novus Biologicals (Littleton, CO). Mouse anti-CD19 was purchased from Imgenex (San Diego, CA). Mouse anti-CD105 was purchased from Exbio (Vestec, Czech Republic). Mouse anti-CD34 was purchased from Cayman Chemical (Ann Arbor, Michigan). The secondary antibodies Alexa Fluor 488-conjugated anti-mouse IgG, Alexa Fluor 488-conjugated anti-mouse IgM and Alexa Fluor 488-conjugated anti-rabbit IgG were purchased from Invitrogen TM (Grand Island, NY). AFM cantilevers were purchased from Bruker (Camarillo, CA) and Novascan Technologies, Inc. (Ames, IA).

2.3.2 Preparation and characterization of micropatterns

Photo-reactive azidophenyl-derivatized poly(vinyl alcohol) (AzPhPVA) was synthesized by introducing azidophenyl groups into PVA according to previous report (Figure 2.1a) [15,16]. Briefly, Dimethyl sulfoxide (DMSO) solution (2 mL) containing dicyclohexylcarbodiimide (234 mg, 1.13 mol, Watanabe Chemical Industries, Ltd.) was added dropwise to 5 mL DMSO solution containing 4-azidobenzoic acid (185 mg, 1.13 mmol, Tokyo Chemical Industry Co., Ltd.) under stirring at room temperature in the dark. Then, 2 mL of DMSO solution dissolving 16.8 mg 4-(1-pyrrolidinyl) pyridine (0.113 mmol, Wako Pure Chemical Industries, Ltd.) was added dropwise to the reaction mixture under stirring. After 10 min, 8 mL of DMSO solution containing 100 mg of poly(vinyl alcohol) (MW 44,000, 2.26 mmol in monomer units, Wako Pure Chemical Industries. Ltd.) was added dropwise to the above reaction mixture under stirring in the dark. After 24 h, dicyclohexylurea that formed during the reaction was filtered off, and the filtrate was collected and purified by dialysis against Milli-Q water. The azidophenyl groups introduced in AzPhPVA were characterized by 1H-NMR (Figure 2.1). The percentage of azidophenyl groups in AzPhPVA was determined by 1H-NMR from the peak intensities of the azidophenyl protons at around 7 ppm, and those of the methylene and methylidyne protons of the polymer main chain at 1.5 and 3.9 ppm, respectively.

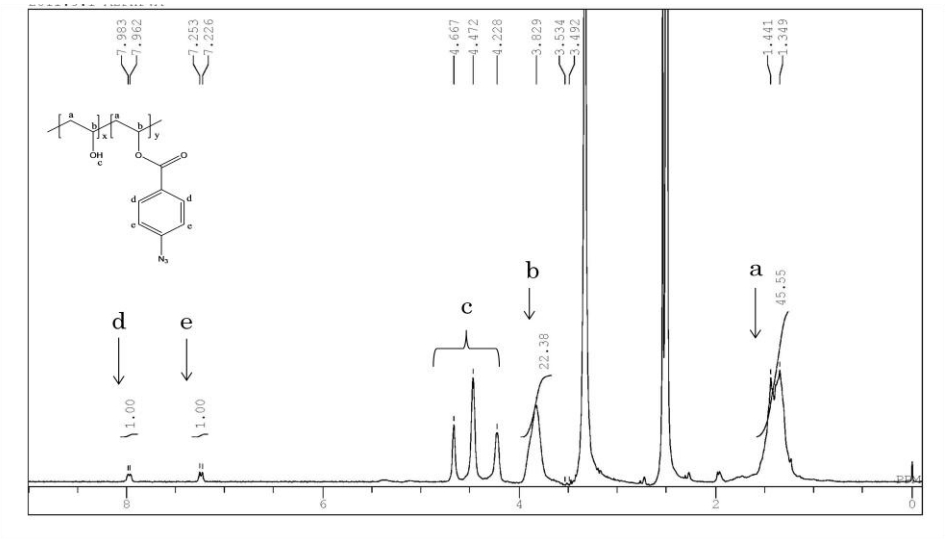

Figure 2.1 ^{1}H-NMR spectrum of the synthesized photo-reactive PVA.

The polystyrene plates were cut from tissue culture flask and coated with 0.2 ml of 0.35 mg/ml AzPhPVA solution and then air-dried at room temperature in the dark. The plates were covered with photomasks of different micropatterns and irradiated with UV light (Funa-UV-linker FS-1500) at 0.25 J/cm^2 from a distance of 15 cm. After irradiation, the plates were immersed in Milli-Q water and ultrasonicated to completely remove any unreacted polymer (Figure 2.2). The micropattrens of different sizes, shapes, and aspect ratios were prepared to control the cell morphogenesis which allowed us to investigate the influences of these biophysical features on stemness of MSCs. The surface topography of PVA-micropatterned polystyrene plates were characterized by a MFP-3D-BIO atomic force microscope (Asylum Research, Santa Barbara, USA). The micropatterns were sterilized with 70% ethanol followed by aseptic water washing and used for cell culture.

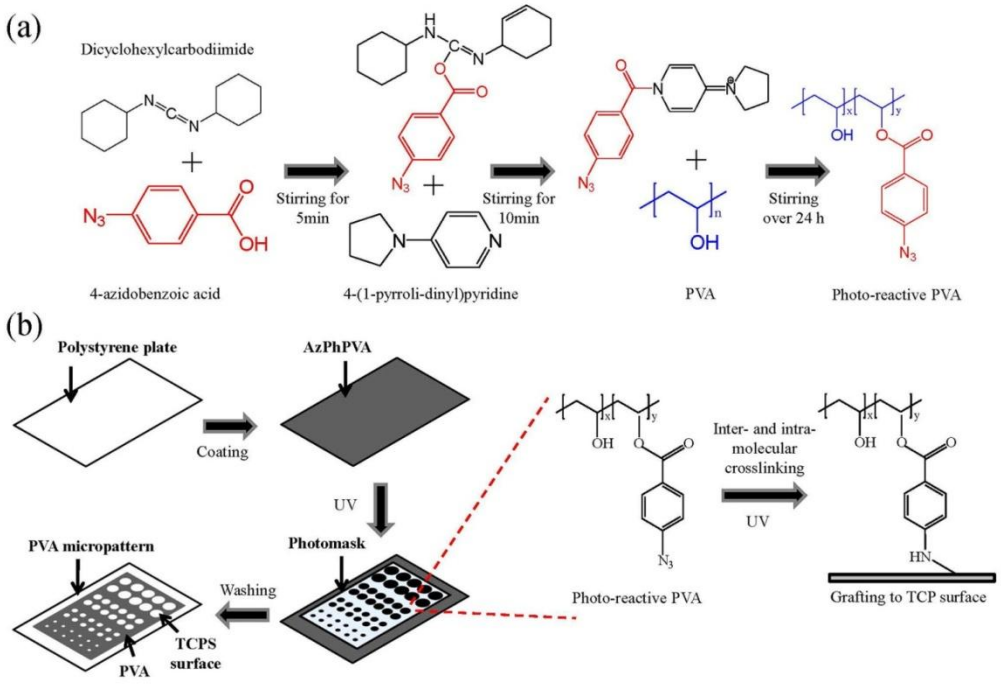

Figure 2.2 Preparation of the PVA micropatterned TCPS surfaces. (a) Photo-reactive PVA was synthesized by

coupling azidobenzoic acid with PVA. (b) The PVA micropatterned TCPS surfaces were prepared using UV photolithography. The photo-reactive PVA was chemically bonded onto TCPs surface upon UV irradiation.

2.3.4 Cell purification and culture

The human MSCs were seeded onto a cell culture dish (58.9 cm^2) at passage 2. Around 20 cells were added into each dish and subcultured with MSCGM medium (Lonza Group Ltd.) for 3 weeks to get cell colonies. 0.3% crystal violet was used to stain the formation of colonies. Colonies greater than 4 mm in diameter were collected and subcultured in 25 cm^2 tissue culture flasks for another 3 weeks to get homogeneous cell mass (Figure 2.3). The cells were treated with serum free low glucose DMEM medium (starvation) for 24 h to obtain the cells at G0/G1 enriched state. Subsequently the cells were collected and seeded on different micropatterns at a density of 3000 cells/cm^2. The cells were then cultured with low glucose DMEM medium supplemented with 10% FBS and 1% penicillin/streptomycin. The cells attached onto the micropatterned surfaces and spread within the micropatterns to show the same geometries as the underling polystyrene micropatterns.

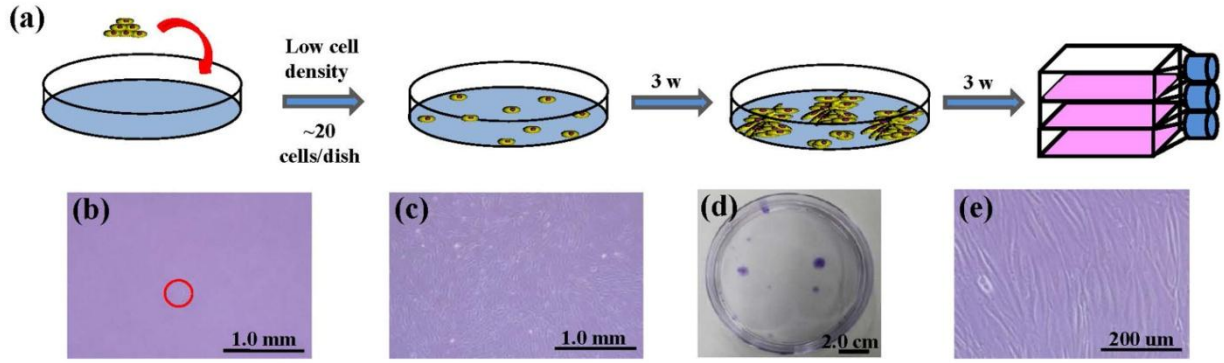

Figure 2.3 Cell purification process. (a) Purification process of the homogeneous MSCs mass. (b) Phase-contrast micrograph of attached single cell on culture dish. (c) Phase-contrast micrograph of MSCs colony after 3 weeks culture. (d) Photograph of MSCs colonies stained by crystal violet to show their size and distribution. (e) Phase-contrast micrograph of the confluent MSCs form one MSCs colony. The confluent MSCs kept stem cell-like spindle shape.

2.3.5 Immunofluorescence staining

Cells were stained for different surface markers to check the multipotency of cells. Cells were fixed with 4% paraformaldehyde for 10 min at room temperature and blocked with 2% BSA and 0.3 M glycine mixture solution for 30 min followed by PBS washing. Primary antibodies were diluted in 1% BSA solution at different concentration according to the protocol. The samples were incubated with the diluted primary antibodies at room temperature for 1.5 h and washed with PBS for three times. Secondary antibody labeling was performed in 1% BSA solution at room temperature for 1 h. Subsequently the cells were permeabilized with 0.2% Triton X-100 in PBS solution for 2 min and stained with Alexa Fluor-594 phalloidin for 20 min. Nuclei were stained with DAPI. The percentage of the cells positively stained with the antibodies was counted with fluorescence microscopy. Only single cell was counted in each experiment and at least 100 single cells were analyzed. Three independent experiments were performed to calculate the means and standard deviations.

2.3.6 Nuclear activity evaluation

After 6 h culture of MSCs on the micropatterns, non-adherent cells were removed by medium change and low glucose DMEM medium supplemented with 10% FBS, 1% penicillin/streptomycin and 1% BrdU labeling reagent (v/v) was added. After 24 h incubation, the cells were washed with PBS and fixed with 70% ethanol for 30 min followed by PBS washing. Cells were denatured with 2 M HCl for 30 min and then 0.2% Triton X-100 was used to permeabilize cells for 10 min. 2% BSA in PBS solution was used to block the cells for 30 min. Cells were incubated with monoclonal mouse anti-BrdU primary antibody (1:200) at room temperature for 1.5 h and then with Alexa Fluor 488-conjugated anti-mouse IgG antibody (1:500) at room temperature for 1 h followed by PBS washing. Mounting medium with DAPI (Vector) was used to mount the samples and stain the nuclei. The percentage of cells staining incorporation of BrdU was counted by using fluorescence microscopy. Three independent experiments were performed to calculate the means and standard deviations.

2.3.7 Cell mechanics measurements by atomic force microscopy

Cell mechanical properties were measured with a commercially available MFP-3D-Bio AFM microscope. An optical microscope was used to find cells and control the position of the AFM tip. Silicon nitride cantilevers with 600 nm diameter glass ball as a probe were used. Although the cantilevers had nominal spring constant (k = 0.06 N/m), the exact spring constant was measured before each experiment using the thermal tuning method [17]. Force-volume height imaging (FVH) was performed to acquire the cell height map. The scan size was set to 20 pixel × 20 lines at a 80 × 80 μm^2 area. The image was recorded at an indentation velocity of 8 μm/s with a trigger force of 3 nN. The acquiring image was used to select the region of interest where the force curves were collected. All the force curves were obtained at the highest region of cells with a loading rate of 4 μm/s and a trigger force of 3 nN. The samples were immersed in DMEM/HEPES serum medium and measured at room temperature. Live/dead staining was performed after the measurement to detect whether the cells were still alive.

The force curves were fitted to Hertz's contact model to calculate the Young's modulus of cells. According to the probe geometry, parabolic model was used and the formula is given by:

$$F(\delta) = \frac{4}{3} \cdot \sqrt{R} \cdot E_r \cdot \delta^{3/2} \qquad (1)$$

where F is the loading force, R is the radius of the tip, Er is the reduced Young's modulus and δ is the indentation depth. The reduced Young's modulus Er is related with the Young's modulus of sample Es and is given by:

$$\frac{1}{E_r} = \frac{1-\nu_t^2}{E_t} + \frac{1-\nu_s^2}{E_s} \qquad (2)$$

where νt and νs are the Poisson ratios of tips and samples. Since the Young's modulus of tips material (SiO2) is much greater than that of living cells, equation (2) can be simplified as following:

$$E_r = \frac{E_s}{1-\nu_s^2} \qquad (3)$$

The Poisson ratio of sample is assumed to be 0.5 since cells can be treated as soft incompressible materials [18].

2.3.8 Statistical analysis

The data was presented as mean ± standard deviation (SD). Statistical analysis was performed using a one-way analysis of variance (ANOVA) with Tukey's post hoc test for multiple comparisons to confirm the significant differences among samples. A value of $p < 0.05$ was considered to indicate statistically significant difference.

2.4 Results

2.4.1Preparation and characterization of the micropatterns and purified cell mass

Photo-reactive PVA was micropatterned on TCPS surface using UV photolithography. A transparent quartz slice with interval nontransparent micro-features was used as the photomask. Cell adhesive TCPS micropatterns were surrounded by non-adhesive PVA. The thin PVA grafted to the substrate surface could resist cells from migrating and spreading across the PSt micropatterns. Three types of micropatterns with different spreading areas, geometries and aspect ratios (Figure 2.4) were prepared. They were circular micropatterns having a diameter of 20, 40, 60 and 80 μm and a respective surface area of 314, 1256, 2826 and 5024 μm^2; 1134 μm^2 micropatterns having a geometry of circle, triangle, square, pentagon and hexagon; and 706 μm^2 ellipse micropatterns having an aspect ratio of 1, 1.5, 4 and 8. The height and 3D images of the micropatterns were observed by AFM in Milli-Q water with a contact mode (Figure 2.5). The diameters of the PSt micropatterns and thickness of the grafted PVA layer were analyzed by section analysis (Table 2.1). The diameters of the PSt micropatterns were nearly the same as those of the designed photomasks indicating good controllability of the micropatterning method. The thickness of grafted PVA varied from 59.66 to 67.98 nm which was effective to constrain cells in the PSt micropatterns. The micropatterns were used for culture of MSCs to systematically compare the influence of different morphogenic cues on stem cells functions.

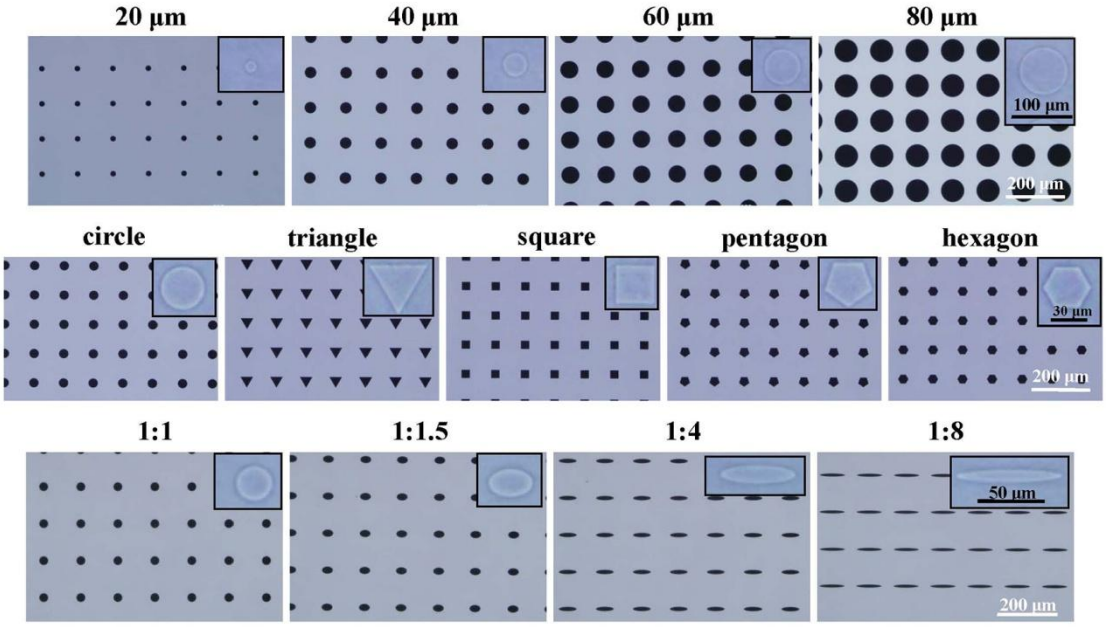

Figure 2.4 Light microscopy images of the photomasks with different size (up), geometry (middle) and aspect ratio (down). Insert images are the prepared micropatterns.

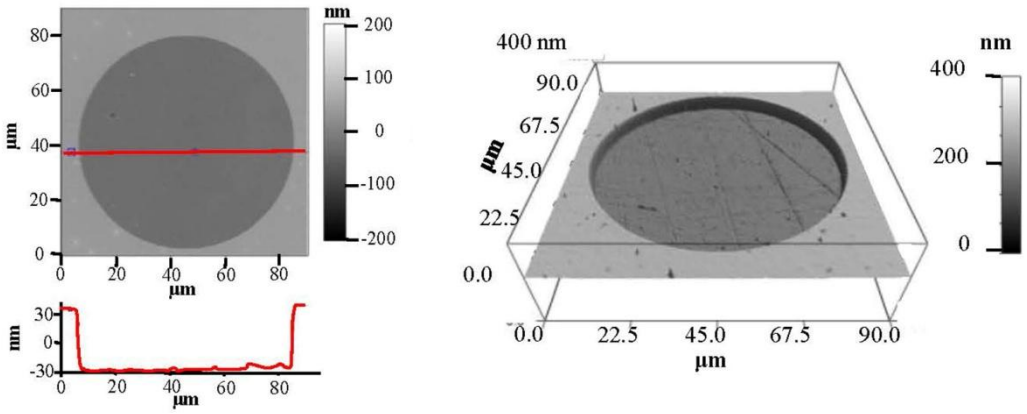

Figure 2.5 AFM scanning images of the 80 µm diameter microdots. Height (left) and 3D view (right) of the micropatterns.

Table 2.1 Designed and measured dimensions of the circular micropatterns with various spreading area. Data represents the mean ± SD (n=3).

Designed diameter (µm)	Measured diameter (µm)	Measured thickness (nm)
20	19.88 ± 0.73	59.66 ± 0.48
40	40.44 ± 0.20	62.92 ± 0.81
60	60.26 ± 0.39	65.40 ± 0.67
80	80.04 ± 0.24	67.98 ± 0.82

Human bone marrow-derived MSCs are usually isolated primarily by their tight adherence to plastic culture dishes which will cause the initial heterogeneity [19]. In order to get the homogeneous cell mass, purification of human MSCs was processed based on clonal culture. The initial state of purified MSCs was checked by immunofluorescence staining. The cells expressed CD73, CD105, CD44, CD106 and STRO-1 surface markers which are commonly used to identify MSCs (Figure 2.6) while lacked expression of CD11b, CD19, CD34 and CD45 (Figure 2.7) [20-22]. The purified homogeneous MSCs were used for culture on the micropatterns. The MSCs attached onto the PSt micropatterns and their morphologies were controlled by underlying polystyrene surfaces (Figure 2.8). Single MSCs arrays with different cellular size, geometry and aspect ratio were formed.

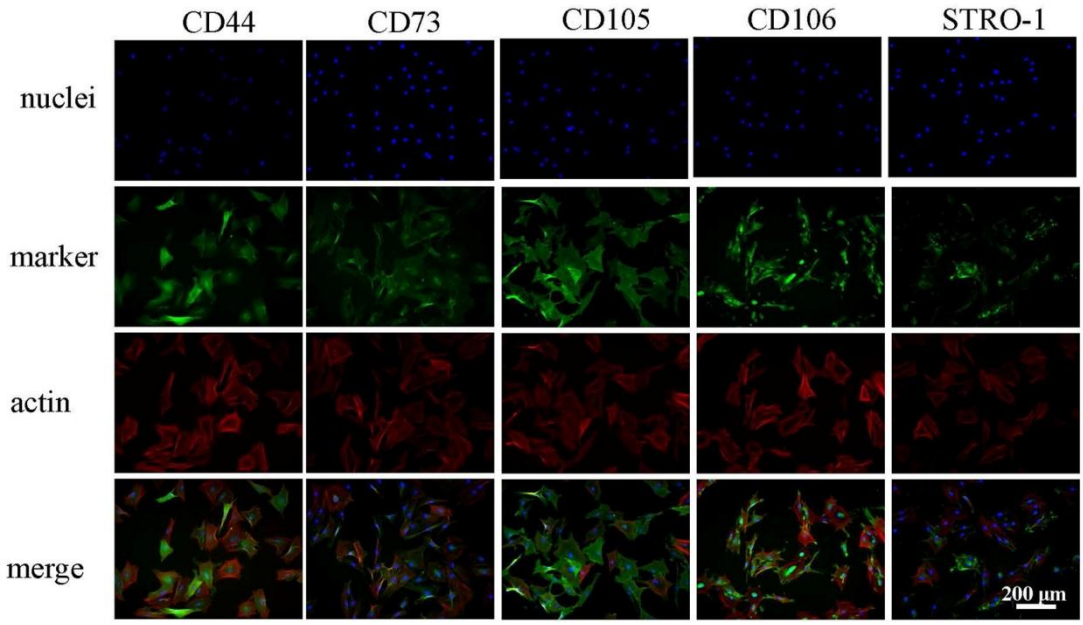

Figure 2.6 Immunofluorescence staining of the positive markers on the purified MSCs after 6 h culture in culture dish. Nuclei (blue), surface markers (green) and F-actin (red) were stained. The purified MSCs were positive for CD44, CD73, CD105,CD106 and STRO-1.

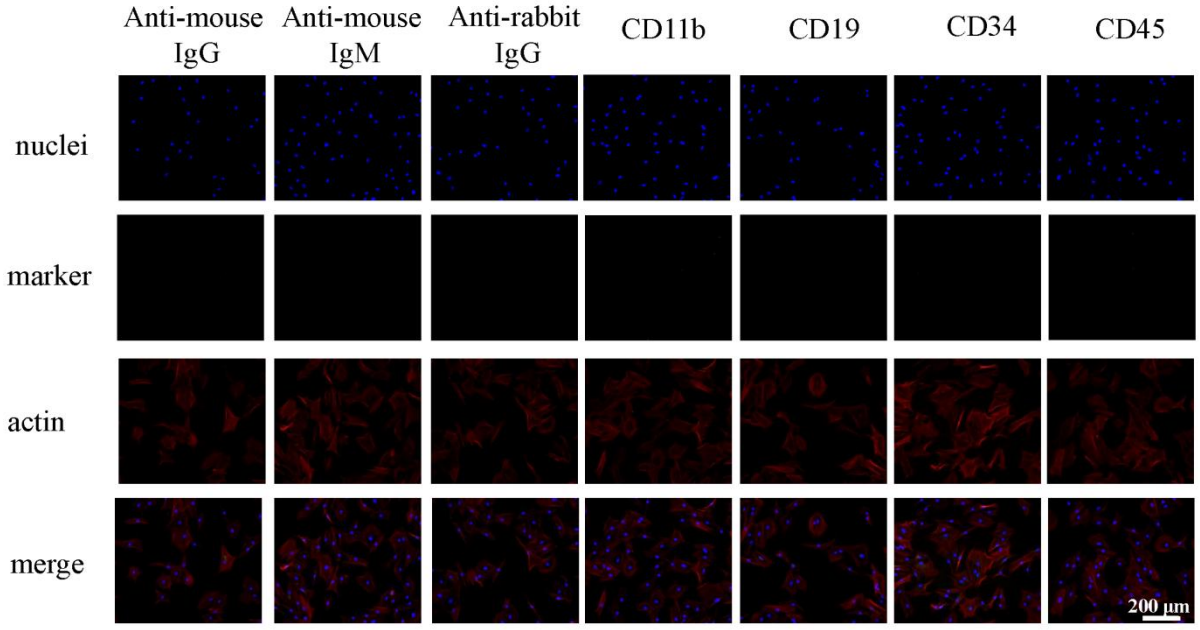

Figure 2.7 Immunofluorescence staining of the negative markers on the purified MSCs after 6 h culture in culture dish. Staining with only second antibodies without primary antibodies were conducted as controls. Nuclei (blue), surface markers (green) and F-actin (red) were stained. The purified MSCs were negative for CD11b, CD19, CD34 and CD45 in accordance with the criteria.

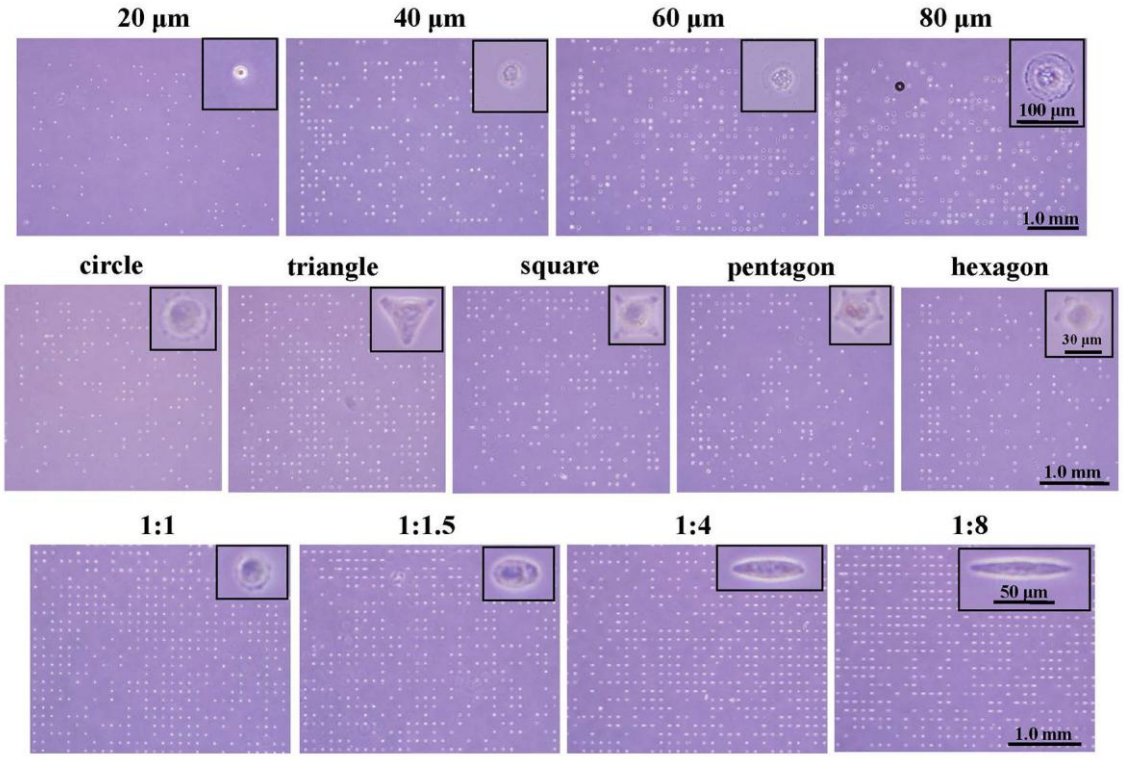

Figure 2.8 Phase-contrast images of single MSCs attached on the micropatterns with different size (up), geometry (middle) and aspect ratio (down). Insert images are the high miganification of typical micropatterned cells with different morphology.

2.4.2 Influence of cell morphology on stemness maintenance of MSCs

After MSCs were cultured on the micropatterns for 2 weeks, the stemness of MSCs was analyzed by expression of surface markers of CD44, CD73, CD105, CD106 and STRO-1. Each surface marker was stained and the percentage of positive stained cells was counted to quantify the influence of micropatterns on stemness variation of MSCs. The expression of CD44, CD73, CD105, CD106 and STRO-1 gradually decreased with increase of spreading area (Figure 2.9). MSCs cultured on the micropatterns with different geometry expressed similar level of CD44, CD73, CD105, CD106 and STRO-1 (Figure 2.10). The expression of CD44, CD73, CD105, CD106 and STRO-1 decreased slightly with increase of aspect ratio. Round cells (AR=1) exhibited significantly higher expression of CD44, CD73, CD105 and CD106 compared to the cells with aspect ratio of 8 or 4 (Figure 2.11). The results indicated that the size and aspect ratio of single cell could affect the stemness of MSCs, while shape showed no influence on stemness of MSCs when spreading was limited. Small size and low aspect ratio were good for the maintenance of MSCs stemness.

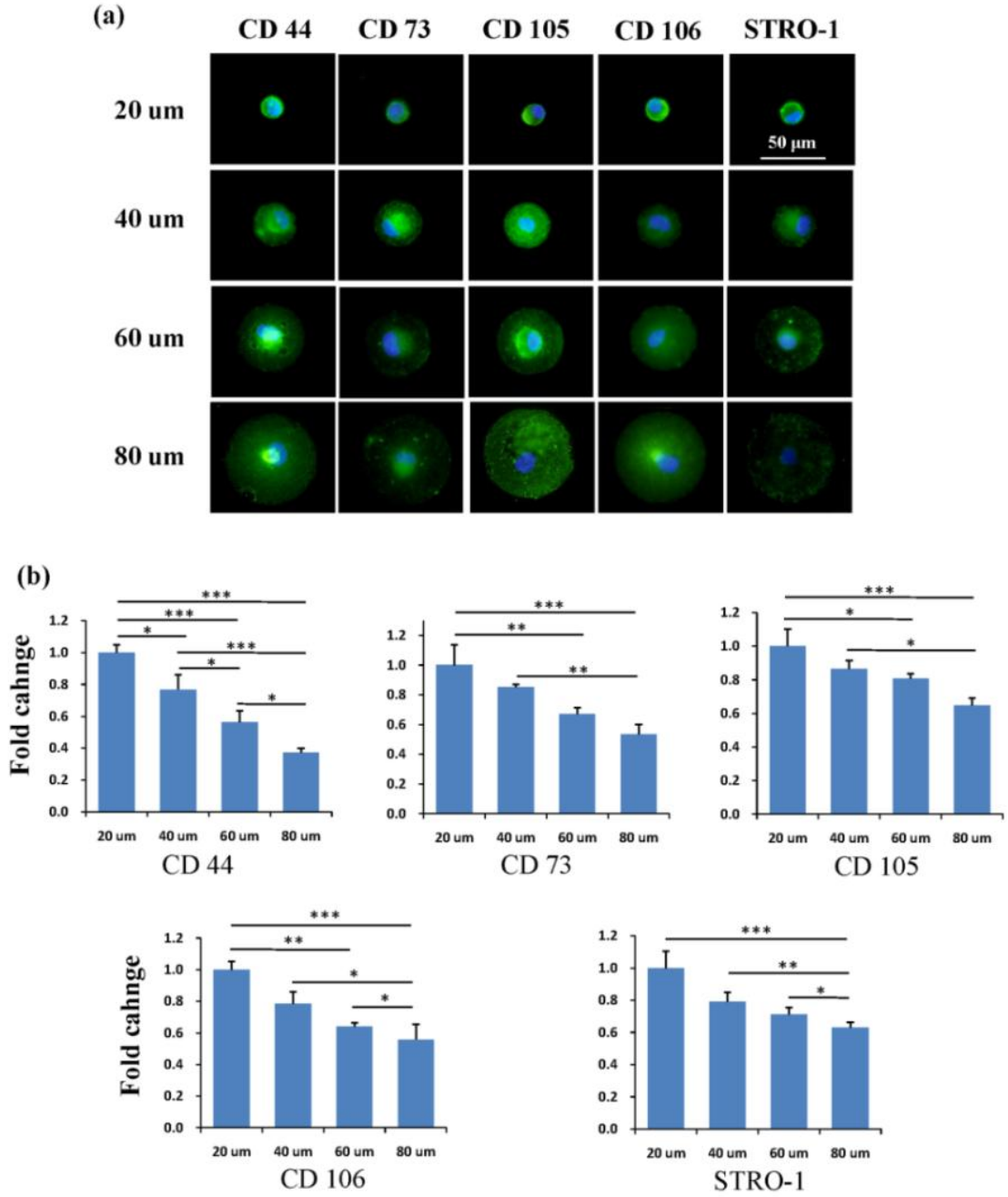

Figure 2.9 Influence of spreading area on expression of surface markers of single MSCs. (a) Representative positively stained MSCs with various spreading area. Nuclei were stained by DPAI (blue) to distinguish single cell from multiple cells. Surface marker was stained (green) to quantify the percentage of positively stained cells to indicate the stemness of MSCs. Small micropatterned cells exhibited higher expression of CD44, CD73, CD105, CD106 and STRO-1 than large one. (b) In general, the number of positively stained cells decreased with the increase of spreading area indicating loss of multipotency of MSCs. The data are represented as the mean ± SD, n > 120. * $p < 0.05$, ** $p < 0.01$ and *** $p < 0.001$.

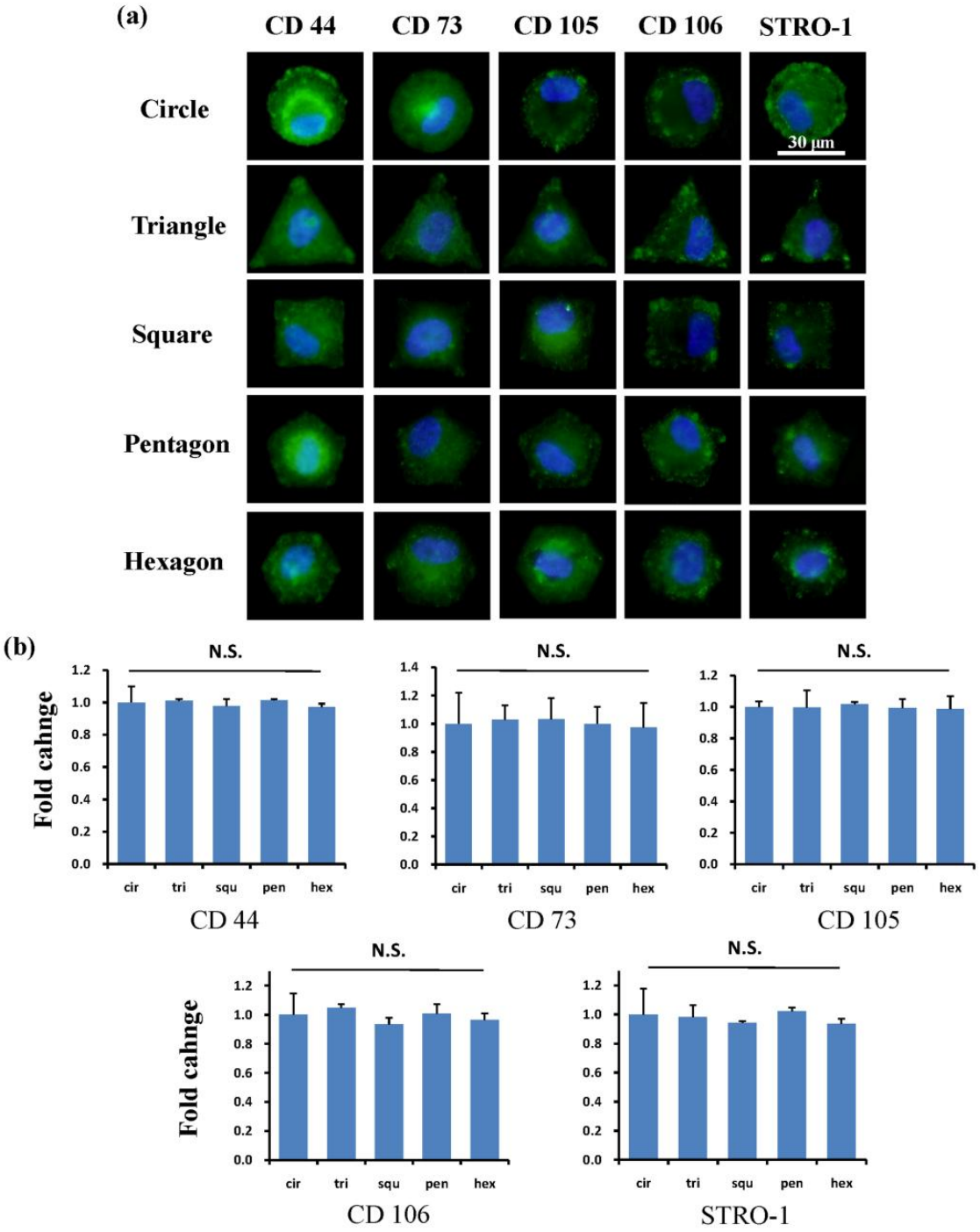

Figure 2.10 Influence of cell geometry on expression of surface markers of single MSCs. (a) Representative positively stained MSCs with various geometries. (b) Cells assembled strong stress fibers at cell edge while cell central part remained disordered. There was no significant difference of expression of surface makers among cells with different geometries. The data are represented as the mean ± SD, n > 120. N.S. means no significant difference.

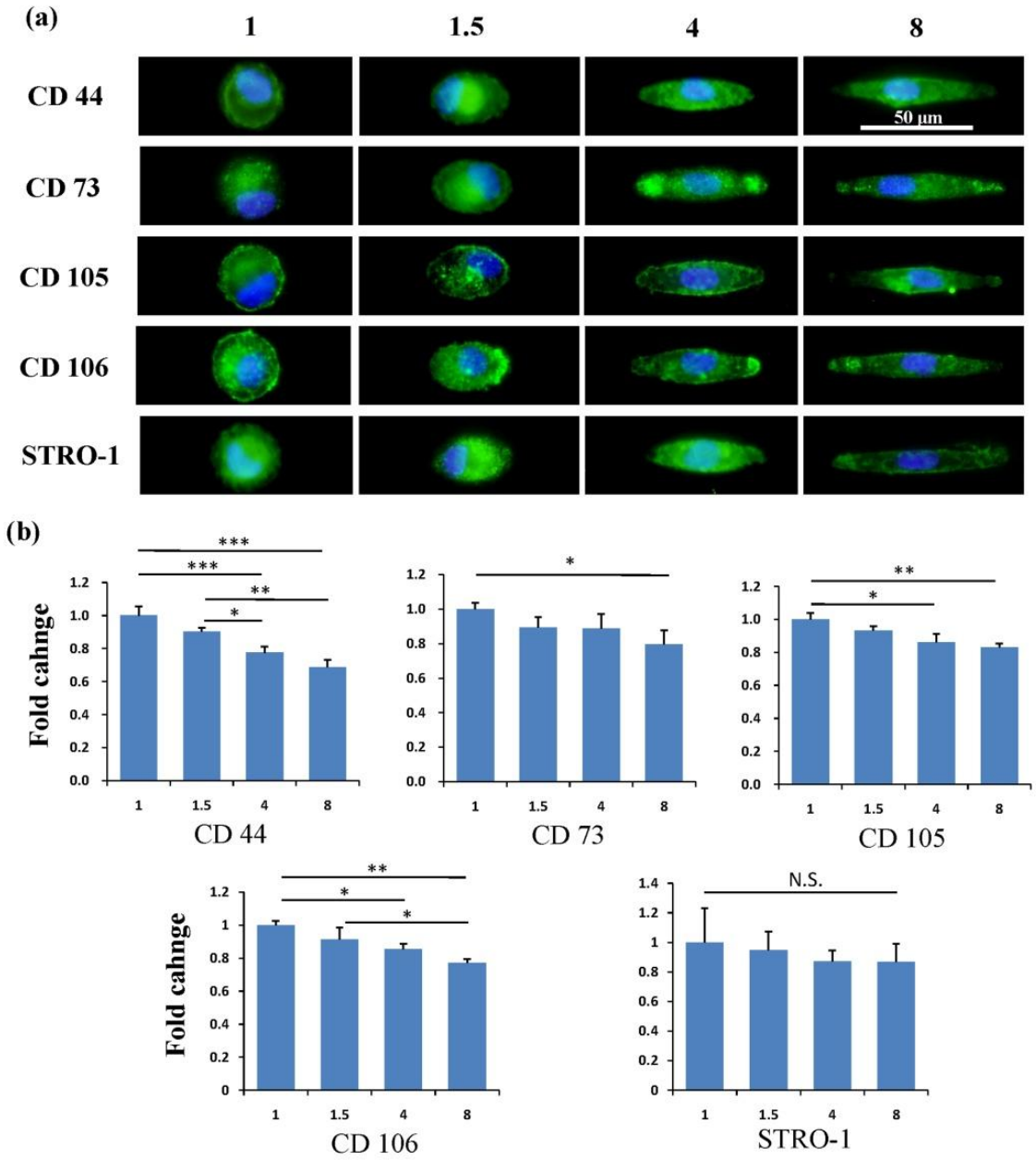

Figure 2.11 Influence of aspect ratio on expression of surface markers of single MSCs. (a) Representative positively stained MSCs with various aspect ratios. (b) Elongation of cell morphology leaded to pronounced nuclear deformation. Elongated cells had lower expression of surface molecules than circular cells. The data are represented as the mean ± SD, n > 120. N.S. means no significant difference, * $p < 0.05$, ** $p < 0.01$, *** $p < 0.001$.

2.4.3 Nuclear activity of MSCs on micropatterns

In vivo, stem cells are quiescent with low activity of nucleus and metabolism which endow them superior long-term reconstitution potential [23]. And growing evidences suggest that stem cells in a quiescent state are prone to maintain their multipotency [24,25]. Thus it was thought that the micropatterns might also affect the stemness through regulation of cell quiescence. To detect the influence of micropatterns on cell

quiescence, BrdU staining which reflects the DNA synthesis of the cells was performed (Figure 2.12a). The results suggested that spreading area had a significant influence on nuclear activity. With the increase of spreading area, more active nuclei were detected on the micropatterns (Figure 2.12b). However, the cells cultured on micropatterns with different geometries but same spreading area did not show significant difference of BrdU staining (Figure 2.12c). Elongation of cells with the same spreading area resulted in gradual enhancement of nuclear activity. When aspect ratio reached to 8, the cells had significantly higher nuclear activity than the round (AR = 1) or ellipse (AR = 1.5) cells (Figure 2.12d). Therefore, it was concluded that single MSC with small size or low aspect ratio preferred to keep a quiescent state with low nuclear activity which contributed to the maintenance of MSCs stemness.

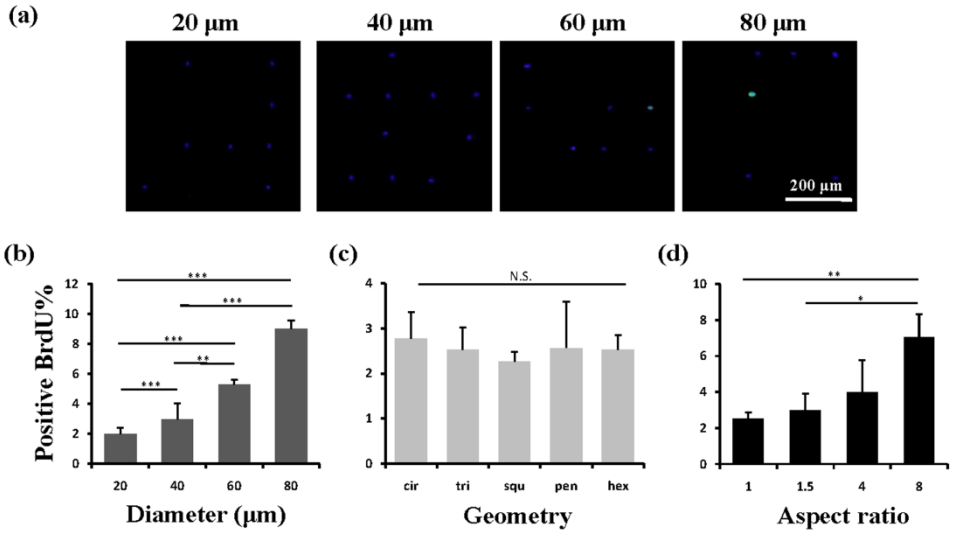

Figure 2.12 Nuclear activity of MSCs evaluated by BrdU staining. (a) Staining images of cell nuclei cultured on circular micropattrens with a diameter of 20, 40, 60 and 80 μm. Quiescent nuclei were stained by DAPI (blue) and activate nuclei were stained by anti-BrdU (green). (b) With the increase of spreading area, the nuclear activity increased. (c) Cells with various geometries had similar nuclear activity. (d) More positively stained nuclei were found in elongated cells. The data are represented as the mean ± SD, n > 120. N.S. means no significant difference, * $p < 0.05$, ** $p < 0.01$, *** $p < 0.001$.

2.4.4 Influence of cytoskeleton on cell mechanics

The next question is how the micropatterns modulated nuclear activity. Previous study showed that cells responded to biophysical stimuli through reorganization of cytoskeleton [26]. F-actin filaments can bind to the nuclear envelope anchoring proteins and generate force to the nucleus to influence its state [27]. Therefore, we thought that the micropatterns should regulate the cytoskeleton and influence the cell mechanical state which activated or passivated nuclear activity and finally determined the stemness of MSCs. To confirm this hypothesis, we firstly investigated the cytoskeleton architecture of single MSCs arrays on the micropatterns from their F-actin staining images. The F-actin structure of single MSCs was significantly influenced by spreading area (Figure 2.13a). The circular cells with large spreading area assembled their actin filaments in both radial and concentric directions of the circle. With the decrease of spreading area, the radial filaments gradually disappeared and the concentric filaments only assembled at cell periphery. MSCs cultured on the micropatterns with different geometries showed similar actin organization (Figure 2.13b). The micropatterned cells predominately assembled their actin filaments at the periphery of the cells and the

formed stress fibers stretched along the edges of micropatterns, while no ordered filament structure was found at the central region of cells. Aspect ratio showed significant effect on F-actin structures. Unlike in circular cells, actin filaments in elongated cells were parallel along the long axis of the cell and spanned over the nucleus (Figure 2.13c). Not only the cytoskeleton, the nuclear geometry was also elongated dramatically with increase of aspect ratio and oriented towards the direction of long cell axis.

Cell mechanics which depends on cytoskeleton structure was then measured by AFM nanoindentation. The AFM measurement of each cell was finished within 1 h to guarantee the cell viability and all the cells attached on the micropatterns were alive after the measurement. The obtained force curves were used to calculate the Young's modulus of cells according to Hertz's model. The final Young's modulus value was determined by fitting the Gaussian function to the histogram created from all the collected data (Figure 2.14). The center of the fitting curve represented the average value of the Young's modulus and the half width at the half height was the standard deviation. The histogram became wider with the increase of spreading area but showed similar shape for the cells with various geometries and aspect ratios. Table 2 shows the obtained Young's modulus of MSCs. The results indicated that Young's modulus of MSCs was regulated by their F-actin structure which assembled according to the micropattens. MSCs with large spreading area formed more stress fibers which assembled in radial and concentric directions of the circle. The highly ordered actin structure resulted in a higher elasticity of the cells. With the decrease of spreading area, cells became soft. While for cells having different geometries but same spreading area, they showed similar Young's modulus. The parallel stress fibers formed in elongated cells also increased the Young's modulus of MSCs.

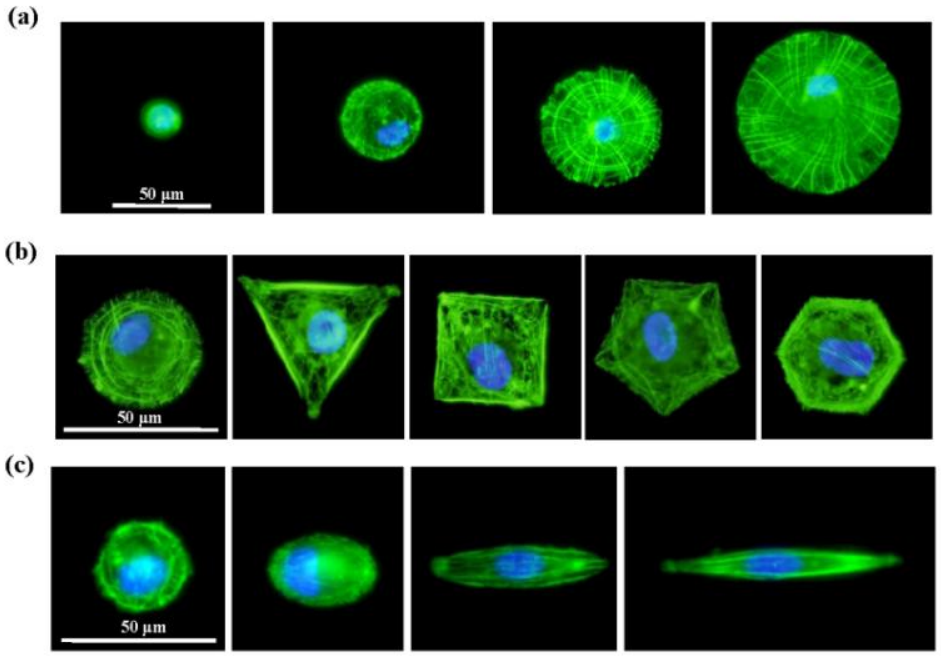

Figure 2.13 F-actin staining of MSCs cultured on micropatterns with various spreading areas (a), geometries (b) and aspect ratios (c). (a) MSCs cultured on circular micropatterns with large spreading area exhibited highly ordered actin network. With the decrease of spreading area, the actin filaments were weakened and became randomly orientated. (b) Cells with different geometries formed strong stress fibers at cell edge, while disrupt actin assembly observed at cell center. (c) With the increase of aspect ratio, MSCs formed straight stress fibers along the long axis of cells.

Table 2. Young's modulus of living MSCs cultured on different micropatterns.

Diameter	E (kPa)	Geometry	E (kPa)	Aspect ratio	E (kPa)
20 μm	0.82 ± 0.65	circle	0.96 ± 0.61	1	0.89 ± 0.60
40 μm	0.99 ± 0.71	triangle	0.97 ± 0.64	1.5	0.93 ± 0.65
60 μm	1.22 ± 0.65	square	0.95 ± 0.63	4	1.16 ± 0.68
80 μm	1.38 ± 0.94	pentagon	0.97 ± 0.59	8	1.23 ± 0.69
		hexagon	0.96 ± 0.64		

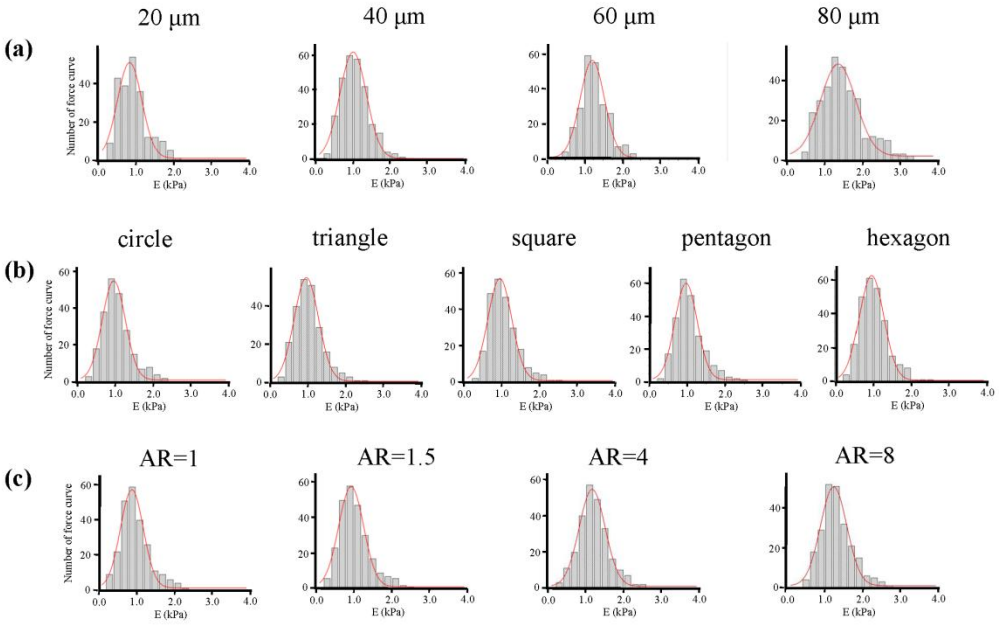

Figure 2.14 Histogram of the value of Young's modulus with Gaussian fittings obtained for MSCs cultured on micropatterns with various (a) spreading areas, (b) geometries and (c) aspect ratios. The data were obtained at 200 nm indentation depths. Bin size: 0.2 kPa (n > 200).

2.5 Discussion

Maintenance of multipotency of stem cells is becoming an attractive topic and various methods have been used to investigate the self-renewal of stem cells. A recent study reported that long time culture of MSCs on a hard unpatterned surface would cause a irreversible effects on stem cell fate by activating YAP and RUNX2 in nucleus [28]. The mechanical dosing effects reminding us that it would be difficult to preserve multipotency of stem cells only use conventional tissue culture plates. In this study, micropatterns with different sizes, geometries and aspect ratios were used for culture of MSCs at single cell level to investigate how these physical cues affect the stemness of stem cells and cytoskeleton change. After two weeks culture on the micropatterns, the expression of CD44, CD73, CD105, CD106 and STRO-1 decreased with increase of spreading area and aspect ratio of MSCs, while kept at similar level in cells with different geometry.

The nuclear activity of the micropatterned cells increased with the increase of spreading area. It is well agreed that spreading area as a crucial parameter of the nuclear deformation process can enhance cell

proliferation. Increasing in spreading area leads to the enlargement of nucleus which activates DNA synthesis [29]. Meanwhile, cells need to maintain an intact actin cytoskeleton which increases cell contraction at the critical time point in the late G1 phase of cell cycle to enter S phase [30]. The ordered actin structure observed in large cells could fulfil this requirement. When being cultured on the micropatterns of different aspect ratios, the elongated cells assembled their parallel actin filaments throughout the cells. And the perinuclear actin filaments formed a cap which has been reported to stimulate cell proliferation [31-33]. On the other hand, the non-elongated cells only assembled their actin filaments at cell periphery. There were few actin filaments at the perinuclear space. Therefore, no nuclear deformation was observed. MSCs on the micropatterns with different geometries had limited spreading area. The cells exhibited similar disrupt actin structure at perinuclear region although they formed intensive stress fibers at cell edge. The results indicated that the cytoskeletal structure might be an important factor for regulation of cell quiescence which contributes to keeping stem cell phenotype.

The cellular tension which depends on cytoskeletal organization is also important for maintenance of multipotency of stem cells. Previous study reported that round ESCs exhibited higher expression of Oct4 and Nanog than flattened ones due to the weak membrane-cytoskeleton linkages [34]. And limited spreading area was revealed to be beneficial for the maintenance of undifferentiated state of ESCs [35]. Human induced pluripotent stem cells (iPSCs) with weak stress fibers were Oct3/4 positive while those formed pronounced stress fibers became Oct3/4 negative [36]. For MSCs, undifferentiated cells were found to have low contractility compared to osteogenic differentiated cells, indicating the low cytoskeletal tension was required to maintain the multipotency [37]. In this study, the elasticity of MSCs cultured on the micropatterns increased with cellular enlargement which was in good accordance with previous work [28]. Similarly, the parallel stress fibers formed in elongated cells also enhanced the elasticity of MSCs. MSCs with different geometries showed disrupt actin structure at cell center, which leaded to low elasticity. Combined with the staining results, high elasticity of MSCs was always accompanied with low expression of surface molecules suggesting partial loss of multipotency.

2.6 Conclusions

In summary, the cell morphogenesis was well controlled by the PSt micropatterns with different size, geometry and aspect ratio. MSCs on the micropatterns showed different expression level of stem cell surface markers, and accompanied with different nuclear activity, cytoskeletal structure and nanomechanics. The micropatterns should directly affect cytoskeletal structures. The resulting cytoskeletal structure could determine cellular nanomechanics, nuclear activity and stemness of MSCs. Large spreading area and high aspect ratio leaded cells to a stressed state with active nuclear synthesis, and therefore resulted in low expression of stem cell surface markers. When spreading area was limited, changes in cell geometries did not influence cell elasticity and nuclear activity. Ordered cytoskeletal structure resulted in high cell elasticity and nuclear activity and decreased the expression of surface markers indicating partial loss of multipotency. MSCs with disrupt cytoskeletal structure exhibited low nanomechanical properties and retained in a quiescent state which promoted stem cell phenotype.

2.7 References

[1] Barry FP, Murphy JM. Mesenchymal stem cells: clinical applications and biological characterization. The International Journal of Biochemistry & Cell Biololgy. 2004;36:568–84.
[2] Pittenger MF. Multilineage Potential of Adult Human Mesenchymal Stem Cells. Science. 1999;284:143–47.
[3] McBeath R, Pirone DM, Nelson CM, Bhadriraju K, Chen CS. Cell shape, cytoskeletal tension, and RhoA regulate stem cell lineage commitment. Developmental Cell. 2004;6:483–95.
[4] Dalby MJ, Gadegaard N, Tare R, Andar A, Riehle MO, Herzyk P, et al. The control of human mesenchymal cell differentiation using nanoscale symmetry and disorder. Nature Materials. 2007;6:997–1003.
[5] Lutolf MP, Gilbert PM, Blau HM. Designing materials to direct stem-cell fate. Nature. 2009;462:433–41.
[6] Kunisaki Y, Bruns I, Scheiermann C, Ahmed J, Pinho S, Zhang D, et al. Arteriolar niches maintain haematopoietic stem cell quiescence. Nature. 2013;502:637–43.
[7] Bonab MM, Alimoghaddam K, Talebian F, Ghaffari SH, Nikbin B. Aging of mesenchymal stem cell *in vitro*. BMC Cell Biololgy. 2006;7:14-21.
[8] McMurray RJ, Gadegaard N, Tsimbouri PM, Burgess KV, McNamara LE, Tare R, et al. Nanoscale surfaces for the long-term maintenance of mesenchymal stem cell phenotype and multipotency. Nature Materials. 2011;10:637-44.
[9] Rustad KC, Wong VW, Sorkin M, Glotzbach JP, Major MR, Rajadas J, et al. Enhancement of mesenchymal stem cell angiogenic capacity and stemness by a biomimetic hydrogel scaffold. Biomaterials. 2012;33:80-90.
[10] Gerecht S, Burdick J, Ferreira LS, Townsend S, Langer R, Vunjak-Novakovic G, et al. Hyaluronic acid hydrogel for controlled self-renewal and differentiation of human embryonic stem cells. Proceedings of the National Academy of Sciences. 2007;104:11298–303.
[11] Gilbert PM, Havenstrite KL, Magnusson KEG, Sacco a, Leonardi N a, Kraft P, et al. Substrate elasticity regulates skeletal muscle stem cell self-renewal in culture. Science. 2010;329:1078–81.
[12] Wen JH, Vincent LG, Fuhrmann A, Choi YS, Hribar KC, Taylor-Weiner H, et al. Interplay of matrix stiffness and protein tethering in stem cell differentiation. Nature Materials. 2014;13:979-987.
[13] Wang PY, Lee HH, Higuchi A, Ling QD, Lin HR, Li HF, et al. Pluripotency maintenance of amniotic fluid-derived stem cells cultured on biomaterials. Journal of Materials Chemistry B. 2015;3:3858-3869.
[14] Thery M. Micropatterning as a tool to decipher cell morphogenesis and functions. Journal of Cell Science. 2010;123:4201.
[15] Wang X, Song W, Kawazoe N, Chen G. The osteogenic differentiation of mesenchymal stem cells by controlled cell-cell interaction on micropatterned surfaces. Journal of Biomedical Materials Research Part A. 2013;101:3388–95.
[16] Wang X, Song W, Kawazoe N, Chen G. Influence of cell protrusion and spreading on adipogenic differentiation of mesenchymal stem cells on micropatterned surfaces. Soft Matter. 2013;9:4160-4166.
[17] Ohler B. Cantilever spring constant calibration using laser Doppler vibrometry. Review of Scientific Instruments. 2007;78:063701.
[18] Costa KD. Single-cell elastography: probing for disease with the atomic force microscope. Disease Markers. 2004;19:139–54.
[19] Zhang S, Jia Z, Ge J, Gong L, Ma Y, Li T, et al. Purified human bone marrow multipotent mesenchymal stem cells regenerate infarcted myocardium in experimental rats. Cell Transplantation. 2005;14:787–98.
[20] Dominici M, Le Blanc K, Mueller I, Slaper-Cortenbach I, Marini F, Krause D, et al. Minimal criteria for defining multipotent mesenchymal stromal cells. The International Society for Cellular Therapy position

statement. Cytotherapy 2006;8:315–7.
[21] Majumdar MK, Keane-Moore M, Buyaner D, Hardy WB, Moorman M a, McIntosh KR, et al. Characterization and functionality of cell surface molecules on human mesenchymal stem cells. Journal of Biomedical Science. 2003;10:228–41.
[22] Docheva D, Haasters F, Schieker M. Mesenchymal stem cells and their cell surface receptors. Current Rheumatology Reviews. 2008;4:155–60.
[23] Li L, Clevers H. Coexistence of quiescent and active adult stem cells in mammals. Science. 2010;327:542–5.
[24] Osawa M, Egawa G, Mak S-S, Moriyama M, Freter R, Yonetani S, et al. Molecular characterization of melanocyte stem cells in their niche. Development. 2005;132:5589–99.
[25] Winer JP, Janmey P a, McCormick ME, Funaki M. Bone marrow-derived human mesenchymal stem cells become quiescent on soft substrates but remain responsive to chemical or mechanical stimuli. Tissue Engineering Part A. 2009;15:147–54.
[26] Engler AJ, Sen S, Sweeney HL, Discher DE. Matrix elasticity directs stem cell lineage specification. Cell. 2006;126:677–89.
[27] Dahl KN, Ribeiro AJS, Lammerding J. Nuclear shape, mechanics, and mechanotransduction. Circulation Research. 2008;102:1307–18.
[28] Yang C, Tibbitt MW, Basta L, Anseth KS. Mechanical memory and dosing influence stem cell fate. Nature Materials. 2014;13:645-652.
[29] Roca-Cusachs P, Alcaraz J, Sunyer R, Samitier J, Farré R, Navajas D. Micropatterning of single endothelial cell shape reveals a tight coupling between nuclear volume in G1 and proliferation. Biophysical Journal. 2008;94:4984–95.
[30] Mammoto A, Huang S, Moore K, Oh P, Ingber DE. Role of RhoA, mDia, and ROCK in cell shape-dependent control of the Skp2-p27kip1 pathway and the G1/S transition. Journal of Biological Chemistry. 2004;279:26323–30.
[31] Khatau SB, Hale CM, Stewart-Hutchinson PJ, Patel MS, Stewart CL, Searson PC, et al. A perinuclear actin cap regulates nuclear shape. Proceedings of the National Academy of Sciences. 2009;106:19017–22.
[32] Li Q, Kumar A, Makhija E, Shivashankar G V. The regulation of dynamic mechanical coupling between actin cytoskeleton and nucleus by matrix geometry. Biomaterials. 2014;35:961–9.
[33] Kurpinski K, Chu J, Hashi C, Li S. Anisotropic mechanosensing by mesenchymal stem cells. Proceedings of the National Academy of Sciences. 2006;103:16095–100.
[34] Veraitch F. Precisely delivered nanomechanical forces induce blebbing in undifferentiated mouse embryonic stem cells. Cell Health Cytoskeleton. 2011;3:23-34.
[35] Bae D, Moon S-H, Park BG, Park S-J, Jung T, Kim JS, et al. Nanotopographical control for maintaining undifferentiated human embryonic stem cell colonies in feeder free conditions. Biomaterials. 2014;35:916–28.
[36] Kim M-H, Kino-Oka M. Switching between self-renewal and lineage commitment of human induced pluripotent stem cells via cell-substrate and cell-cell interactions on a dendrimer-immobilized surface. Biomaterials. 2014;35:5670–8
[37] Tsimbouri PM, McMurray RJ, Burgess K V, Alakpa E V, Reynolds PM, Murawski K, et al. Using nanotopography and metabolomics to identify biochemical effectors of multipotency. ACS Nano. 2012;6:10239–49.

Chapter 3

Regulation of single cell nanomechanics on micropatterns

3.1 Summary

In this chapter, the micropatterned surfaces with various sizes were prepared using photolithographic micropatterning of photo-reactive poly(vinyl alcohol) on cell-culture polystyrene plates to provide controllable and reproducible cell morphology. The nanomechanics of stem cells, normal cells and cancer cells were compared on the micropatterned surfaces. The three types of cells showed different responses and nanomechanics on the micropatterned surfaces. Especially, cancer cells showed less dependence on their microenvironments compared to the stem cells and normal cells. The results suggest that the nanomechanical differences between normal and cancer cells can be used as a biomarker to enhance the diagnosis of cancers. The use of micropatterns should be a very useful technique to compare the nanomechanics of cells.

3.2 Introduction

Since developed, micropatterning technology has been widely used in various fields. Recent applications of micropatterns in biomedical researches enable manipulation of cytoskeletal structures by restraining cells in a controlled size and geometry, which plays crucial role in regulating cell spatial and mechanical functions [1-2]. Micropatterned surfaces with various geometrical features can provide controllable and reproducible cell morphology with relatively stable cytoskeletal structure which cannot be fulfilled with conventional uniform cell culture substrates [3]. The quantitative description of the influence of subcellular structures can also be achieved on micropatterns without the influence caused by the diversity of cell morphology [4]. Therefore, systematical investigation of cell nanomechanics on micropatterned surfaces is required to elucidate the relationship between nanomechanics and subcellular structures.

Several techniques have been developed to measure the nanomechanical properties of individual cells such as magnetic twisting cytometry (MTC), micropipette aspiration (MA), optical stretcher (OS), traction force microscopy (TFM) and atomic force microscopy (AFM) [5-12]. Compared with the other techniques, AFM has the highest spatial resolution and the largest force range. It was proved to be one of the least invasive techniques for nanomechanical measurement of cells. In this study, we prepared micropatterns

with various sizes using UV photolithography. The nanomechanical properties of the major osteosarcoma microenvironment cells (NHOst, MSCs and MG-63) were compared on micropatterned surfaces. These three types of cells represent the normal somatic cells, stem cells and cancer cells, respectively. The influence of cytoskeletal organization regulated by micropatterns on cell stiffness and non-specific adhesion was investigated using AFM nanoindentation. The results of this study should inspire the development of the novel way for cancer diagnosis and therapy, and provide information to reveal how the nanomechanics of individual cells can be manipulated by their surrounding microenvironment.

3.3 Materials and methods

3.3.1 Preparation and characterization of the PVA micropatterned TCPS surfaces

The synthesis process of photo-reactive PVA, preparation scheme of the PVA micropatterned TCPS surfaces and AFM scanning of the micropatterns were performed in the same way as described in Chapter 2.3.2.

3.3.2 Cell culture

Human bone marrow-derived mesenchymal stem cells (MSCs) and normal human osteoblast cells (NHOst) were purchased from Lonza Walkersville, Inc. (Walkersville, MD) and subcultured using their growth medium got from the same company. MG-63 cells were acquired from Japanese Collection of Research Bioresources (JCRB) Cell Bank (Osaka, Japan) and subcultured using minimum essential medium eagle (EMEM, Sigma) supplemented with 10% fetal bovine serum (FBS), 2 mM glutamine and 1% non essential amino acids (NEAA). Prior to use, the micropatterns were sterilized with 70% ethanol followed by exhaustive Milli-Q rinsing. The micropatterns were put in 6-well cell culture plates and a glass ring was placed over each PVA-micropatterned polystyrene plate. A 3 mL aliquot of growth medium was added to each well and 200 μl cell suspension solution (2.7×10^3 cells/ml) was added within the glass ring (3000 cells/cm^2). After 6 h, the glass rings were taken out and the unattached cells were removed by changing medium. After 24 h, cells were washed with warm PBS and then merged in HEPES medium and directly used for AFM indentation or cell migration assay. HEPES was reported to have better capability at maintaining physiological pH compared to bicarbonate buffer which was commonly used in commercially available medium [13]. The medium was composed of 13.4 g/L DMEM powder (Sigma) and 20 mM HEPES (Sigma). The pH value of the medium was adjusted to 7.2 using NaOH solution. HEPES can maintain the pH value of the medium at 7.2 after exposure to 5% CO_2 atmosphere or air in 2 h. Meanwhile, the HEPES medium was serum free which can exclude the influence of serum protein on measurement of non-specific adhesion force and cell migration. To disrupt actin structure, 0.2 μg/ml cytochalasin D (Sigma) in growth medium was applied to cells after 6 h post-seeding. After incubation for another 18 h, cytochalasin D containing medium was replaced with HEPES medium and the cytochalasin D treated cells were used for AFM nanoindentation.

3.3.3 Immunofluorescence staining

Cells were fixed with 4% paraformaldehyde after incubation for 24 h. For F-actin staining, cells

were permeabilized with 0.2% Triton X-100 for 2 min and blocked with 2% bovine serum albumin (BSA) solution for 30 min followed by PBS washing. Actin filaments were stained with either Alexa Fluor-488 or Alexa Fluor-594 phalloidin (1:40, Invitrogen) for 20 min. Nuclei were stained with DAPI. To stain phosphoezrin, cells were permeabilized with 0.2% Triton X-100 for 2 min and blocked with 2% BSA solution for 30 min followed by PBS washing. Primary phosphoezrin antibody (Cell Signaling Technology) was diluted in 1% BSA solution (1:500). The samples were incubated with the diluted primary antibody at room temperature for 1.5 h and washed with PBS for three times. Secondary antibody (donkey anti-rabbit IgG, 1:1000) labeling was performed at room temperature for 1 h. For visualization of vinculin, cells were permeabilized with 1% Triton X-100 and 0.02% Tween-20. After PBS washing, the samples were blocked with 2% BSA in PBS solution for 30 min at room temperature. The samples were incubated with the diluted primary antibodies (1:100 in Can Get Signal solution) at 37 °C for 1.5 h and washed with 0.02% Tween-20 for three times. Secondary antibody (1:500) was diluted in Can Get Signal solution and the labeling was performed at 37 °C for 1 h followed by PBS washing. Fluorescence micrographs of the stained cells were captured using an Olympus BX51 microscope with a DP-70 CCD camera (Olympus, Tokyo, Japan).

3.3.4 Nanomechanics measurement by atomic force microscopy

The nanomechanical properties of living NHOst, MSCs and MG-63 cells were measured using a commercially available MFP-3D-BIO AFM instrument in a contact mode. An optical microscope was used to visualize the samples and the position of the AFM tip. Each measurement was performed within a maximum of 1.5 h to minimize the influence on cells during the experiment. To perform the nanoindentation, a silicon nitride cantilever (Novascan, Ames, USA) coated with reflective gold were used for force curve detection. The exact spring constant of the cantilever was measured before each set of experiment using the thermal tuning method [14]. The cantilever has a silica glass ball with a diameter of 600 nm attached to the end as the probe. The indentation rate was 4 μm/s and the trigger force was set to 2 nN to avoid any damage to the cell surface. The AFM indentation was performed at the highest part of cells (usually cell center). Ten force curves were collected on each cell to decrease cell damage. To acquire the non-specific adhesion force, the tip was set to dwell on cell membrane for 30 s. In order to correlate cell surface to its nanomechanical property, membrane roughness of micropatterned cells was recorded using AFM scanning. To process the scanning, a cantilever with spring constant of 0.06 N/m was used to reduce the damage of cell during scanning. There is a conical tip at the end of the cantilever with radius of 20 nm which can provide high resolution scanning images. The scanning rate was set to 0.5 Hz and the set point was 0.8 V. The scan size was 90 × 90 μm^2. The height and deflection images of 20 micropatterned cells were recorded to evaluate the membrane roughness of cells.

The force curves were fitted to Hertz's contact model to calculate the Young's modulus of cells. The ten force curves acquired from the same cell were used to calculate the average rigidity of the single cell. And the average Young's modulus of 20 single cells was calculated to represent the stiffness of the cells on the same micropattern. According to the probe geometry, parabolic model was used and the formula is given by:

$$F(\delta) = \frac{4}{3} \cdot \sqrt{R} \cdot E_r \cdot \delta^{3/2} \qquad (1)$$

where F is the loading force, R is the radius of the tip, Er is the reduced Young's modulus and δ is the indentation depth. In this study, the Young's Modulus was calculated at indentation depth of 200 nm which

has been reported to be the region rich in actin network [15]. The reduced Young's modulus Er correlates with the Young's modulus of sample Es and is given by:

$$\frac{1}{E_r} = \frac{1-\nu_t^2}{E_t} + \frac{1-\nu_s^2}{E_s} \qquad (2)$$

where ν_t and ν_s are the Poisson ratios of tips and samples. Since the Young's modulus of tips material (SiO_2) is much greater than that of living cells, equation (2) can be simplified as following:

$$E_r = \frac{E_s}{1-\nu_s^2} \qquad (3)$$

The Poisson ratio of sample is assumed to be 0.5 since cells can be treated as soft incompressible materials [16]. The maximum adhesion force was analyzed by Asylum Research data processing software Igor Pro 6.37.

3.3.5 Cell migration assay

Before migration, the number of adhering cells on each micropatterns was firstly counted according to the micrographs. The micropatterned TCPS plates with cells were moved to a new cell culture dish. A new TCPS plate (2.5 x 2.5 cm2) without micropattern, defined as transferring plate, was placed onto each micropatterned TCPS plates with adhering cells. 50 μl serum-free medium was added between the micropatterned plate and the transferring plate. This "contact transfer assay" was then put into incubator to induce the cell migration. A timelapse system (Olympus, Tokyo, Japan) was used to capture the migrating process. After 45 min incubation, the two plates were separated and the remaining cell number on micropatterned plate was counted again. Decrease of cell number was defined as the cells that moved from micropatterned plate to the plate without micropattern.

3.3.6 Statistical analysis

The data were presented as means ± standard deviations (SDs). Statistical analysis of surface roughness and cell migration percentage of micropatterned cells was performed using a one-way analysis of variance (ANOVA) with Tukey's post hoc test for multiple comparisons to confirm the significant differences among samples. And Student's t-test was used to compare the differences between cytochalasin D treated and untreated samples. A value of $p < 0.05$ was considered to indicate statistically significant difference.

3.4 Results and discussion

3.4.1 Preparation and observation of PVA-micropatterned surfaces

UV photolithography was used to prepare the micropatterned surfaces. Azidophenyl-derivatized photo-reactive poly(vinyl alcohol) (AzPhPVA) was synthesized as cell resistant material. It was immobilized to the tissue culture polystyrene (TCP) surfaces upon UV irradiation. A photomask containing microdots with various sizes (suitable for single cell) were designed to control the shape and spreading area of cells. The designed diameters of the microdots were 20, 40, 60 and 80 μm (Figure 3.1). The 3D images of the microdots were observed by AFM which can be used to detect their exact size and depth. According to the

analysis results, the diameters of the microdots were nearly the same as those of the designed photomasks indicating good controllability of this method. The thickness of the micropatterns could be adjusted by controlling the concentration of photo-reactive PVA solution. In this study, the thickness of PVA layer was around 60 nm that was effective to resist cell adhesion on PVA layer but did not influence cell attachment and spreading on TCP microdots. When cells were cultured on the micropatterned surfaces, the cells were constrained in the TCP microdots (Figure 3.2). MSCs and NHOst cells occupied all the micropatterned TCP dots area and showed the same circular geometry as that of underlying TCP microdots. MG-63 cells could spread and occupy the whole TCP microdots when the diameters were smaller than 80 μm, but they did not fully occupy the microdots with a diameter of 80 μm.

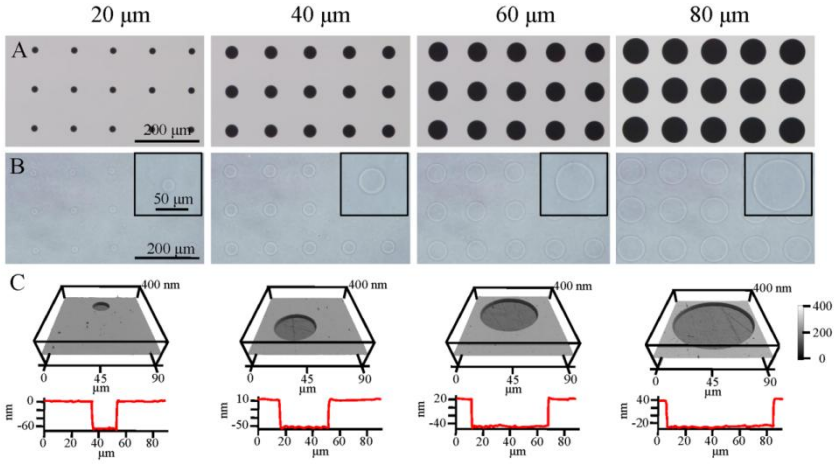

Figure 3.1 Characterization of the prepared micropatterns. (a) and (b) are the phase-contrast micrographs of the photomasks and prepared micropatterns. (c) The 3D and section view of the micropatterns visualized by AFM. The diameters of the microdots were 20, 40, 60 and 80 μm to control cell spreading area and shape.

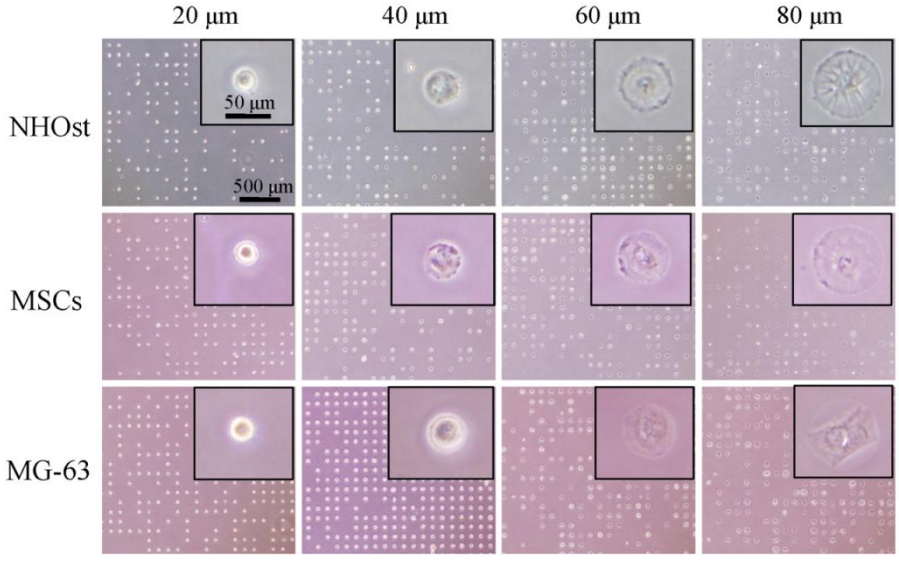

Figure 3.2 Phase-contrast micrographs of NHOst, MSCs and MG-63 cells cultured on the micropatterned surfaces. The values (20, 40, 60, 80 μm) indicate the diameter of the microdots. Except MG-63 cells cultured on 80 μm diameter microdots, all other micropatterned cells showed the same round geometry as the underlying adhesive TCP microdots.

3.4.2 Influence of cell size on cell stiffness

The nanomechanical properties of the micropatterned cells were measured by AFM nanoindentation (Figure 3.3a). During the approach and retract process, cell stiffness and adhesion information was acquired (Figure 3.3b). The nanoindentation was performed at the highest part of cells. This could reduce the influence of substrate on the measured stiffness of micropatterned cells [17]. The Young's modulus of micropatterned cells was calculated to compare the influence of spreading area on nanomechanics of various cell types. Because the morphology of MG-63 cells on 80 μm diameter microdots was not stable, their stiffness on 80 μm diameter microdots was not compared with the other micropatterned cells. According to the analysis results, the stiffness of micropatterned cells increased with increase of cell size (Figure 3.4 and Table 1). However, the influence of cell size on cancer cells stiffness was not as evident as the somatic cells and stem cells, indicating the cancer cells behaved less dependently on their microenvironment compared to their normal counterparts. This should be reasonable because cancer cells, especially the metastatic cancer, require the ability to survive in the physiological microenvironment that differ from their original tissues [18]. Behaving less dependent on microenvironment should provide a relative stable condition which benefits the proliferation and colony forming of cancer cells in a new microenvironment. On small diameter patterns (20 μm), the difference of cell stiffness among the three types of cells was not significant. With increase of spreading area, cell stiffness increased and the difference among the three types of cells became significant. Cell stiffness had the order of NHOst > MSCs > MG-63. The result was in accordance with previous report that the adherent cancer cells were softer than their normal counterparts, which should endow them high ability to penetrate tissues and the extracellular matrix, and hence promote their invasiveness [19]. NHOst cells had larger Young's modulus than MSCs indicating that the mature osteoblast was stiffer than their 'progenitor' stem cells. Several studies have also reported a higher Young's modulus of osteoblasts or osteogenic differentiated MSCs compared to that of undifferentiated MSCs [20,21]. It is quite interesting to notice that the Young's modulus of MSCs and MG-63 cells was similar on 20 and 40 μm diameter microdots which would not happen if the cell stiffness was compared on a uniform TCP surface without micropatterning. The low mechanical state of MSCs should be considered in a state close to the quiescent MSCs *in vivo*, which can preserve the multipotency of MSCs and should enhance the homing capacity of MSCs for penetration and migration among tissues [22,23].

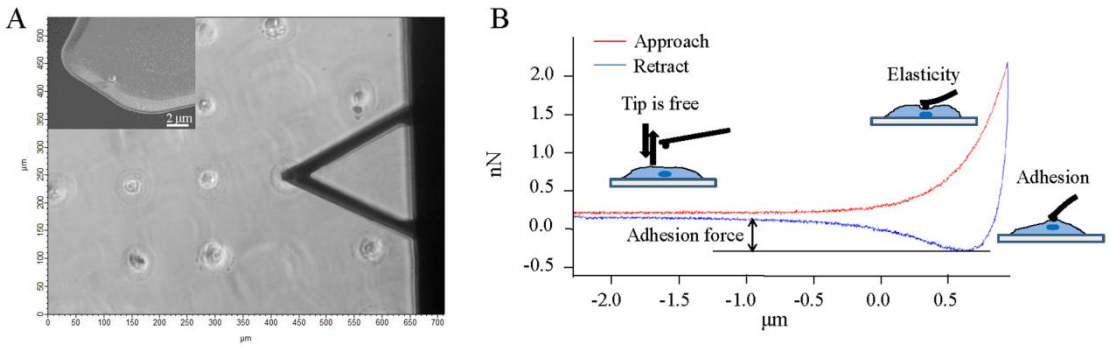

Figure 3.3 Measurement of cell nanomechanics under AFM nanoindentation. (a) Bright field images of the micropatterned cells and AFM probe. The tip was above a cell and processing the nanoindentation. Insert is the SEM image of the AFM cantilever with a 600 nm diameter glass ball as the tip. (b) A typical force curve of the micropatterned cells measured by AFM. During indentation and stretching, the stiffness and adhesion force of cells can be acquired.

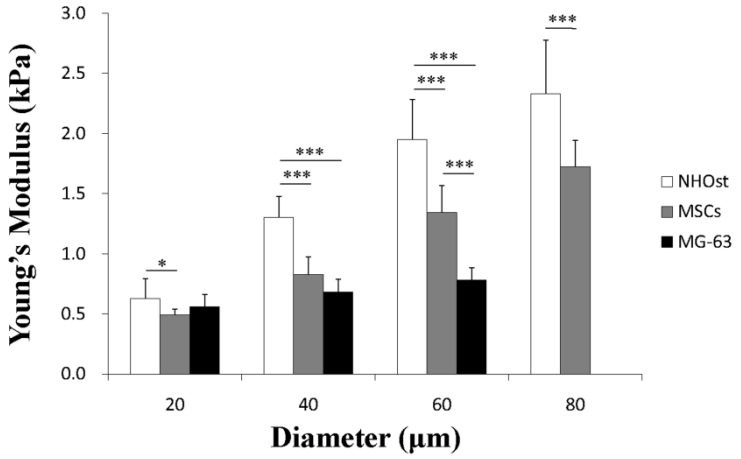

Figure 3.4 The Young's modulus of NHOst, MSCs and MG-63 cells on micropatterns with various spreading area. The data are represented as the means ± SDs, n = 20, *$p < 0.05$, ***$p < 0.001$ and unlabelled columns mean no significant difference.

Table 1. The Young's modulus of NHOst, MSCs and MG-63 cells on micropatterned surfaces with various spreading area.

Cell \ Size / E (kPa)	20 μm	40 μm	60 μm	80 μm
NHOst	0.63 ± 0.19	1.30 ± 0.17	1.95 ± 0.33	2.33 ± 0.44
MSCs	0.49 ± 0.04	0.83 ± 0.15	1.34 ± 0.22	1.72 ± 0.21
MG-63	0.56 ± 0.11	0.68 ± 0.10	0.78 ± 0.12	

3.4.3 Cytoskeletal organization depends on cell size and type

Nanomechanical properties of cells are intimately related with their cytoskeletal organization. The F-actin structure of the micropatterned cells was examined since actin filaments were reported to be the major component of the cytoskeleton which localizes beneath the cellular membrane and were supposed to play a crucial role in regulating cell mechanical properties [24,25]. The actin filament organization of the micropatterned cells was dependent on spreading area and cell type (Figure 3.5). MSCs and NHOst cells on large microdots (60 and 80 μm) assembled their actin in both radial and concentric directions which formed integrated actin network. The actin filaments of NHOst cells were denser than those of MSCs. According to previous studies, the radially and concentrically assembled actin filaments are defined as dorsal stress fibers and transverse arcs, respectively [26,27]. The dorsal stress fibers have one end attaching to the focal adhesion site at the cell-substrate interface and growing to cell center weave into actin cortex around nucleus beneath cell membrane [28]. The transverse arcs are contractive because they are abundant of motor protein myosin. The transverse arcs are connected to the dorsal fibers. The contractive force generated in transverse arcs can be transferred to the actin cortex through dorsal fibers to influence the cortex tension. Therefore, highly ordered F-actin structures should generate high cortex tension which leads to the enhanced cell stiffness. When spreading area decreased, MSCs and NHOst cells assembled their actin structure in different ways. On 40 μm diameter microdots, MSCs predominately assembled concentric actin filaments at periphery

region, while NHOst cells still showed organized radial and concentric actin filaments. On the smallest microdots (20 μm), actin structure of MSC cells were randomly oriented and no obvious filament could be observed. But NHOst cells still had thin and short actin filaments along the cell body. MG-63 cells exhibited less ordered thin actin filaments at cell edge on 60 μm diameter microdots and it disappeared with the decrease of spreading area. The staining results of cytoskeleton are in consistent with the measure cell stiffness. When cells had well organized F-actin filament structure, their stiffness was high like the MSCs and NHOst cells on large micropatterns. By decreasing the spreading area, the F-actin assembly was inhibited and cell stiffness decreased. The cancer cells always showed less ordered F-actin structure and their stiffness was low.

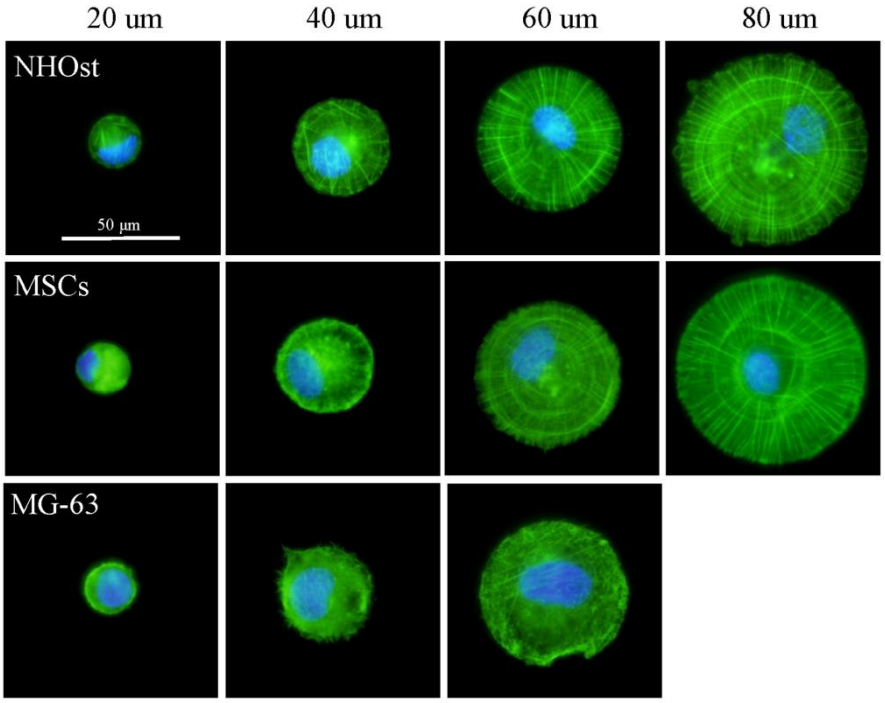

Figure 3.5 The F-actin (green) organization of NHOst, MSCs and MG-63 cells with various spreading area controlled by micropatterns. Nuclei (blue) were stained by DAPI to show the single patterned cells.

3.4.4 Disruption of cytoskeleton reduced cell stiffness

To further investigate the relationship between cell nanomechanics and cytoskeletal structure, the micropatterned cells were treated with cytochalasin D which is known as a reagent to inhibit actin filament polymerization [29]. The integrated actin network observed in the large micropattern MSCs and NHOst cells was disrupted after cytochalasin D treatment (Figure 3.6a). The ratios of the Young's modulus of cytochalasin D treated cells to that of untreated cells are shown in Figure 3.6b. Significant decrease of cell stiffness was observed after cytochalasin D treatment. The ratio further decreased with increase of spreading area indicating that the influence of cytochalasin D was more evident on cells cultured on large microdots. This should be attributed to the disruption of F-actin structures. On large microdots, the highly ordered actin structures played a major role for supporting cell nanomechanics. When the actin structures were disrupted, cell stiffness would significantly decrease. However, on small microdots, the F-actin filaments in cells already disappeared. Therefore, the influence of cytochalasin D treatment on cell stiffness was not evident.

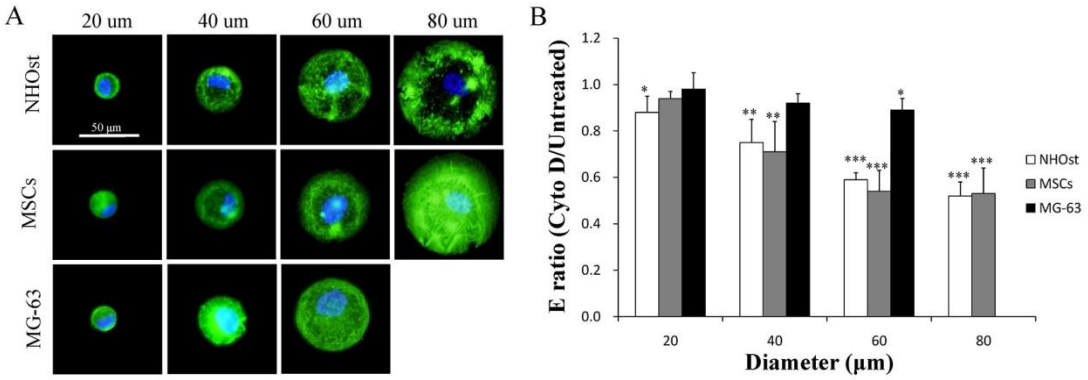

Figure 3.6 Disruption of F-actin filaments by cytochalasin D. (a) The F-actin staining images of NHOst, MSCs and MG-63 cells with various spreading area after treatment with cytochalasin D. (b) Three independent experiments were performed to evaluate the ratio of the Young's modulus of cytochalasin D treated cells to that of untreated cells. The data are represented as the means ± SDs, $*p < 0.05$, $**p < 0.01$, $***p < 0.001$ and unlabelled columns mean no significant difference.

3.4.5 Non-specific adhesion force of micropatterned cells

Cell adhesion which is critical for cell migration and invasion has been investigated using various techniques [30-37]. Previous studies mainly focus on the interaction between certain type of proteins (fibronectin, laminin, etc.) and integrin receptors [38-40] Such interactions are definitely important since the specific adhesion of cell to the ECM proteins is essential process during cell attachment. However, the real adhesion process is usually more complex and generally accepted to occur in two stages, an initial stage dominated by non-specific adhesion and a second stage depended on the specific adhesion [41]. Therefore, understanding non-specific adhesion force is also important. Herein, the non-specific adhesion of micropatterned cells was evaluated basing on the maximum adhesion force recorded during retract process. The force curves were collected at the highest part of cells to predict the cell migration in the following experiment. The non-specific adhesion force showed negatively correlation with spreading area. It decreased with increase of spreading area (Figure 3.7 and Table 2). There was no significant difference of adhesion force among the three types of cells on small diameter patterns (20 μm). With increase of spreading area, non-specific adhesion decreased and it became significantly different among the three types of cells. The adhesion force had an order of MG-63 > MSCs > NHOst. Larger adhesion force of micropatterned MG-63 cells indicated the cancer cells were more deformable compared with their normal counterparts.

Table 2. The non-specific adhesion force of NHOst, MSCs and MG-63 cells on micropatterned surfaces with various spreading area.

Size / Cell / F (pN)	20 μm	40 μm	60 μm	80 μm
NHOst	473.1 ± 53.4	404.3 ± 32.8	322.96 ± 27.5	280.69 ± 17.2
MSCs	501.7 ± 55.2	440.2 ± 46.4	362.24 ± 32.2	323.87 ± 37.3
MG-63	511.9 ± 48.9	456.5 ± 41.8	412.39 ± 34.8	

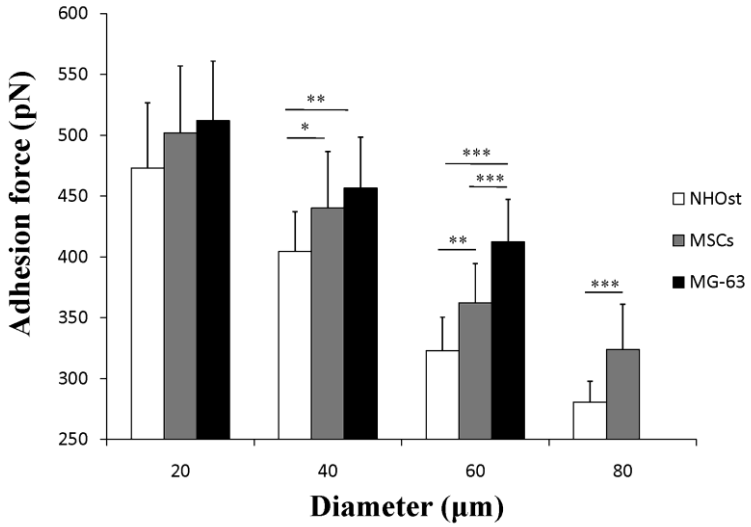

Figure 3.7 The adhesion force of NHOst, MSCs and MG-63 cells on micropatterns with various spreading area. The data are represented as the means ± SDs, n = 20, *p < 0.05, **p < 0.01, ***p < 0.001 and unlabelled columns mean no significant difference.

3.4.6 Membrane roughness of micropatterned cells

The non-specific adhesion force was dominated by the physical interactions between the interfaces of AFM probe and cell membrane. Any change in membrane would affect the interactions. Therefore, we supposed that changing cell spreading area should alter the cell membrane property such as roughness. To confirm this hypothesis, the micropatterned cells were scanned to characterize their membrane properties (Figure 3.8a and b). The roughness of micropatterned cells was in an order of MG-63 > MSCs > NHOst cells (Figure 3.8c). Previous study reported the different membrane proteins and structures of these three types of cells when being cultured on uniform surfaces [42]. Interestingly, the present study disclosed that the surface roughness of cells decreased with increase of spreading area. As mentioned, the spreading area influenced the cytoskeletal structure of cells. Assembly of cytoskeleton further determined cell stiffness through regulation of cortex tension. Large force enhanced the cortex tension which would stretch cell membrane to become smooth. Furthermore, phosphoezrin was stained to check its expression and localization in the micropatterned cells. Ezrin as a membrane-actin linker restricted to the apical membrane has been proved to involve in the membrane ruffling which plays a key role in cell surface structure organization [43]. Change of the expression of ezrin should affect cell membrane roughness. According to the staining results, the expression of phosphoezrin decreased with the increase of spreading area (Figure 3.9). Cells on 20 μm diameter microdots showed condensed ezrin network while those on 80 μm diameter microdots showed faint signal. Therefore, we could conclude that the spreading area would influence cell membrane through regulation of cytoskeleton. On one hand, cytoskeletal assembly would determine the cortex tension force which exerted on membrane to stretch cell surface. Meanwhile, spreading area controlled the actin cortex protrusion through regulating expression of ezrin. Small micropattern cells had weak cortex tension but strong expression of ezrin leading to rough surface. Large micropattern cells had strong cortex tension but weak expression of ezrin leading to smooth surface.

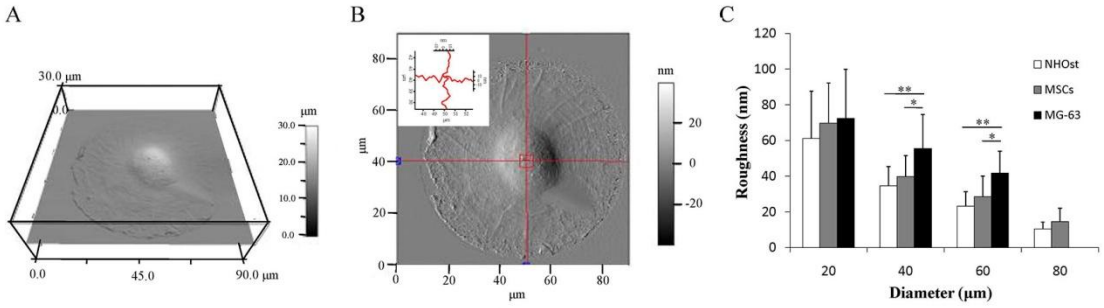

Figure 3.8 The influence of spreading area on cell membrane roughness. (a) 3D scanning images of a micropatterned cells. (b) Deflection image of the same cell. Red square (5 x 5 μm^2) is the highest region of the cell (based on section image of (a) in which the roughness was calculated. Red lines are the horizontal and vertical line pass through the region of interest. Insert is the section images of the two red lines in red square of (b) which indicates the roughness. (c) The surface roughness of micropatterned NHOst, MSCs and MG-63 cells.The data are represented as the means ± SDs, n = 20, $*p < 0.05$, $**p < 0.01$ and unlabelled columns mean no significant difference.

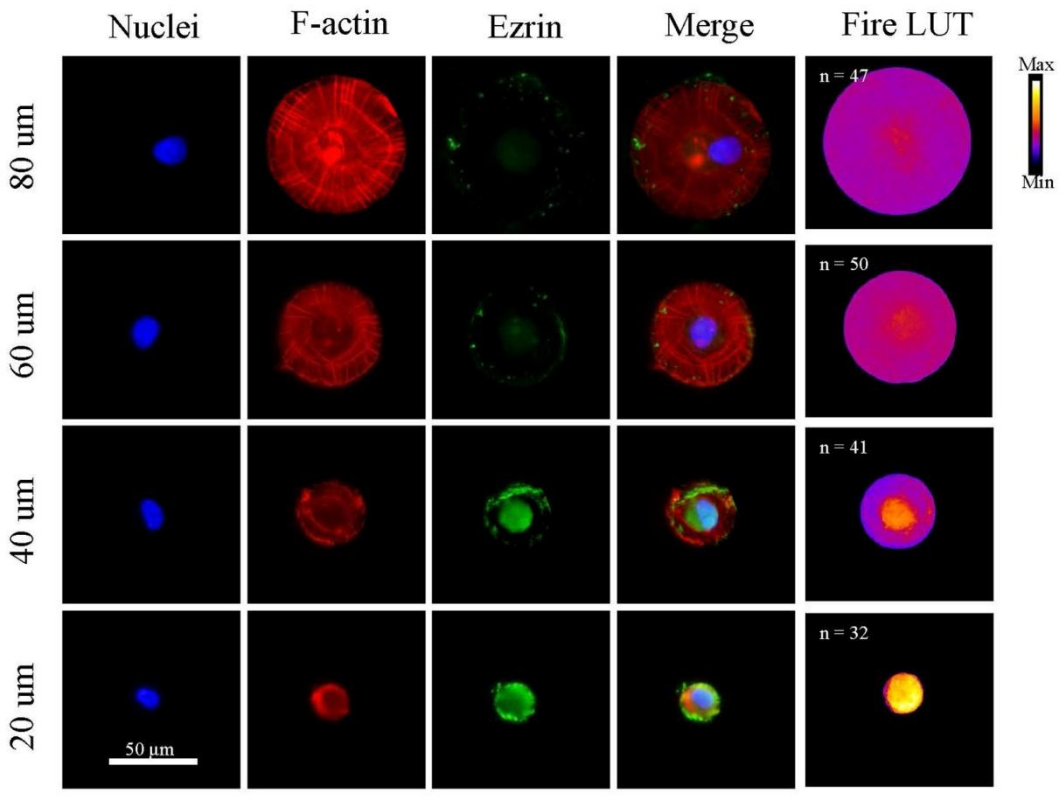

Figure 3.9 Phosphoezrin staining images of micropatterned MSCs. The fluorescence intensity decreased with the increase of spreading area. The staining images of several cells with the same spreading area were stacked along Z axis and their mean intensity was projected on a single image shown in fire look up table.

3.4.7 Cell migration regulated by spreading area and cell type

To confirm how the initial non-specific adhesion will affect cell migration, the migration rate of the

cells with different spreading area was measured. Since the micropatterned cells were restricted within the microdots, conventional test assay such as scratch assay and transmembrane assay cannot be used [44]. Instead, a simple method, as called “contact transfer assay”, was designed to measure the cell migration percentage of the micropatterned cells (Figure 3.10a). A cell adhesive surface without micropatterning, defined as transferring plate, was allowed to contact with the micropatterned cells. Upon contact, cells restricted on the micropatterns would migrate from the patterned surfaces to the transferring plate. After contacting for 15 min, most of the micropatterned cells (MSCs on 40 μm diameter microdots) started to adhere to the transferring plate (Figure 3.10b). And 45 min later, the cells were confirmed to migrate onto the transferring plate with clear migration leading edge. The results indicated that the “contact transfer assay” was effective to study the migration of micropatterned cells. Compared with conventional migration assay, the newly developed method involved the cell migration in Z-axis which mimics the spatial migration of cells *in vivo*. By comparing the cell number on micropatterns before and after migration, the migration percentage of the micropatterned cells was obtained (Figure 3.11). The results indicated that the migration of micropatterned cells was influenced by both cell type and cell spreading area. The migration potential of the three cell types was in an order of MG-63 > MSCs > NHOst cells. This confirmed that cancer cells were more invasive than their normal counterpart. Cell motility decreased with increase of spreading area which showed the same trend as the non-specific adhesion force. After contacting with the unpatterned surface, cells remained on the micropatterns showed contracted morphology, especially the cells with large spreading area. This indicated that the migration of the micropatterned cells was dominated not only by the attachment to the transferring plate but also by the adhesion on the micropatterned surface. Therefore, vinculin was stained to evaluate the adhesion of cells on micropatterned surfaces (Figure 3.12). The results showed that cells with large spreading area formed mature focal adhesion, while those with small spreading area did not.

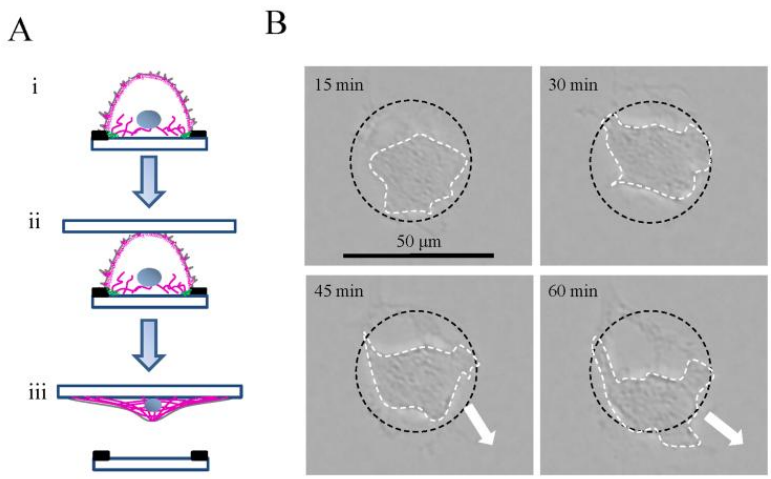

Figure 3.10 Contact transfer assay for cell migration analysis. (a) Scheme of the contact transfer assay. The micropatterned cells (i) were allowed to contact with the unpatterned adhesive surface (ii). After a period, the patterned cells would migrate to the unpatterned surface (iii). (b) The migration process of the MSCs on 40 μm diameter microdots. Black dashed lines indicate the original micropattern area. White dashed lines indicate the contacting area of the cells with unpatterned surface. Arrows indicate the major migration direction of the cells after transfer to the unpatterned surface.

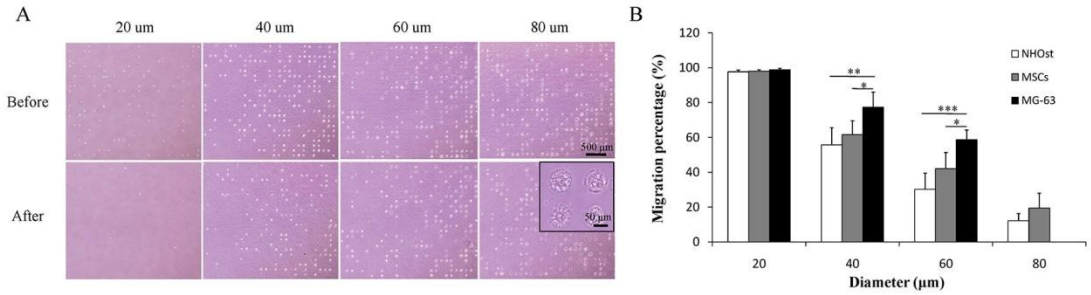

Figure 3.11 Influence of cell size and type on cell migration. (a) The micrographs of the micropatterned MSCs before and after migration. Insert is the high magnification of the cells remaining on the microdots with a diameter of 80 μm. (b) The migration percentage of micropatterned NHOst, MSCs and MG-63 cells. The data are represented as the means ± SDs, n = 3, $*p < 0.05$, $**p < 0.01$ and unlabelled columns mean no significant difference.

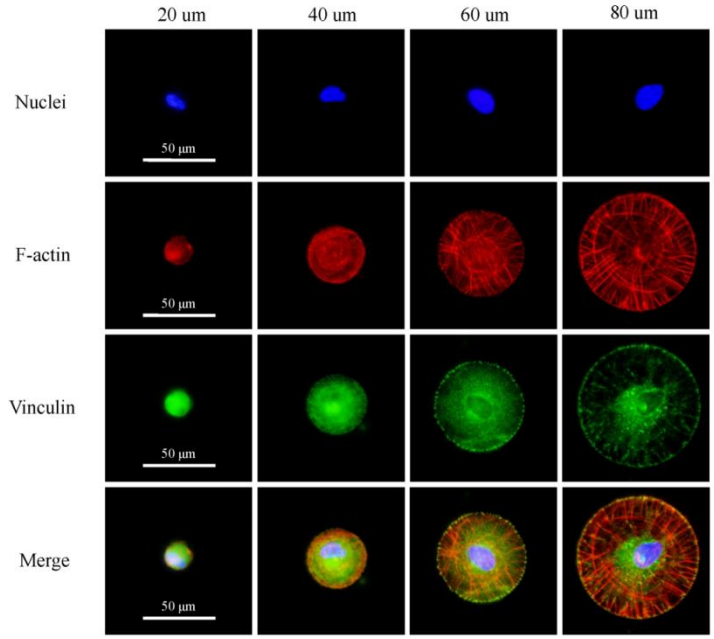

Figure 3.12 Vinculin staining images of micropatterned MSCs. More mature force adhesion complexes were observed with increase of spreading area.

3.4.8 Relationship between cell size and cell nanomechanics

Based on our results, we concluded that cell nanomechanics were intimately related with their spreading area, especially for normal cells (e.g. NHOst and MSCs). Large spreading area facilitated the assembly of cytoskeleton (Figure 3.13a). The dorsal stress fibers and transverse arcs formed the integrated actin network in large micropattern cells. Highly ordered actin network would generate high cortex tension force stretching cell membrane. On one hand, high cortex tension counteracted with AFM indentation force leading to the increase of measured cell stiffness. On the other hand, high cortex tension stretched cell membrane and inhibited expression of ezrin which resulted in the smooth membrane surface. A stretched smooth cell surface would decrease the local density of membrane protein which reduced the non-specific adhesion between AFM tip and cell membrane as measured. Weak non-specific adhesion inhibited cells from

forming new adhesion to transferring plate. Meanwhile, mature focal adhesions formed on large micropatterns reduced cell motility. Opposite to large spreading area, small spreading area inhibited cells from forming integrated cytoskeletal network. Weak organization of actin reduced the intracellular force to counteract with AFM indentation and stretch membrane. But high expression of ezrin enabled membrane ruffling to increase local density of membrane protein which endowed strong interaction between cell and AFM tip. Therefore, small spreading cells had low stiffness but high non-specific adhesion. Initial non-specific adhesion might stimulate cells to produce specific adhesion proteins to form stable adhesion site on the transferring plate. Strong adhesion to transferring plate and immature adhesion on small micropatterns enhanced cell motility. Depending on the intrinsic properties, cancer cells (e.g. MG-63) did not form well organized cytoskeleton in regardless of spreading area (Figure 3.13b). They usually showed low stiffness but high motility.

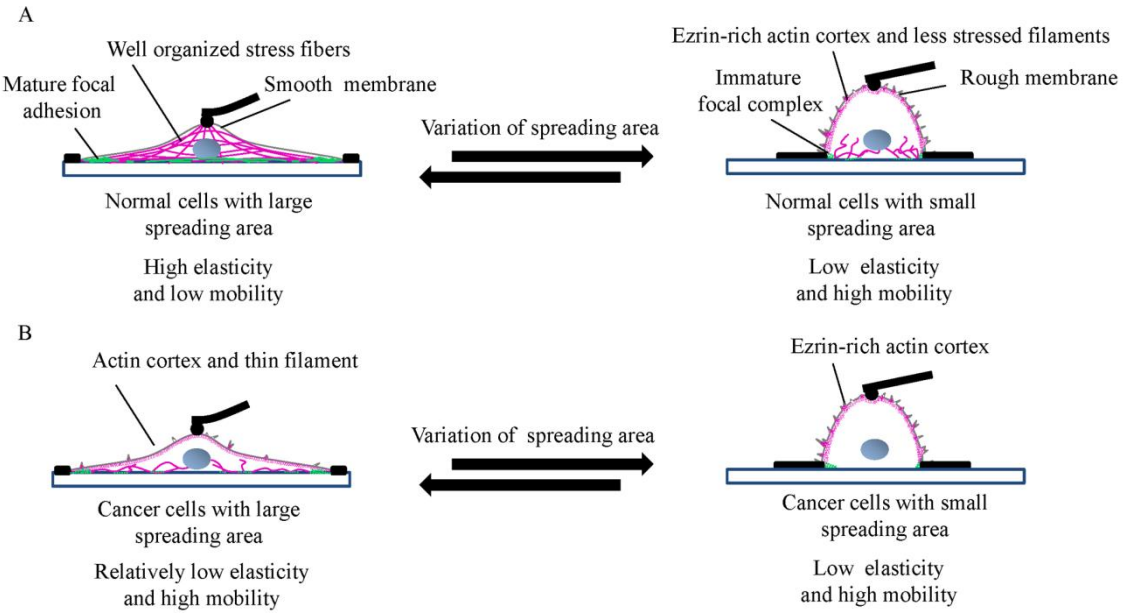

Figure 3.13 Illustration of the influence of spreading area on nanomechanical properties of normal cells and cancer cells. (a) Altering of spreading area significantly influenced cytoskeletal organization and membrane properties of normal cells which resulted in the big variation of cell nanomechanics. (b) Cancer cell behaviors were less dependent on their microenvironment since the influence of spreading area on cell nanomechanics was not evident.

3.5 Conclusions

In summary, the nanomechanical properties of osteosarcoma microenvironment cells (NHOst, MSCs and MG-63 cells) were compared on micropatterned surfaces by AFM. The PVA micropatterned polystyrene surfaces were prepared by UV lithography. They were used to control the cell size and shape to reveal the relationship between the cytoskeletal organization and the nanomechanical properties of cells. Ordering of the cytoskeleton enhanced cell stiffness while disruption of cytoskeleton by cytochalasin D treatment reduced cell stiffness. Meanwhile, cell spreading area influenced the expression of phosphoezrin that affected the surface roughness of cells. Rough membrane was accompanied with high non-specific adhesion force and migration rate. Compared to normal cells, cancer cells behaved less dependently on their microenvironment as their cytoskeleton did not change much by manipulating the spreading area. These

differences of the nanomechanical properties between normal cells and cancer cells can be used to distinguish cancer cells from their microenvironment cells. Cell nanomechanics showed the potential to be applied for cancer diagnosis and therapy. The use of micropatterned surfaces provides a stable way to manipulate the cytoskeletal organization to investigate the nanomechanical properties of individual cells based on cytoskeletal signatures.

3.6 References

[1] Théry M. Micropatterning as a tool to decipher cell morphogenesis and functions. Journal of Cell Science. 2010;123:4201-13.
[2] Sterner O, Giazzon M, Zürcher S, Tosatti S, Liley M, Spencer ND. Delineating Fibronectin Bioadhesive Micropatterns by Photochemical Immobilization of Polystyrene and Poly (vinylpyrrolidone). ACS Applied Materials & Interfaces. 2014;6:18683-92.
[3] Roca-Cusachs P, Alcaraz J, Sunyer R, Samitier J, Farré R, Navajas D. Micropatterning of single endothelial cell shape reveals a tight coupling between nuclear volume in G1 and proliferation. Biophysical Journal. 2008;94:4984-95.
[4] Rigato A, Rico F, Eghiaian F, Piel M, Scheuring S. Atomic Force Microscopy Mechanical Mapping of Micropatterned Cells Shows Adhesion Geometry-Dependent Mechanical Response on Local and Global Scales. ACS Nano. 2015;9:5846-56.
[5] Wang N, Butler JP, Ingber DE. Mechanotransduction across the cell surface and through the cytoskeleton. Science. 1993;260:1124-7.
[6] Hochmuth RM. Micropipette aspiration of living cells. Journal of Biomechanics. 2000;33:15-22.
[7] Guck J, Schinkinger S, Lincoln B, Wottawah F, Ebert S, Romeyke M, et al. Optical deformability as an inherent cell marker for testing malignant transformation and metastatic competence. Biophysical Journal. 2005;88:3689-98.
[8] Legant WR, Choi CK, Miller JS, Shao L, Gao L, Betzig E, et al. Multidimensional traction force microscopy reveals out-of-plane rotational moments about focal adhesions. Proceedings of the National Academy of Sciences. 2013;110:881-6.
[9] Weder G, Guillaume-Gentil O, Matthey N, Montagne F, Heinzelmann H, Vörös J, et al. The quantification of single cell adhesion on functionalized surfaces for cell sheet engineering. Biomaterials. 2010;31:6436-43.
[10] Rianna C, Ventre M, Cavalli S, Radmacher M, Netti PA. Micropatterned Azopolymer Surfaces Modulate Cell Mechanics and Cytoskeleton Structure. ACS Applied Materials & Interfaces. 2015;7:21503-10.
[11] Wang X, Song W, Kawazoe N, Chen G. The osteogenic differentiation of mesenchymal stem cells by controlled cell–cell interaction on micropatterned surfaces. Journal of Biomedical Materials Research Part A. 2013;101:3388-95.
[12] Wang X, Song W, Kawazoe N, Chen G. Influence of cell protrusion and spreading on adipogenic differentiation of mesenchymal stem cells on micropatterned surfaces. Soft Matter. 2013;9:4160-6.
[13] Baicu SC, Taylor MJ. Acid–base buffering in organ preservation solutions as a function of temperature: new parameters for comparing buffer capacity and efficiency. Cryobiology. 2002;45:33-48.
[14] Ohler B. Cantilever spring constant calibration using laser Doppler vibrometry. Review of Scientific Instruments. 2007;78:063701.

[15] Pogoda K, Jaczewska J, Wiltowska-Zuber J, Klymenko O, Zuber K, Fornal M, et al. Depth-sensing analysis of cytoskeleton organization based on AFM data. European Biophysics Journal. 2012;41:79-87.
[16] Costa KD. Single-cell elastography: probing for disease with the atomic force microscope. Disease Markers. 2004;19:139-54.
[17] Lekka M, Laidler P. Applicability of AFM in cancer detection. Nature Nanotechnology. 2009;4:72-.
[18] Matthews HK, Baum B. The metastatic cancer cell cortex: An adaptation to enhance robust cell division in novel environments? Bioessays. 2012;34:1017-20.
[19] Rother J, Nöding H, Mey I, Janshoff A. Atomic force microscopy-based microrheology reveals significant differences in the viscoelastic response between malign and benign cell lines. Open Biology. 2014;4:140046.
[20] Yourek G, Hussain MA, Mao JJ. Cytoskeletal changes of mesenchymal stem cells during differentiation. ASAIO journal (American Society for Artificial Internal Organs: 1992). 2007;53:219.
[21] Darling EM, Topel M, Zauscher S, Vail TP, Guilak F. Viscoelastic properties of human mesenchymally-derived stem cells and primary osteoblasts, chondrocytes, and adipocytes. Journal of Biomechanics. 2008;41:454-64.
[22] Winer JP, Janmey PA, McCormick ME, Funaki M. Bone marrow-derived human mesenchymal stem cells become quiescent on soft substrates but remain responsive to chemical or mechanical stimuli. Tissue Engineering Part A. 2008;15:147-54.
[23] Sohni A, Verfaillie CM. Mesenchymal stem cells migration homing and tracking. Stem Cells International. 2013;2013.
[24] Haga H, Sasaki S, Kawabata K, Ito E, Ushiki T, Sambongi T. Elasticity mapping of living fibroblasts by AFM and immunofluorescence observation of the cytoskeleton. Ultramicroscopy. 2000;82:253-8.
[25] Pesen D, Hoh JH. Micromechanical architecture of the endothelial cell cortex. Biophysical Journal. 2005;88:670-9.
[26] Hotulainen P, Lappalainen P. Stress fibers are generated by two distinct actin assembly mechanisms in motile cells. The Journal of Cell Biology. 2006;173:383-94.
[27] Tee YH, Shemesh T, Thiagarajan V, Hariadi RF, Anderson KL, Page C, et al. Cellular chirality arising from the self-organization of the actin cytoskeleton. Nature Cell Biology. 2015;17:445-57.
[28] Stricker J, Falzone T, Gardel ML. Mechanics of the F-actin cytoskeleton. Journal of Biomechanics. 2010;43:9-14.
[29] Schliwa M. Action of cytochalasin D on cytoskeletal networks. The Journal of Cell Biology. 1982;92:79-91.
[30] Connors WL, Heino J. A duplexed microsphere-based cellular adhesion assay. Analytical Biochemistry. 2005;337:246-55.
[31] Forrester J, Lackie J. Adhesion of neutrophil leucocytes under conditions of flow. Journal of Cell Science. 1984;70:93-110.
[32] Hunter A, Archer C, Walker P, Blunn G. Attachment and proliferation of osteoblasts and fibroblasts on biomaterials for orthopaedic use. Biomaterials. 1995;16:287-95.
[33] Helenius J, Heisenberg C-P, Gaub HE, Muller DJ. Single-cell force spectroscopy. Journal of Cell Science. 2008;121:1785-91.
[34] Sung K, Sung LA, Crimmins M, Burakoff SJ, Chien S. Determination of junction avidity of cytolytic T cell and target cell. Science. 1986;234:1405-8.
[35] Walter N, Selhuber C, Kessler H, Spatz JP. Cellular unbinding forces of initial adhesion processes on nanopatterned surfaces probed with magnetic tweezers. Nano Letters. 2006;6:398-402.

[36] Matthews BD, Overby DR, Alenghat FJ, Karavitis J, Numaguchi Y, Allen PG, et al. Mechanical properties of individual focal adhesions probed with a magnetic microneedle. Biochemical and Biophysical Research Communications. 2004;313:758-64.
[37] Neuman KC, Nagy A. Single-molecule force spectroscopy: optical tweezers, magnetic tweezers and atomic force microscopy. Nature Methods. 2008;5:491.
[38] Li F, Redick SD, Erickson HP, Moy VT. Force measurements of the α5β1 integrin–fibronectin interaction. Biophysical Journal. 2003;84:1252-62.
[39] Sun Z, Martinez-Lemus LA, Trache A, Trzeciakowski JP, Davis GE, Pohl U, et al. Mechanical properties of the interaction between fibronectin and α5β1-integrin on vascular smooth muscle cells studied using atomic force microscopy. American Journal of Physiology-Heart and Circulatory Physiology. 2005;289:H2526-H35.
[40] Taubenberger AV, Woodruff MA, Bai H, Muller DJ, Hutmacher DW. The effect of unlocking RGD-motifs in collagen I on pre-osteoblast adhesion and differentiation. Biomaterials. 2010;31:2827-35.
[41] Donaldson SH, Valtiner M, Gebbie MA, Harada J, Israelachvili JN. Interactions and visualization of bio-mimetic membrane detachment at smooth and nano-rough gold electrode surfaces. Soft Matter. 2013;9:5231-8.
[42] Docheva D, Padula D, Popov C, Mutschler W, Clausen-Schaumann H, Schieker M. Researching into the cellular shape, volume and elasticity of mesenchymal stem cells, osteoblasts and osteosarcoma cells by atomic force microscopy. Journal of Cellular and Molecular Medicine. 2008;12:537-52.
[43] Pitaval A, Tseng Q, Bornens M, Théry M. Cell shape and contractility regulate ciliogenesis in cell cycle–arrested cells. The Journal of Cell Biology. 2010;191:303-12.
[44] Kramer N, Walzl A, Unger C, Rosner M, Krupitza G, Hengstschläger M, et al. *In vitro* cell migration and invasion assays. Mutation Research/Reviews in Mutation Research. 2013;752:10-24.

Chapter 4

Cellular uptake of gold nanoparticles regulated by cell size

4.1 Summary

In this chapter, photo-reactive PVA micropatterned TCPS surfaces were used to control the cell size and investigated how the cell size affected the cellular uptake of polyethylene glycol modified gold NPs (PEG-AuNPs). The cell morphology was precisely controlled by micropatterned surfaces. Cells cultured on the micropatterned surfaces had the same shape and dimension as those of micropatterns. Uptake of FITC labeled PEGylated gold NPs by the micropatterned cells was investigated to disclose the influence of cell size on cellular uptake behavior. The results showed that the total uptake amount increased with the increase of cell size, but uptake capacity per unit cell area decreased with the increase of cell size. The results were correlated with interaction between NPs and micropatterned cells and cell membrane tension. The results should open new avenues for engineering the NPs based biomedicine for more effective delivery, and inspire understanding the influence of cell microenvironment on cell behaviors.

4.2 Introduction

Nanoparticles (NPs) have been widely used to improve the diagnosis and treatment of disease in biomedicine due to their unique physical and structural properties [1-6]. Recent studies have reported that NPs are able to regulate stem cell differentiation which holds great promise for tissue engineering [7-9]. Efficient cellular uptake of NPs plays a key role in the cell-based biomedical applications of NPs. Therefore, understanding the interaction between NPs and cells including cellular uptake becomes the cornerstone for the possible biomedical applications of NPs. Plenty of studies have concentrated on the influence of particle properties including size, shape and surface chemistry on the cellular uptake of NPs [10-16]. However, how the cell morphogenesis would affect the cellular uptake remains elusive. Cells develop their morphology depending on their surrounding microenvironment. Recent studies have reported that the biophysical stimuli from cell microenvironment (elasticity, topography, etc.) affect cell size that is involved in determination of cell fate [17-24]. Meanwhile, cell size plays crucial roles in organ development and human disease progression [25]. Understanding the influence of cell size on cellular uptake should provide useful information to guide the NPs-based biomedical applications.

Among numerous NPs, gold NPs (AuNPs) in particular have attracted plenty of interests due to their chemical stability, easily modified surface chemistry and tunable optical properties [26-30]. AuNPs are usually modified with biocompatible molecules such as polyethylene glycol (PEG) to improve their biocompatibility and to prevent aggregation [31,32]. Thiol-end PEG can be easily bound onto the surfaces of AuNPs through gold-thiol interaction. The modified PEG monolayer on gold surface can enhance the biocompatibility and blood retention time of AuNPs which is important for biomedical applications [33].

In this study, the cell size was controlled by culturing cells on micropatterned surfaces having microdots of different diameters. PEG-AuNPs with a diameter around 50 nm were synthesized and used for cellular uptake. Fluorescein isothiocyanate (FITC) was used to label the PEG-AuNPs to trace cellular uptake process. Cells with different sizes assembled cytoskeleton in different manners which further affected cell membrane tension that was disclosed by atomic force microscope (AFM) nanoindentation. The endocytosis of PEG-AuNPs was investigated to reveal the influence of cell size on cellular uptake.

4.3 Materials and methods

4.3.1 Synthesis and characterization of FITC-PEG-AuNPs

AuNPs were synthesized using Turkevich method as previously described [34,35]. Briefly, 1 ml 1% wt HAuCl4 (Wako Pure Industries, Ltd, Tokyo, Japan) solution was added to 98 ml pure water and heated in oil bath (110 °C) with stirring (700 rpm) for 20 min. Subsequently, 1 ml 1% wt tri-sodium citrate (Wako Pure Industries, Ltd, Tokyo, Japan) solution was added as the reducing and capping agent. After 15 min, the solution was slowly cooled down to room temperature. The synthesized AuNPs were collected and washed with water under centrifugation at 8,000 rpm. Finally, the mixture of mPEG-SH (5 kDa, Nanocs, MA, USA) and FITC-PEG-SH (5 kDa, Nanocs, MA, USA) at a ratio of 3:2 was added into 3.3 nM AuNPs solution to reach the final PEG concentration of 100 μM. The reaction mixture was treated with ultrasonic for 30 min and stirred for another 24 h at room temperature at a condition protected from light. The FITC-PEG-AuNPs were collected and washed with water using centrifugation at 8,000 rpm and then characterized with field-emission scanning electron microscopy (FE-SEM, Hitachi, Tokyo, Japan), transmission electron microscopy (TEM, JEOL, Tokyo, Japan) and dynamic light scattering (DLS, JASCO, Tokyo, Japan). The fluorescence intensity of the FITC-PEG-AuNPS was tested with excitation wavelength of 490 nm and emission wavelength from 500 to 600 nm using fluorescence microscopy (JASCO, Tokyo, Japan).

4.3.2 Preparation and characterization of the PVA micropatterned TCPS surfaces

The synthesis process of photo-reactive PVA, preparation scheme of the PVA micropatterned TCPS surfaces and AFM scanning of the micropatterns were performed in the same way as described in Chapter 2.3.2.

4.3.3 Cell culture

Human mesenchymal stem cells (hMSCs, passage 2) were purchased from Lonza Walersville, Inc. and subcultured using MSCGM medium (Lonza). The hMSCs at passage 4 were used for the cellular uptake study. Prior to use, micropattern plates were sterilized using 70% ethanol followed by washing with sterile

water for 3 times. The micropattern plates were then placed in 6-well plates and glass rings were placed on the plates to protect cell leakage during cell seeding. An aliquot of 3 mL growth medium (DMEM supplemented with 4500 mg/L glucose, 584 mg/L glutamine, 100 μg/mL penicillin-sterptomycin, 0.1 mM nonessential amino acids, 0.4 mM proline, 50 mg/L ascorbic acid, and 10% FBS) was added inside the glass rings. And then 200 μL cell suspension solution (2.7 x 10^4 cells/mL) was added within the glass ring (3000 cells/cm^2). After being cultured for 6 h, the glass rings were taken out and the medium was changed using the growth medium supplemented with FITC-PEG-AuNPs. The culture condition of the micropatterned cells was similar to the normal stem cell expansion condition to exclude the effect of artificial culture condition on cellular uptake. After being culture for another 24 h, the samples were fixed with 4% paraformaldehyde for quantification of the uptake amount and immunofluorescence staining.

4.3.4 In vitro cytotoxicity

To evaluate the cytotoxicity of the FITC-PEG-AuNPs, cell viability was tested using WST-1 assay. The hMSCs were seeded in 96 well plates at a density of 3,000 cells/cm^2. After 6 h culture, the medium was changed to medium containing FITC-PEG-AuNPs at a concentration of 0, 0.1, 0.5 and 1.0 nM. After 24 h incubation, the medium was replaced with 110 μl WST-1 working solution (Roche, Germany, 10 μl of WST-1 stock solution diluted with 100 μl of growth medium). After 3 h incubation, the absorbance in each well at 440 nm was measured using a plate reader (Benchmark Plus, USA) to evaluate cell viability. Live/dead staining was processed using a Cellstain Live-Dead Double Staining kit (Dojindo, Japan). The hMSCs were seeded in 24 well plates at a density of 3,000 cells/cm^2. After 6 h culture, the medium was changed to medium containing FITC-PEG-AuNPs at a concentration of 0, 0.1, 0.5 and 1.0 nM. After 24 h incubation, the cells were washed thrice with PBS and incubated with 2 mM calcein-AM and 4 mM propidium iodide (PI) in serum-free medium for 15 min at 37 °C. The staining images were observed using an inverted fluorescence microscope (Olympus, Japan).

4.3.5 Immunofluorescence staining

For myosin and F-actin staining, cells were fixed with 4% paraformaldehyde, permeabilized with 1% Triton X-100 and blocked with 1% BSA solution for 30 min. The samples were then incubated with rabbit anti-myosin IIA antibody (Sigma, 1:100) at 4 °C overnight followed by PBS washing. Alexa Fluor-488 labeled donkey anti-rabbit IgG antibody (Invitrogen, 1:800) and Alexa Fluor-594 phalloidin (Invitrogen, 1:40) were diluted in PBS solution and the labeling was performed at room temperature for 1 h. Cell nuclei were stained with 4',6-diamidino-2-phenylindole (DAPI). Fluorescence micrographs of the stained cells were captured using an Olympus BX51 microscope with a DP-70 CCD camera (Olympus, Tokyo, Japan). The obtained fluorescence images were analyzed using the ImageJ software. The images were converted to 16 bit images and the background was subtracted. Gray plot profile was processed across the filaments and fitted with Gaussian fitting. The full width at half maximum was considered as the thickness of the actin filaments.

4.3.6 Evaluation of cell membrane tension

The membrane tension of the micropatterned cells were evaluated based on cell elasticity measured using AFM nanoindentation. Briefly, the micropatterned cells were cultured in growth medium for 6 h and directly used for mechanical test under a living state. A silicon nitride cantilever (Novascan, Ames, USA)

coated with reflective gold was used for force indentation. The cantilever has a silica glass ball with a diameter of 600 nm attached to the end as the probe. Using the thermal tuning method, the exact spring constant of the cantilever was measured [36]. An optical microscope was used to visualize the micropatterned cells and the position of the cantilever. The measurement was performed within 1.5 h to minimize the death of cells during the experiment. The force distance curves were collected in the central region of cells at an indentation rate of 4 μm/s with a trigger force of 2 nN to avoid any damage to the cell surface. For 80 μm diameter micropatterned cells, the indentation was performed at both cell central and periphery region. The obtained force curves were fitted to Hertz's contact model to calculate the Young's modulus of cells. For each sample, 200 force curves were collected from 20 cells and used for calculation. The average Young's modulus of the 20 cells was considered as the cell elasticity.

4.3.7 Cellular uptake of FITC-PEG-AuNPs

Cells cultured on the micropatterned surfaces were incubated with 1 nM FITC-PEG-AuNPs for 24 h. After thrice washing with warm PBS buffer, the micropatterned cells were washed with 0.4 % trypan blue solution (Sigma) to quench the extracellular FITC fluorescence [37]. And then the cells were fixed with 4% paraformaldehyde for 10 min. After that, the samples were completely washed with PBS and mounted. To confirm the endocytosis of the FITC-PEG-AuNPs, the confocal images of the micropatterned cells were taken under a confocal fluorescence microscope (Zeiss, Germany). Cell membrane was stained with 0.25 μg/mL CellMaskTM Deep Red plasma membrane stain (Invitrogen, CA, USA) solution for 5 min followed by PBS washing. The fluorescence images of the micropatterned cells were obtained to evaluate the cellular uptake. The software ImageJ was used to analyze the fluorescence intensity of the micropatterned cells. Briefly, the micropatterned cells were selected as regions of interest. The area (A) and integrated intensity (I) of the micropatterned cells were measured. Subsequently, the mean fluorescence intensity (M) of the unoccupied micropatterns was measured as the background. The corrected total fluorescence (CTF) can be described as: $CTF = I - (A \times M)$. While the average fluorescence intensity per unit area (AFI) can be described as: $AFI = CTF/A$ [38].

4.3.8 Statistical analysis

Statistical analysis was performed using a one-way analysis of variance (ANOVA) with Tukey's post hoc test for multiple comparisons to confirm the significant differences among samples. The data was presented as means ± standard deviations (SDs). It was considered to be statistically significant different when $p < 0.05$.

4.4 Results and discussion

4.4.1 Preparation of FITC-PEG-AuNPs

The size and shape of the citrate-AuNPs and FITC-PEG-AuNPs were characterized using SEM and TEM (Figure 4.1). The NPs were well dispersed and showed homogeneous size and nearly spherical shape. The size of the NPs was analyzed using TEM and DLS (Table 1). The diameter of FITC-PEG-AuNPs was around 50 nm which should have high cellular uptake amount according to previous studies [39-41]. After

PEG modification, the surface potential of AuNPs changed from -24.6 ± 4.1 mV (citrate AuNPs) to -0.7 ± 1.3 mV (PEG-AuNPs) indicating the PEG layer was successfully coated onto the surface of AuNPs. The fluorescence spectra of citrate-AuNPs, FITC-PEG-AuNPs and pure FITC-PEG solution were measured to check whether the FITC-PEG was coated onto the AuNPs (Figure 4.2). Citrate-AuNPs did not show any fluorescence peak in the range of 500-600 nm, while the pure FITC-PEG solution had strong peak at 520 nm. The FITC-PEG-AuNPs also showed a peak at 520 nm indicating the PEG-AuNPs were successfully labeled with FITC. The fluorescence intensity was proportional to the concentration of FITC-PEG-AuNPs. Higher particle concentration resulted in higher fluorescence intensity. Live/dead staining was processed to check the cytotoxicity of the FITC-PEG-AuNPs (Figure 4.3a). Nearly no dead cells were observed after incubation with the FITC-PEG-AuNPs for 24 h even the concentration reached to 1 nM. The WST-1 assay was performed to confirm the cell viability after incubation with the FITC-PEG-AuNPs. Once more, the results showed that the cells still had high viability after treatment of the FITC-PEG-AuNPs at the studied concentration of 0.1 – 1.0 nM (Figure 4.3b). Therefore, the FITC-PEG-AuNPs did not show obvious cytotoxicity to the hMSCs.

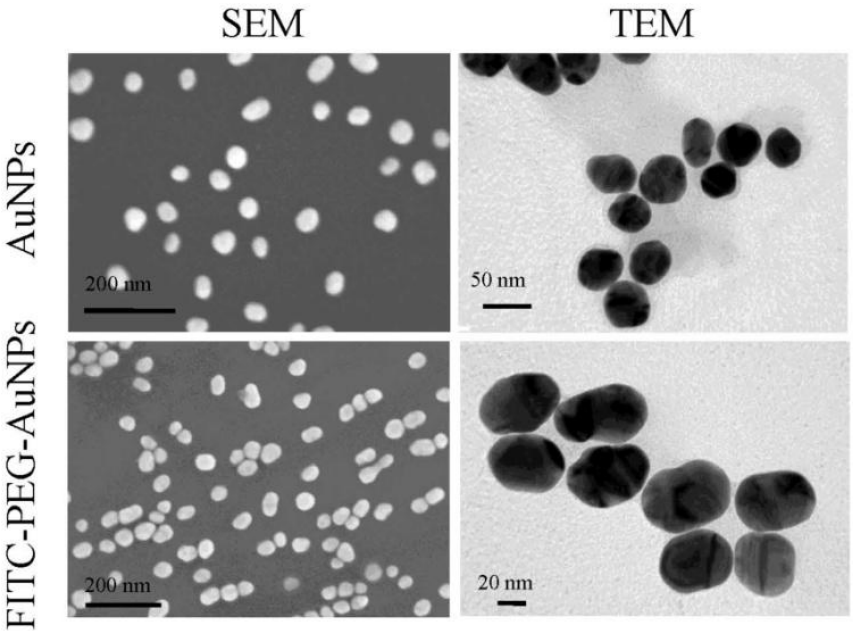

Figure 4.1 The SEM and TEM images of the AuNPs and FITC-PEG-AuNPs were acquired to characterize the size and shape of the prepared NPs.

Table 4.1 Characterization of citrate-AuNPs and FITC-PEG-AuNPs.

Gold NPs	Diameter (nm)		Zeta-potential (mV)
	TEM	DLS	
AuNPs (Citrate)	43.7 ± 12.9	46.6 ± 15.5	-24.6 ± 4.1
FITC-PEG-AuNPs	48.1 ± 17.1	59.3 ± 16.3	-0.7 ± 1.3

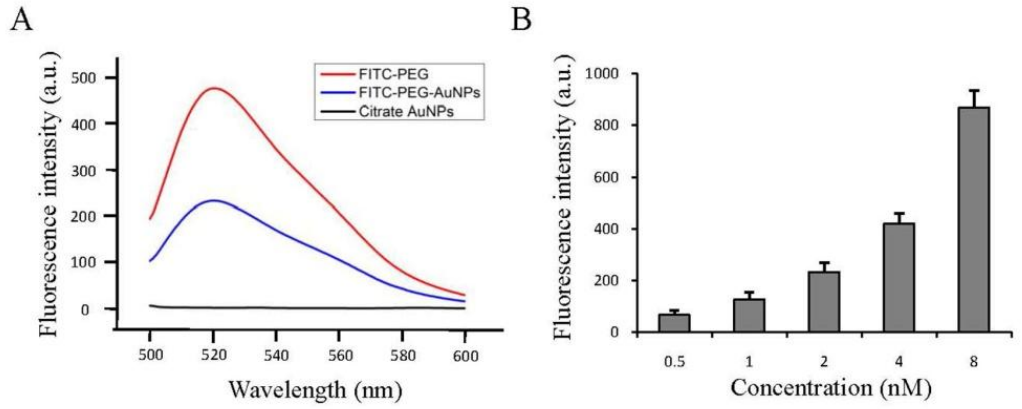

Figure 4.2 Characterization of FITC conjugation. (a) The fluorescence spectra of citrate-AuNPs (black), FITC-PEG-AuNPs (blue) and pure FITC-PEG (red) solution. (b) The fluorescence intensity (at 520 nm) increased with the increase of concentrations of FITC labeled PEG-AuNPs.

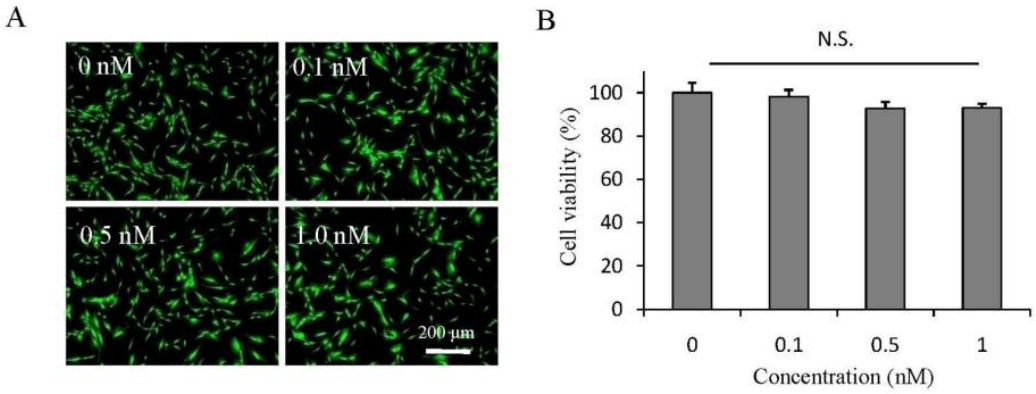

Figure 4.3 Evaluationof cell viability after being cultured with the FITC-PEG-AuNPs. (a) Live/dead staining of the cells after treatment with various concentrations of FITC-PEG-AuNPs for 24 h. Green staining indicates live cells and red staining indicates dead cells. (b) Cell viability after treatment of FITC-PEG-AuNPs with various concentrations for 24 h. N. S. means no significant difference.

4.4.2 Cell size regulated by PVA micropatterns

Photo-reactive PVA as cell resistant material was micropatterned onto cell adhesive TCPS plate surface using UV photolithography (Figure 4.4a). Photo-reactive PVA contained the azide groups which can be irradiated by UV light. In this study, we fabricated the photomasks composed of microdots with various diameters to control the size of cells. The diameters of the designed microdots were 20, 40, 60 and 80 μm that were suitable for single hMSCs adhesion and spreading. AFM scanning of the micropatterned surfaces showed that the size of the microdots was nearly same as the designed photomasks indicating the good controllability of this method (Figure 4.4b). The section analysis of the microdots showed that the average depth of the PVA layer was 60 nm which should be effective to constrain the cells in the microdots [42,43]. The hMSCs were used in this study to investigate the influence of cell size on stem cells cellular uptake of NPs which hold great promise for tissue engineering and cell therapy. The hMSCs attached onto the TCPS surfaces and showed the same size and shape as the underlying microdots (Figure 4.4c). Therefore, both the

size and shape of hMSCs were well controlled by the micropatterned surfaces.

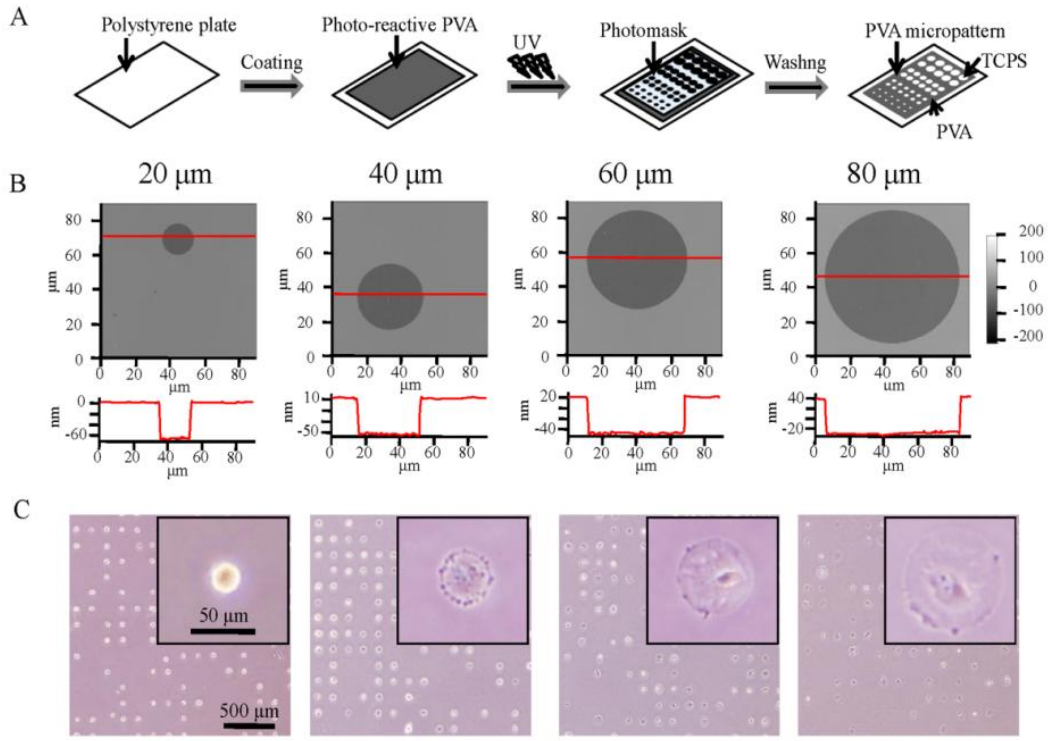

Figure 4.4 Preparation scheme and characterization of the PVA micropatterned TCPS surfaces. (A) Preparation scheme of the micropatterns with microdots of different diameters. (B) AFM scanning images of the microdots with diameters of 20, 40, 60 and 80 μm. (C) Cell attachment on the micropatterns after culture for 24 h. Insert is the typical image of attached MSCs.

4.4.3 Influence of cell size on cytoskeleton assembly

F-actin filaments as one of the major cytoskeletal components were stained to check the cytoskeletal assembly of micropatterned cells. Myosin as the major actin binding motor protein was stained to estimate the cellular mechanical state (Figure 4.5). According to the staining results, the hMSCs with large spreading area formed integrated actin network. Meanwhile they showed fibrous pattern of myosin. The merged images showed the colocalization of actin and myosin indicating a strong binding of myosin to actin filaments in the large hMSCs. Cells with large spreading area assembled the actin filaments in both radial and concentric direction of the microdtos. The thick radial actin filaments abundant of myosin are defined as ventral stress fibers (VSFs), while thin radial actin filaments deplete of myosin are defined as dorsal stress fibers (DSFs) [44]. The concentrically assembled actin filaments are defined as the transverse arcs (TAs) [45]. Myosin abundant VSFs are highly contractive and play an important role in regulating intracellular tension [46]. DSFs are non-contractive but they weave into actin cortex network around nucleus beneath cell membrane during their growth from cell edge to center region [47]. TAs are contractive since they are reported to have periodic α-actinin-myosin distribution in the assembled fibers [48]. TAs are linked to DSFs, thus the contractive force generated in TAs can transfer to other organelle through DSFs. The integrated actin gradually disassembled with decrease of cell spreading area. The thickness of actin filaments decreased with decrease of spreading area indicating small spreading area inhibited the recruitment of F-actin filaments (Figure 4.6). Meanwhile, fibrous pattern of myosin became ambiguous as cell spreading area decreased and

this would affect cell mechanical state.

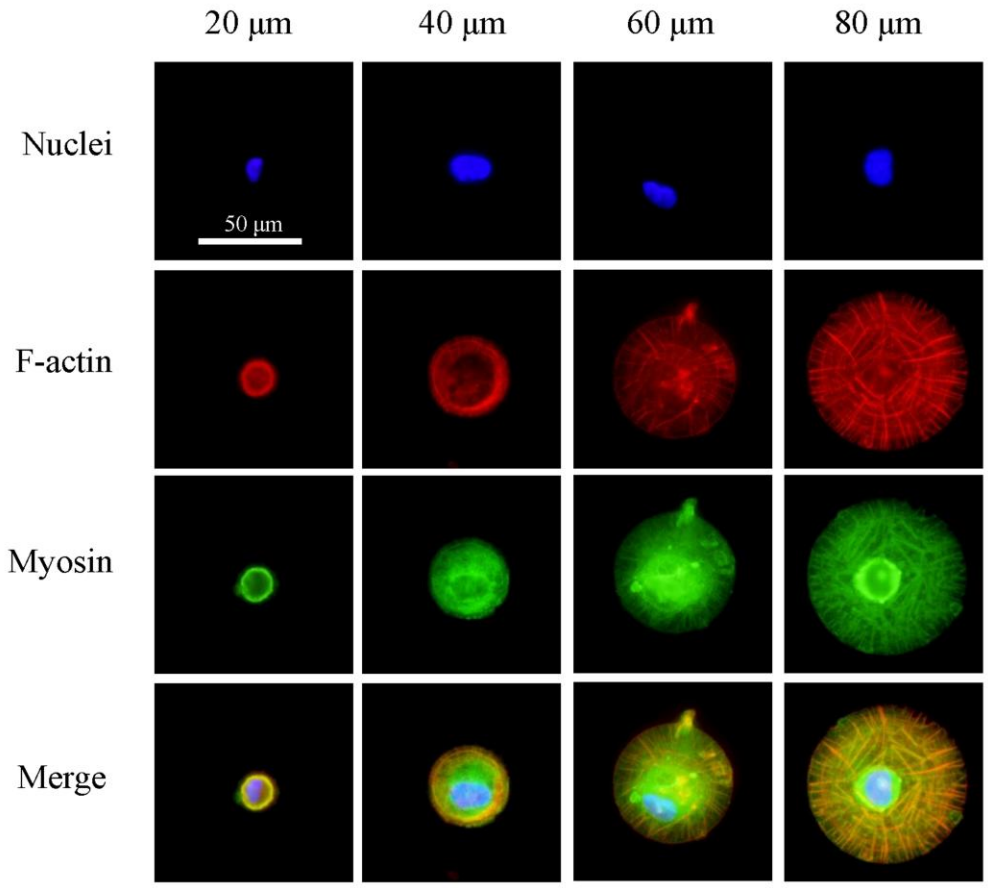

Figure 4.5 F-actin, myosin and nucleus staining images of the micropatterned MSCs that were cultured on the micropatterns with microdots having diameters of 20, 40, 60 and 80 μm for 6 h.

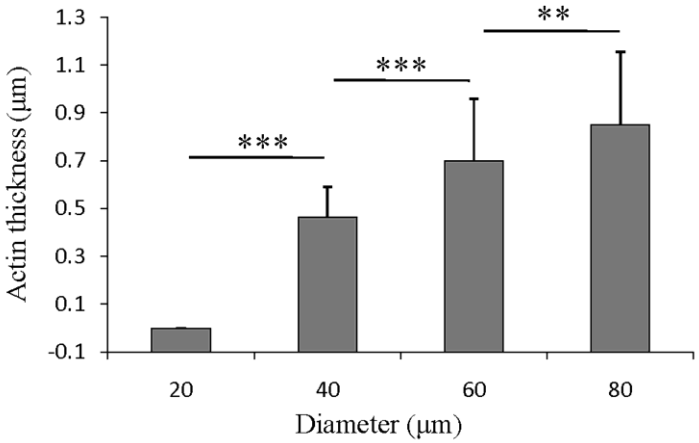

Figure 4.6 The thickness of the F-actin filaments of the micropatterned MSCs that were cultured on the micropatterns with microdots having diameters of 20, 40, 60 and 80 μm for 6 h. **$p < 0.01$ and ***$p < 0.001$ ($n = 80$).

4.4.4 Influence of cell size on membrane tension

It is well accepted that cell membrane tension is intimately related with cell mechanical state [49-51]. Therefore, the cytoskeletal tension of micropatterned cells was measured using AFM nanoindentation to evaluate cell membrane tension. Firstly, the nanoindentation was performed at the cell center to compare the average elasticity of each micropatterned cells. According to the results, the Young's modulus of cells significantly increased with increase of spreading area (Figure 4.7). This was in good accordance with the cytoskeletal staining results. The well organized cytoskeletal network in the large cells enhanced cell cytoskeletal tension, while the disordered cytoskeletal network formed in small cells reduced cytoskeletal tension. The cytoskeletal tension at periphery regions of the large cells (80 μm) was further tested to show the heterogeneous mechanical state at different cell regions. The results showed that the Young's modulus at cell edge was significantly higher than that measured at cell center indicating the cytoskeletal tension at cell edge should be higher than that of cell central region. Previous study has also reported higher cellular tension at cell periphery region compared to that in cell center [52]. This was also attributed to the cytoskeletal assembly since the actin filaments were denser at cell edge than those at cell center. Therefore, the results suggested that the cell membrane tension would increase with the increase of cell spreading area and it was higher in cell periphery region than in central region.

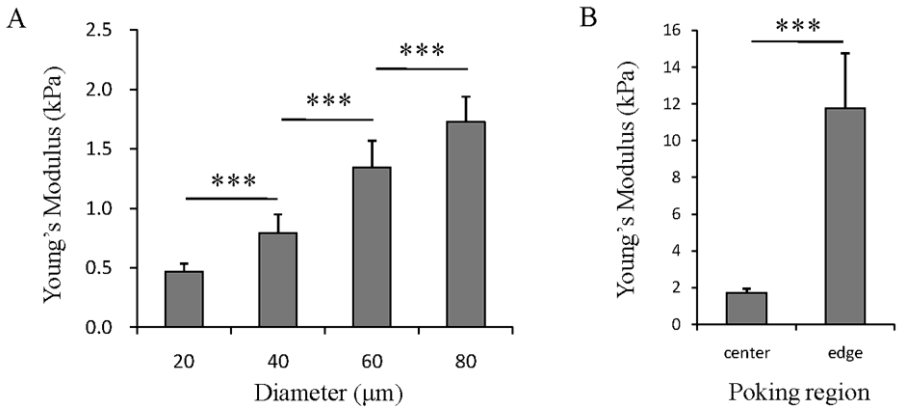

Figure 4.7 Cellular mechanical properties measured by AFM nanoindentation. (A) The Young's modulus of MSCs that were cultured on the micropatterns with microdots having diameters of 20, 40, 60 and 80 μm for 6 h, which was measured from the center of micropatterned MSCs. (B) The Young's modulus of MSCs cultured on the micropatterns with microdots having a diameter of 80 μm for 6 h, which was measured from the center and edge regions of the micropatterned MSCs. ***$p < 0.001$ ($n = 20$).

4.4.5 Influence of cell size on cellular uptake

The typical confocal micrographs of the micropatterned cells treated with FITC-PEG-AuNPs were shown in Figure 4.8. Cell membrane was stained to distinguish the intra- and extra-cellular environments. In order to quench the extracellular fluorescence, the micropatterned cells were pre-treated with 0.4 % trypan blue solution. The confocal micrographs confirmed that the fluorescence intensity mainly accounted for the internalized FITC-PEG-AuNPs. The majority of FITC-PEG-AuNPs accumulated at the cell center region rather than cell periphery region. However, the NPs did not enter cell nuclei since there was always a dark region at nucleus position. Furthermore, the fluorescence images of the micropatterned cells were acquired to calculate the total and average fluorescence yield of the internalized NPs (Figure 4.9a). Semi-quantitative

analysis of the fluorescence images of the micropatterned cells showed that the total fluorescence yield increased with increase of cell spreading area but the average intensity per unit membrane area decreased with increase of spreading area (Figure 4.9b and c). Herein, the cell spreading area was regarded as the cell membrane area. This would lead to overestimation of the average intensity of the micropatterned cells, especially for the cells with small spreading area. However, even the small micropatterned cells were treated as hemispherecial, and the hemispherecial surface area was used for calculation, the average intensity per unit membrane area was still significantly higher than that of the large cells. These results indicated that the large cells had higher total cellular uptake amount than the small ones, while their uptake capacity per unit membrane area was lower than the small ones.

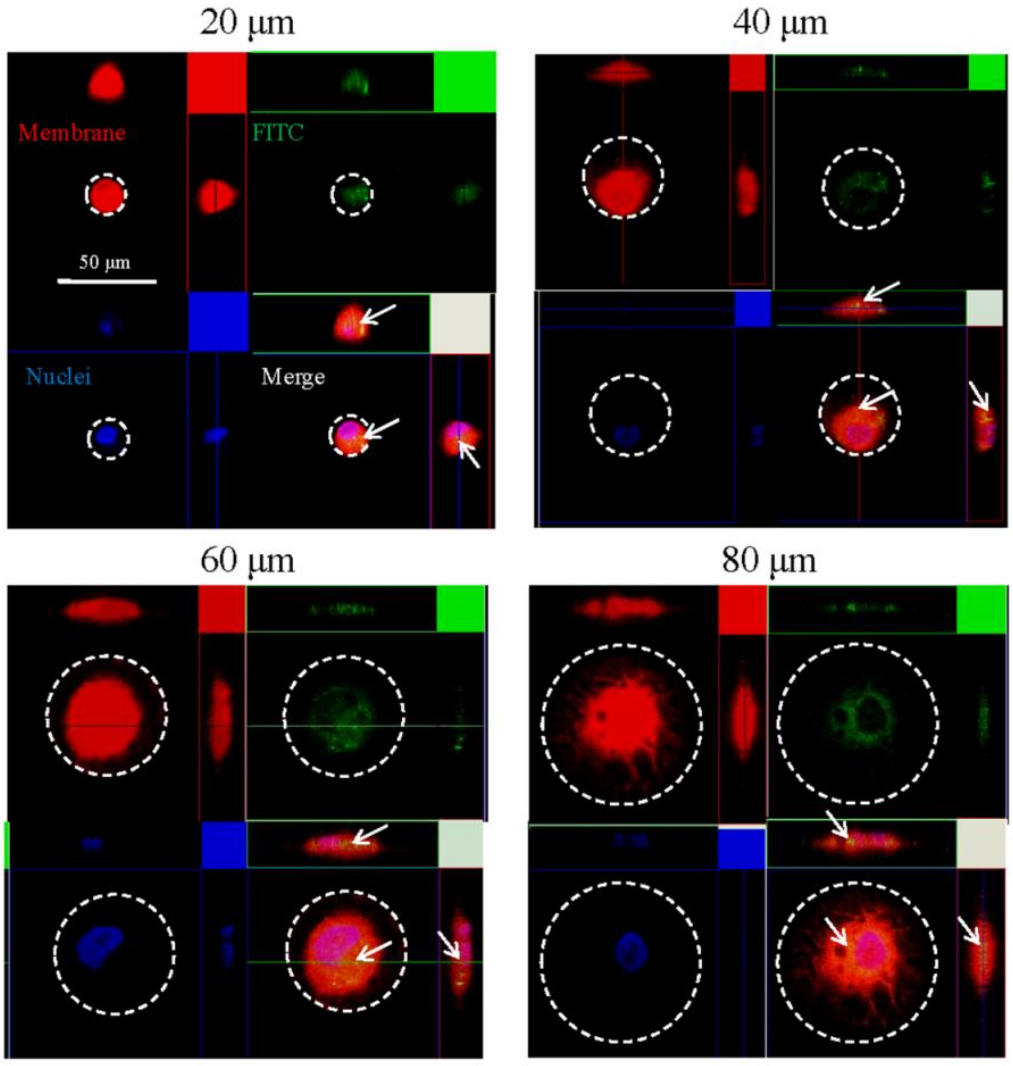

Figure 4.8 Confocal images of the micropatterned MSCs showing cellular uptake of the FITC-PEG-AuNPs after being cultured on the micropatterns with 1.0 nM FITC-PEG-AuNPs for 24 h. Cell membrane was stained red and nucleus was stained blue.

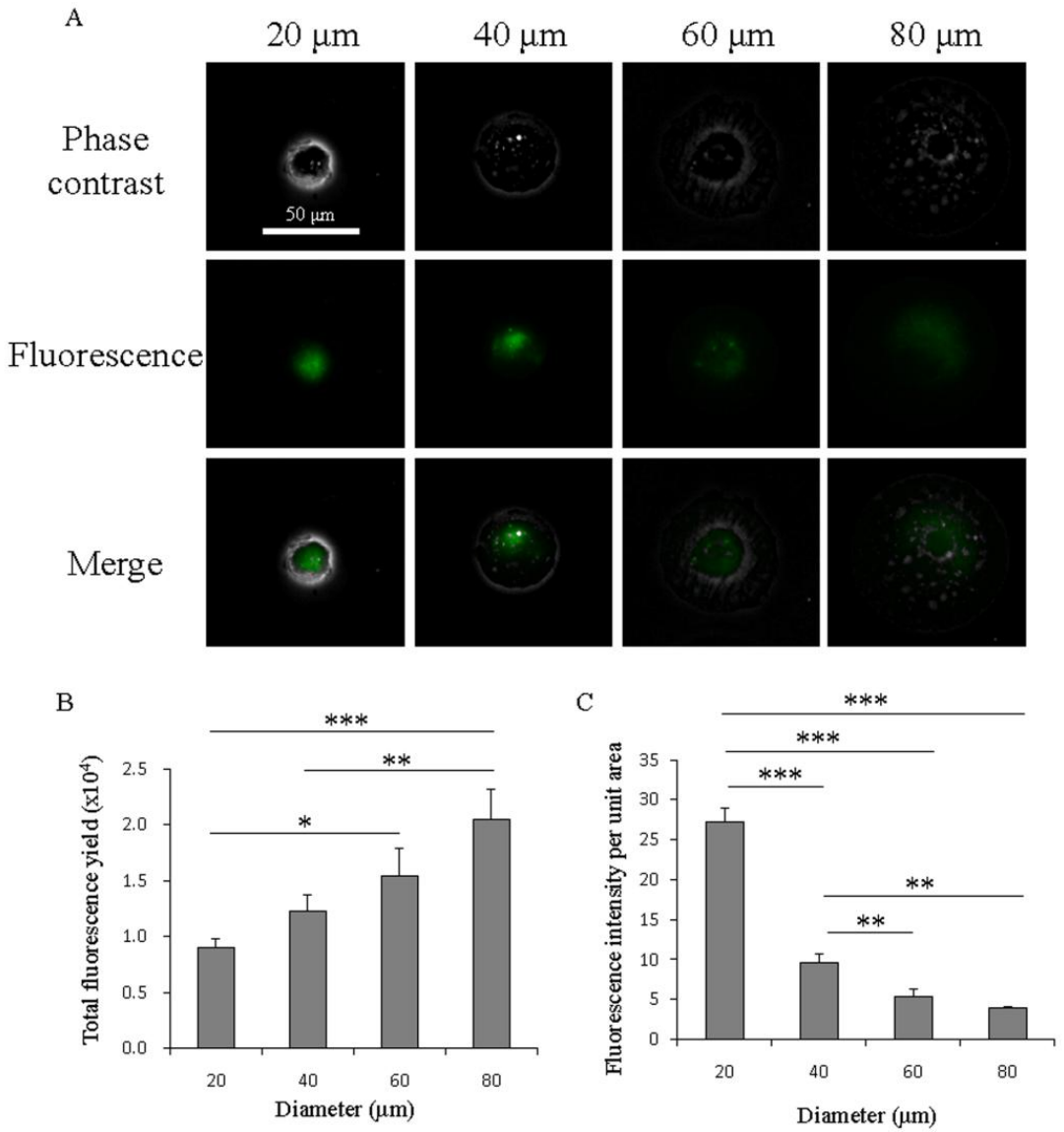

Figure 4.9 Influence of cell size on cellular uptake of the PEG-AuNPs. (A) The phase contrast, fluorescence and merged images of micropatterned MSCs after being cultured on the micropatterns with 1.0 nM FITC-PEG-AuNPs for 24 h. (B) Total fluorescence yield of the micropatterned cells. (C) Average fluorescence intensity per unit projection area of the micropatterned cells. *$p < 0.05$, **$p < 0.01$ and ***$p < 0.001$ ($n = 3$).

Cellular uptake is a complex behavior and many different possible pathways should involve in the process [53]. The size, shape and surface properties of NPs dominated the interactions between NPs and cell membrane (contact area, orientation, etc) which leads the NPs to enter cells through phagocytosis, macropinocytosis, caveolin-dependent, clathrin-dependent, receptor-mediated, non-specific and translocation pathways [54]. Because the PEG layer coated on the surface of NPs can resist protein adsorption, the PEG-AuNPs were likely to be engulfed through non-specific endocytosis.16 Previous studies have reported that the stiffness and topography of substrate could affect non-specific cellular uptake of NPs through regulating cell membrane tension and cell spreading [55,56]. In this study, the cell size was controlled using micropatterns without change of the stiffness and topography of substrate. And all the cells showed round shape that was regulated by the micropatterns. This could exclude the influence of diverse cell shape on cell

functions. It was found that the large cell size facilitated cellular uptake, while high membrane tension inhibited cellular uptake. Large cell size provided large membrane area for NPs adhesion which would enhance cellular uptake efficiency [57]. High membrane tension required high membrane deformation energy during the wrapping of NPs which reduced the cellular uptake efficiency [54]. Furthermore, the cell geometry was controlled in our study which provided a relative stable cytoskeletal network. This enabled us to evaluate the influence of local mechanical state of different cell region on cellular uptake behavior. It was found that NPs mainly accumulated at cell center rather than cell edge in micropatterned cells. And the cellular tension at cell center was lower than that at cell edge. Therefore, it can be concluded that NPs mainly accumulated at low cellular tension region (cell center) rather than at high cellular tension region (cell edge). This also confirmed that high cellular tension may reduce the uptake capacity of NPs.

4.5 Conclusions

In summary, FITC-PEG-AuNPs were synthesized and showed no obvious cytotoxicity to hMSCs at the studied concentration. Photo-reactive PVA micropatterned TCPS surfaces were prepared using UV photolithography and showed good capability to control cell size. Large cells had large contacting areas with AuNPs which enhanced total cellular uptake while their ordered cytoskeletal network induced high membrane tension which reduced average cellular uptake capacity per unit membrane area. Small cells had low total uptake amount but showed high average uptake per unit area. Therefore, the cellular uptake of PEG-AuNPs was positively correlated with cell/NPs contacting area, but negatively correlated with cell membrane tension. The overall effect of cell size on cellular uptake of NPs would be positive since the total uptake amount increased with the increase of cell size.

4.6 References

[1] Xie J, Lee S, Chen X. Nanoparticle-based theranostic agents. Advanced drug delivery reviews. 2010;62:1064-79.
[2] De M, Ghosh PS, Rotello VM. Applications of nanoparticles in biology. Advanced Materials. 2008;20:4225-41.
[3] Stark WJ. Nanoparticles in biological systems. Angewandte Chemie International Edition. 2011;50:1242-58.
[4] Suarez S, Almutairi A, Christman K. Micro-and nanoparticles for treating cardiovascular disease. Biomaterials science. 2015;3:564-80.
[5] Tian Y, Luo S, Yan H, Teng Z, Pan Y, Zeng L, et al. Gold nanostars functionalized with amine-terminated PEG for X-ray/CT imaging and photothermal therapy. Journal of Materials Chemistry B. 2015;3:4330-7.
[6] Loh XJ, Lee T-C, Dou Q, Deen GR. Utilising inorganic nanocarriers for gene delivery. Biomaterials science. 2016;4:70-86.
[7] Ko W-K, Heo DN, Moon H-J, Lee SJ, Bae MS, Lee JB, et al. The effect of gold nanoparticle size on osteogenic differentiation of adipose-derived stem cells. Journal of colloid and interface science. 2015;438:68-76.
[8] Choi SY, Song MS, Ryu PD, Lam ATN, Joo S-W, Lee SY. Gold nanoparticles promote osteogenic differentiation in human adipose-derived mesenchymal stem cells through the Wnt/β-catenin signaling

pathway. International journal of nanomedicine. 2015;10:4383.
[9] Kohl Y, Gorjup E, Katsen-Globa A, Büchel C, von Briesen H, Thielecke H. Effect of gold nanoparticles on adipogenic differentiation of human mesenchymal stem cells. Journal of Nanoparticle Research. 2011;13:6789-803.
[10] Herd H, Daum N, Jones AT, Huwer H, Ghandehari H, Lehr C-M. Nanoparticle geometry and surface orientation influence mode of cellular uptake. ACS nano. 2013;7:1961-73.
[11] Wang C, Sun A, Qiao Y, Zhang P, Ma L, Su M. Cationic surface modification of gold nanoparticles for enhanced cellular uptake and X-ray radiation therapy. Journal of Materials Chemistry B. 2015;3:7372-6.
[12] Gratton SE, Ropp PA, Pohlhaus PD, Luft JC, Madden VJ, Napier ME, et al. The effect of particle design on cellular internalization pathways. Proceedings of the National Academy of Sciences. 2008;105:11613-8.
[13] Voigt J, Christensen J, Shastri VP. Differential uptake of nanoparticles by endothelial cells through polyelectrolytes with affinity for caveolae. Proceedings of the National Academy of Sciences. 2014;111:2942-7.
[14] Tatini F, Landini I, Scaletti F, Massai L, Centi S, Ratto F, et al. Size dependent biological profiles of PEGylated gold nanorods. Journal of Materials Chemistry B. 2014;2:6072-80.
[15] Oh E, Delehanty JB, Sapsford KE, Susumu K, Goswami R, Blanco-Canosa JB, et al. Cellular uptake and fate of PEGylated gold nanoparticles is dependent on both cell-penetration peptides and particle size. Acs Nano. 2011;5:6434-48.
[16] Cho EC, Zhang Q, Xia Y. The effect of sedimentation and diffusion on cellular uptake of gold nanoparticles. Nature nanotechnology. 2011;6:385-91.
[17] Engler AJ, Sen S, Sweeney HL, Discher DE. Matrix elasticity directs stem cell lineage specification. Cell. 2006;126:677-89.
[18] Bartczak D, Muskens OL, Nitti S, Sanchez‐Elsner T, Millar TM, Kanaras AG. Interactions of human endothelial cells with gold nanoparticles of different morphologies. Small. 2012;8:122-30.
[19] Rostam H, Singh S, Vrana N, Alexander M, Ghaemmaghami A. Impact of surface chemistry and topography on the function of antigen presenting cells. Biomaterials science. 2015;3:424-41.
[20] Zhao C, Xia L, Zhai D, Zhang N, Liu J, Fang B, et al. Designing ordered micropatterned hydroxyapatite bioceramics to promote the growth and osteogenic differentiation of bone marrow stromal cells. Journal of Materials Chemistry B. 2015;3:968-76.
[21] Schvartzman M, Palma M, Sable J, Abramson J, Hu X, Sheetz MP, et al. Nanolithographic control of the spatial organization of cellular adhesion receptors at the single-molecule level. Nano letters. 2011;11:1306-12.
[22] Dalby MJ, Gadegaard N, Tare R, Andar A, Riehle MO, Herzyk P, et al. The control of human mesenchymal cell differentiation using nanoscale symmetry and disorder. Nature materials. 2007;6:997-1003.
[23] Higuchi A, Ling Q-D, Kumar SS, Chang Y, Alarfaj AA, Munusamy MA, et al. Physical cues of cell culture materials lead the direction of differentiation lineages of pluripotent stem cells. Journal of Materials Chemistry B. 2015;3:8032-58.
[24] Yang C, Tibbitt MW, Basta L, Anseth KS. Mechanical memory and dosing influence stem cell fate. Nature materials. 2014;13:645.
[25] Yang X, Xu T. Molecular mechanism of size control in development and human diseases. Cell research. 2011;21:715-29.
[26] Li J, Cai R, Kawazoe N, Chen G. Facile preparation of albumin-stabilized gold nanostars for the targeted photothermal ablation of cancer cells. Journal of Materials Chemistry B. 2015;3:5806-14.

[27] Gao J, Huang X, Liu H, Zan F, Ren J. Colloidal stability of gold nanoparticles modified with thiol compounds: bioconjugation and application in cancer cell imaging. Langmuir. 2012;28:4464-71.
[28] Zhang Z, Van Steendam K, Maji S, Balcaen L, Anoshkina Y, Zhang Q, et al. Tailoring Cellular Uptake of Gold Nanoparticles Via the Hydrophilic‐to‐Hydrophobic Ratio of their (Co) polymer Coating. Advanced Functional Materials. 2015;25:3433-9.
[29] Giljohann DA, Seferos DS, Daniel WL, Massich MD, Patel PC, Mirkin CA. Gold nanoparticles for biology and medicine. Angewandte Chemie International Edition. 2010;49:3280-94.
[30] Islam MA, Reesor EK, Xu Y, Zope HR, Zetter BR, Shi J. Biomaterials for mRNA delivery. Biomaterials science. 2015;3:1519-33.
[31] Walkey CD, Olsen JB, Guo H, Emili A, Chan WC. Nanoparticle size and surface chemistry determine serum protein adsorption and macrophage uptake. Journal of the American Chemical Society. 2012;134:2139-47.
[32] Fratoddi I, Venditti I, Cametti C, Russo M. Gold nanoparticles and gold nanoparticle-conjugates for delivery of therapeutic molecules. Progress and challenges. Journal of Materials Chemistry B. 2014;2:4204-20.
[33] Larson TA, Joshi PP, Sokolov K. Preventing protein adsorption and macrophage uptake of gold nanoparticles via a hydrophobic shield. Acs Nano. 2012;6:9182-90.
[34] Kawazoe N, Chen G. Gold nanoparticles with different charge and moiety induce differential cell response on mesenchymal stem cell osteogenesis. Biomaterials. 2015;54:226-36.
[35] Wang X, Nakamoto T, Dulińska-Molak I, Kawazoe N, Chen G. Regulating the stemness of mesenchymal stem cells by tuning micropattern features. Journal of Materials Chemistry B. 2016;4:37-45.
[36] Mao H, Li J, Dulińska-Molak I, Kawazoe N, Takeda Y, Mamiya H, et al. Cellular effects of magnetic nanoparticles explored by atomic force microscopy. Biomaterials science. 2015;3:1284-90.
[37] Rejman J, Oberle V, Zuhorn IS, Hoekstra D. Size-dependent internalization of particles via the pathways of clathrin-and caveolae-mediated endocytosis. Biochemical Journal. 2004;377:159-69.
[38] Burgess A, Vigneron S, Brioudes E, Labbé J-C, Lorca T, Castro A. Loss of human Greatwall results in G2 arrest and multiple mitotic defects due to deregulation of the cyclin B-Cdc2/PP2A balance. Proceedings of the National Academy of Sciences. 2010;107:12564-9.
[39] Shuaidong H, Ma H, Huang K, Liu J, Wei T, Jin S, et al. Superior penetration and retention behavior of 50 nm gold nanoparticles in tumors. Cancer Research. 2012:canres. 2071.12.
[40] Kettler K, Veltman K, van de Meent D, van Wezel A, Hendriks AJ. Cellular uptake of nanoparticles as determined by particle properties, experimental conditions, and cell type. Environmental Toxicology and Chemistry. 2014;33:481-92.
[41] Chithrani BD, Ghazani AA, Chan WC. Determining the size and shape dependence of gold nanoparticle uptake into mammalian cells. Nano letters. 2006;6:662-8.
[42] Wang X, Song W, Kawazoe N, Chen G. Influence of cell protrusion and spreading on adipogenic differentiation of mesenchymal stem cells on micropatterned surfaces. Soft Matter. 2013;9:4160-6.
[43] Wang X, Song W, Kawazoe N, Chen G. The osteogenic differentiation of mesenchymal stem cells by controlled cell–cell interaction on micropatterned surfaces. Journal of Biomedical Materials Research Part A. 2013;101:3388-95.
[44] Vallenius T. Actin stress fibre subtypes in mesenchymal-migrating cells. Open biology. 2013;3:130001.
[45] Tee YH, Shemesh T, Thiagarajan V, Hariadi RF, Anderson KL, Page C, et al. Cellular chirality arising from the self-organization of the actin cytoskeleton. Nature cell biology. 2015;17:445-57.
[46] Tay CY, Wu Y-L, Cai P, Tan NS, Venkatraman SS, Chen X, et al. Bio-inspired micropatterned hydrogel

to direct and deconstruct hierarchical processing of geometry-force signals by human mesenchymal stem cells during smooth muscle cell differentiation. NPG Asia Materials. 2015;7:e199.
[47] Stricker J, Falzone T, Gardel ML. Mechanics of the F-actin cytoskeleton. Journal of biomechanics. 2010;43:9-14.
[48] Hotulainen P, Lappalainen P. Stress fibers are generated by two distinct actin assembly mechanisms in motile cells. The Journal of cell biology. 2006;173:383-94.
[49] Titushkin I, Cho M. Distinct membrane mechanical properties of human mesenchymal stem cells determined using laser optical tweezers. Biophysical journal. 2006;90:2582-91.
[50] Nambiar R, McConnell RE, Tyska MJ. Control of cell membrane tension by myosin-I. Proceedings of the National Academy of Sciences. 2009;106:11972-7.
[51] Lieber AD, Yehudai-Resheff S, Barnhart EL, Theriot JA, Keren K. Membrane tension in rapidly moving cells is determined by cytoskeletal forces. Current Biology. 2013;23:1409-17.
[52] Roca-Cusachs P, Alcaraz J, Sunyer R, Samitier J, Farré R, Navajas D. Micropatterning of single endothelial cell shape reveals a tight coupling between nuclear volume in G1 and proliferation. Biophysical journal. 2008;94:4984-95.
[53] Doherty GJ, McMahon HT. Mechanisms of endocytosis. Annual review of biochemistry. 2009;78:857-902.
[54] Zhang S, Gao H, Bao G. Physical principles of nanoparticle cellular endocytosis. ACS nano. 2015;9:8655-71.
[55] Huang C, Butler PJ, Tong S, Muddana HS, Bao G, Zhang S. Substrate stiffness regulates cellular uptake of nanoparticles. Nano letters. 2013;13:1611-5.
[56] Huang C, Ozdemir T, Xu C, Butler PJ, Siedlecki C, Brown JL et al. The role of topography on the cellular uptake of nanoparticles. Journal of Biomedical Materials Research Part B. 2016;104:488-95.
[57] Lesniak A, Salvati A, Santos-Martinez MJ, Radomski MW, Dawson KA, Åberg C. Nanoparticle adhesion to the cell membrane and its effect on nanoparticle uptake efficiency. Journal of the American Chemical Society. 2013;135:1438-44.

Chapter 5

Independent influence of cell adhesion and spreading area on stem cell fate determination

5.1 Summary

In this chapter, the micropatterns were prepared to provide the same spreading area and different adhesion area or different spreading area and the same adhesion area to precisely control the cell adhesion and spreading separately. The results showed that adhesion area had more significant influences on stem cell functions including differentiation than did the spreading area. This study should provide new insight of the influence of cell adhesion and spreading on cell functions and inspire the design of new functional materials and devices to process in an effective manner for manipulation of cell functions.

5.2 Introduction

As the basic behaviors of anchorage-dependent cells, adhesion and spreading play crucial roles in regulating cell functions including migration [1-4], proliferation [5,6] and differentiation [7-11]. When cells attach to a surface, they initially bind to the extracellular matrix (ECM) molecules adsorbed on the surface through integrin receptors [12]. Lateral clustering of the integrin receptors, together with other associated proteins, leads to the formation of focal adhesions (FAs) that constitute a structural link between the cytoskeleton and the ECM [13]. The FAs can respond to biochemical and biophysical stimulus by initiating a cascade of events including cytoskeleton reorganization which results in outside-in signaling activities [14]. In the meantime, the cytoskeletal force also affects the formation of FAs and is exerted to outside through the adhesion site to give feedback to their microenvironment [15]. As a consequence, the cell adhesion and spreading were manipulated by the cell/ECM interactions. Many studies have reported that the physical properties of ECM including geometry [16,17], anisotropy [18], topography [19,20] and rigidity [21,22] can influence the mechanosensing of the microenvironment through regulating cell adhesion and spreading. However, it is unclear whether cell adhesion or spreading is the predominant factor to influence cell functions because it has been difficult to separate the two effects by conventional cell culture using uniform surfaces.

To discriminate the influence of adhesion and spreading on cell functions, the micropatterning technology is needed because conventional ECM coating method results in parallel changes of cell adhesion and spreading areas. Several previous studies using micropatterned surfaces have reported controversial results on independent influence of adhesion and spreading areas to cell functions [23-26]. The controversially observed phenomena require further detailed investigation to reveal the influence of cell adhesion and spreading on cell functions. Meanwhile, how the differentiation, the most attractive point of stem cell research, is influenced by adhesion and spreading areas remains unclear. In this study, the independent influence of adhesion and spreading area on differentiation of human mesenchymal stem cells (MSCs) was investigated by using micropatterning method to precisely control cell adhesion and spreading areas. A series of micropatterns having the same size and different cell adhesion area or having different size and the same cell adhesion area were prepared by UV photolithography for cell culture. The formation of FAs and the cytoskeletal organization in the cells cultured on the micropatterns were investigated to evaluate cell adhesion and spreading state. The mechanical properties of micropatterned cells and the transduction of cytoskeletal force into nucleus were characterized to reveal the mechanism of the influence. The osteogenic and adipogenic differentiation of MSCs were investigated to show how the adhesion and spreading areas independently influenced cell fate determination (Figure 5.1).

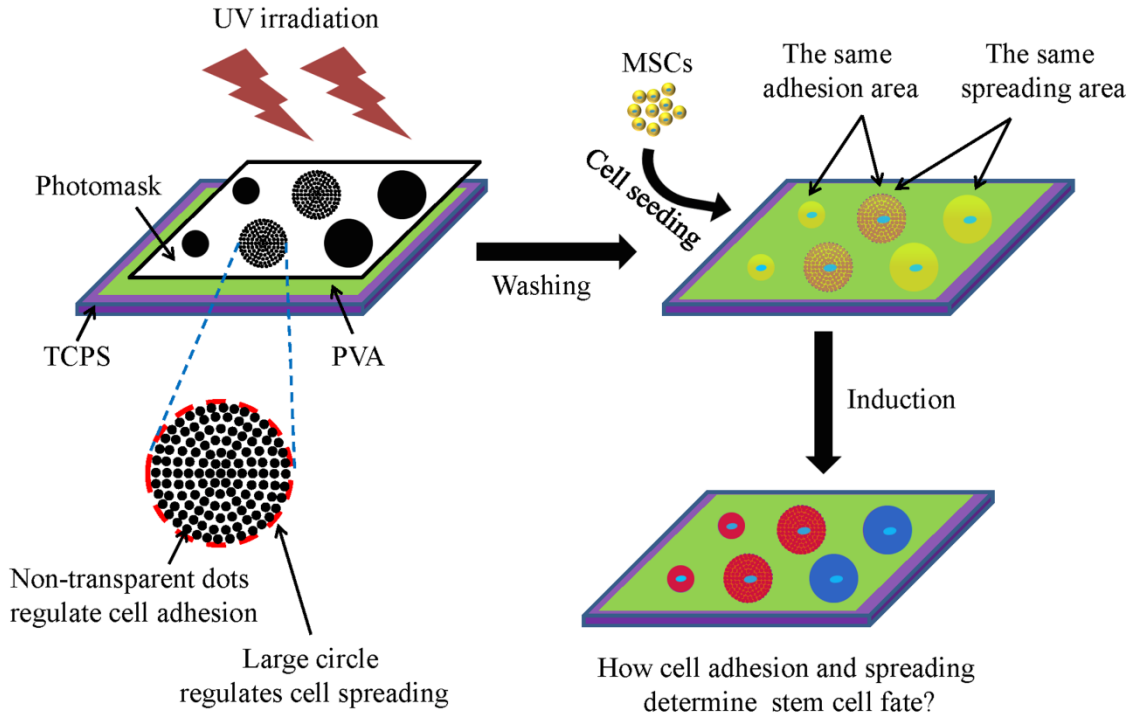

Figure 5.1 Schematic illustration of this study. Photo-reactive PVA micropatterned TCPS surfaces were prepared using UV photolithography. The designed photomask contains the circles composed of numerous non-transparent microdots. The area of the circle represents cell spreading area, while the sum area of non-transparent microdots represents cell adhesion area. Micropatterned MSCs are induced into adipogenic and osteogenic differentiation to investigate the influence of cell adhesion and spreading on stem cell fate determination.

5.3 Materials and methods

5.3.1 Preparation and characterization of the micropatterns

The synthesis process of photo-reactive PVA, preparation scheme of the PVA micropatterned TCPS surfaces and AFM scanning of the micropatterns were performed in the same way as described in Chapter 2.3.2.

To enhance cell adhesion and guarantee cell spreading, the sterilized micropatterns were incubated with 20 μg/ml fibronectin (Sigma-Aldrich) in NaHCO3 (pH = 8.4) solution for 1 h followed by exhaustive washing in NaHCO3 and aseptic water. To confirm the adsorption of fibronectin, the coated micropatterns were incubated with mouse anti-fibronectin (1:100, Santa Cruz Biotechnology) at 4 ℃ overnight. And then the micropatterns were washed and incubated with Alexa Fluor-488 labeled goat anti-mouse IgG antibody (1:800, Invitrogen) at room temperature for 1 h. The fluorescence images were observed with an Olympus BX51 microscope with a DP-70 CCD camera (Olympus, Tokyo, Japan).

5.3.2 Cell culture

Human bone marrow-derived MSCs were purchased from Osiris Therapeutics, Inc. (Columbia, MA) and subcultured in MSCGM medium (MSCBM supplemented with 10% serum, 2% L-glutamine and 0.1% gentamicin sulfate amphotericin b, Lonza Group Ltd.). The fibronectin coated micropatterns were put in 6-well plates and a glass ring (inner diameter 1.5 cm) was placed over each micropattern plate. An aliquot of 3 mL serum-free medium (DMEM medium supplemented with 4500 mg/L glucose, 584 mg/L glutamine, 100 U/mL penicillin, 100 μg/mL streptomycin, 0.1 mM nonessential amino acids, 0.4 mM proline, 50 mg/L ascorbic acid) was added to each well. And then 200 μL cell suspension solution (2.7 x 104 cells/mL in serum-free DMEM medium) was added within the glass ring (3000 cells/cm2). After 6 h culture for cell attachment, the glass rings were taken out and the medium was changed to serum-containing medium for cytoskeleton development. Before medium change, cell morphology was observed by an optical microscope. After another 18h culturein serum medium (totally 24 h), the samples were used for immunofluorescence staining and cell mechanical test.

5.3.3 Immunofluorescence staining

After 24 h culture, the cells were fixed with 4% cold paraformaldehyde for 10 min. For visualization of F-actin filaments and vinculin, cells were treated with 1% Triton X-100 and 0.02% Tween-20 for 30 min. After PBS washing, the samples were blocked with 1% bovine serum albumin (BSA) in PBS for 30 min at room temperature. The samples were then incubated with the diluted mouse anti-vinculin antibodies (Merck Millipore, 1:100 in Can Get Signal solution) at 37 °C for 1.5 h followed by washing with 0.02% Tween-20 for three times. Finally the samples were incubated with Alexa Fluor-488 labeled goat anti-mouse IgG antibody (Invitrogen, 1:800) and Alexa Fluor-594 phalloidin (Invitrogen, 1:40) at 37 °C for 1 h for visualization. For myosin staining, the fixed cells were permeated with 1% Triton X-100 and blocked with 1% BSA solution for 30 min. The samples were incubated with rabbit anti-myosin IIA antibody (1:100, Sigma) at 4 °C overnight followed by PBS washing. And then the labeling was performed with Alexa Fluor-488 labeled donkey anti-rabbit IgG antibody (1:800, Invitrogen) and Alexa Fluor-594

phalloidin (Invitrogen, 1:40) at room temperature for 1 h. For YAP/TAZ staining, the fixed cells were permeated with 1% Triton X-100 and blocked with 1% BSA solution for 30 min. The samples were incubated with mouse anti-YAP/TAZ (1:50, Santa Cruz Biotechnology) at 4 °C overnight followed by PBS washing. Secondary antibody labeling was performed with Alexa Fluor-488 labeled goat anti-mouse IgG antibody (1:800, Invitrogen) at room temperature for 1 h. Nuclei were stained with DAPI. Fluorescence micrographs of the stained cells were captured using an Olympus BX51 microscope with a DP-70 CCD camera (Olympus, Tokyo, Japan).

5.3.4 Image analysis

The vinculin and F-actin staining images were analyzed using an ImageJ software according to previous report [28]. Firstly, the obtained fluorescence images were converted to 16 bit images. And then the images were processed with the following commands including 'subtracting background', 'enhancing local contrast', 'minimizing background' and 'adjusting brightness and contrast'. After that, the 'Laplacian of Gaussian or Mexican Hat filter' (available at: http://bigwww.epfl.ch/sage/soft/LoG3D) and 'threshold' command was run to get the final processed images (Figure 5.2). Finally, 'analyze particles' command was executed to calculate the focal adhesion area. The thickness of actin filaments was analyzed based on their fluorescence intensity. Gray plot profile was processed across the filaments and fitted with Gaussian fitting. The full width at half maximum was considered as the thickness of the actin filaments (Figure 5.3).

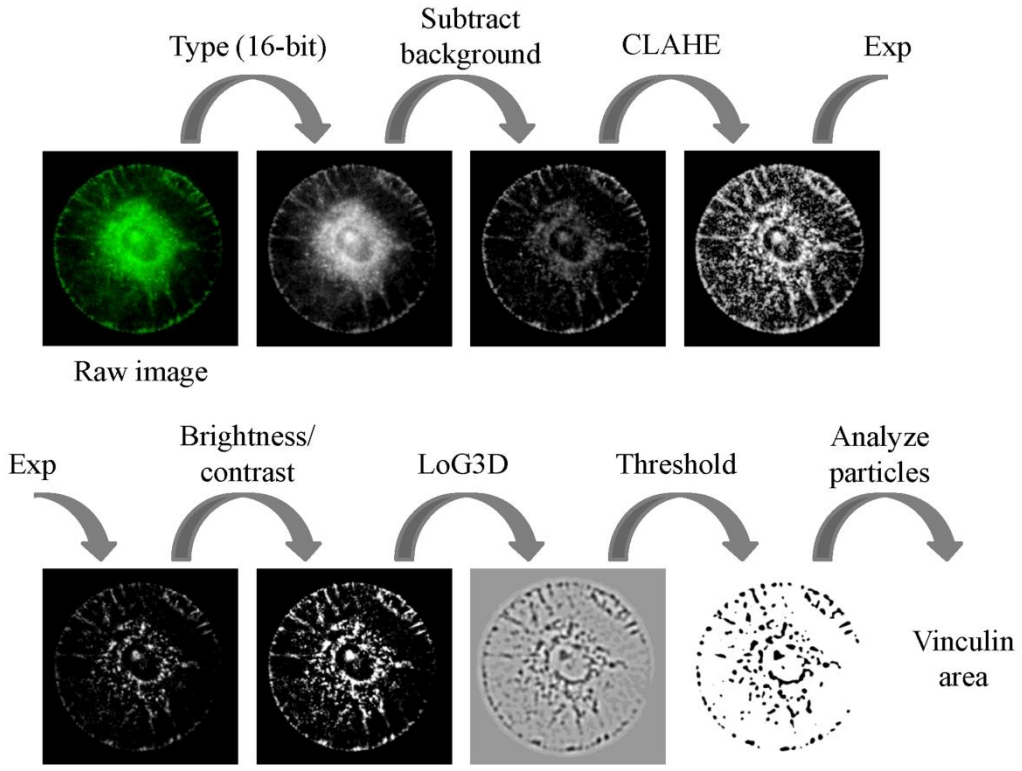

Figure 5.2 Scheme of the analysis process to calculate vinculin area.

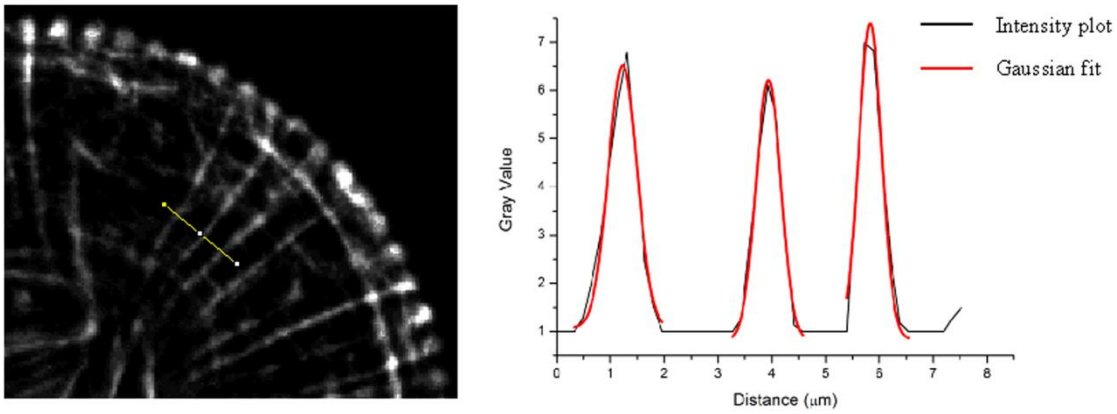

Figure 5.3 Analysis of the thickness of actin fibers. Gray intensity plot of the actin fibers (right) was processed along the yellow lines (left). The intensity plot (black) was fitted to Gaussian distribution (red) to evaluate the thickness of the actin fibers.

5.3.5 Atomic force microscopy measurement

The cytoskeletal tension of living MSCs with various adhesion and spreading areas was evaluated using a commercially available MFP-3D-BIO AFM instrument in a force mode. A silicon nitride cantilever (Novascan, Ames, USA) coated with reflective gold was used for the AFM nanoindentation. At the end of the cantilever, there was a probe made of a silica glass ball with a diameter of 600 nm. An optical microscope was used to visualize the samples and the position of AFM tip. The exact spring constant of the cantilever was measured using the thermal tuning method [29]. The trigger force was set to 2 nN to avoid any damage to the cell surface. The force versus distance curves were collected at the highest region of cells at an indentation rate of 4 μm/s.

The obtained force curves were fitted to Hertz's contact model to calculate the Young's modulus of cells. Since the probe was a spherical ball, the parabolic model was used for calculation. The relationship between the loading force F and the indentation δ can be described in formula of:

$$F(\delta) = \frac{4}{3} \cdot \sqrt{R} \cdot E_r \cdot \delta^{3/2} \qquad (1)$$

where R is the radius of the tip and Er is the reduced Young's modulus. In this study, the Young's modulus of cells was calculated at 200 nm indentation depth where was reported to be abundant of actin network [30]. The reduced Young's modulus Er correlates with the Young's modulus of sample Es and is given by:

$$\frac{1}{E_r} = \frac{1-\nu_t^2}{E_t} + \frac{1-\nu_s^2}{E_s} \qquad (2)$$

where νt and νs are the Poisson ratios of tips and samples. Since the Young's modulus of tips material (SiO2) is much greater than that of living cells, equation (2) can be simplified as following:

$$E_r = \frac{E_s}{1-\nu_s^2} \qquad (3)$$

The Poisson ratio of cell is assumed to be 0.5 [31].

Ten force curves were collected from each cell. Twenty cells on each micropattern were measured to evaluate the average stiffness of the cell population. Each measurement was performed within a maximum of 1.5 hours to minimize the death of cells during the experiment.

5.3.6 Osteogenic and adipogenic differentiation of micropatterned MSCs

After 1 d culture, the growth medium was replaced by osteogenic and adipogenic induction medium, respectively. The osteogenic induction medium was prepared by supplementing the DMEM medium with 1000 mg/L glucose, 584 mg/L glutamine, 100 U/mL penicillin, 100 μg/mL streptomycin, 0.1mM nonessential amino acids, 50 mg/L ascorbic acid, 10% FBS, 100 nM dexamethasone and 10 mM β-glycerophosphate disodium salt hydrate. The adipogenic induction medium was DMEM medium supplemented 4500 mg/L glucose, 584 mg/L glutamine, 100 U/mL penicillin, 100 μg/mL streptomycin, 0.1 mM nonessential amino acids, 0.4 mM proline, 50 mg/L ascorbic acid, 10% FBS, 1 μM dexamethasone, 0.5 mM methylisobutylxanthine, 10 μg/mL insulin and 100 μM indomethacin. The induction medium was changed every 3 d. The induction culture was continued for 2 weeks.

5.3.7 Osteogenic and adipogenic analysis

After 2 weeks induction, the samples were fixed with 4% cold paraformaldehyde for 10 min at room temperature. The alkaline phosphatase (ALP) activity was examined by staining method to evaluate the osteogenesis of MSCs. To perform ALP staining, the fixed cells were soaked in 0.1 wt% naphthol AS-MX phosphate (Sigma) and 0.1 wt% Fast Blue RR salt (Sigma) in 56 mM 2-amino-2-methyl-1,3-propanediol (pH 9.9, Sigma) for 10 min at room temperature followed by PBS washing. The fat droplets which can be stained by Oil Red O was chosen as the maker of adipogenic differentiated MSCs. To perform Oil Red O staining, cells were firstly immersed in 60% isopropanol for 5 min and then stained with fresh Oil Red O working solution for 5 min. The Oil Red O working solution was prepared by mixing three parts 0.3% Oil Red O in isopropanol (stock solution) with two parts Milli-Q water and filtering through a 0.2 μm filter. After staining, samples were observed using an optical microscope with a DP-70 CCD camera (Olympus, Tokyo, Japan). Cells positive for ALP or fat droplets were considered as osteogenically or adipogenically differentiated. The probability of osteogenic or adipogenic differentiation of MSCs on different micropatterns was investigated by calculating the percentage of differentiated MSCs to the total cells. Three parallel experiments were carried out to calculate the means and standard deviations (SDs).

5.3.8 Statistical analysis

The data was presented as means ± SDs. Statistical analysis was performed using a one-way analysis of variance (ANOVA) with Tukey's post hoc test for multiple comparisons to confirm the significant differences among samples. A value of $p < 0.05$ was considered to indicate statistically significant difference.

5.4 Results

5.4.1 Preparation and observation of the micropatterns

The micropatterns were prepared by micropatterning non-adhesive PVA on cell adhesive TCPS surface. Upon UV irradiation, the photo-reactive PVA under the transparent part of the photomask was corsslinked and grafted to the TCPS surface, while those under the non-transparent microdots of the

photomask remained un-reacted and were washed away by ultrasonic washing. The micropattern structures were designed and prepared to control cell adhesion area and cell spreading area separately. Totally ten kinds of micropatterns were prepared. Four from the ten micropatterns were micropatterned TCPS round circles having a diameter of 70, 60, 50 and 40 μm that are shown in dark in Figure 5.4. The dark region in Figure 5.4 was TCPS while white region was PVA. The other six micropatterns were composed of many TCPS microdots having a diameter of 2 μm in a round circle having a diameter of 70, 60 and 50 μm. The TCPS microdots and round circles were surrounded by PVA. Each row of the micropatterns in Figure 5.4 had the same size of round circle. The four rows of micropatterns had the round circles with a diameter of 70, 60, 50 and 40 μm and corresponding area of 3846, 2826, 1962 and 1256 μm^2, respectively. However, the total area of TCPS region (cell adhesion region) of each micropattern in the same row was different. The cells in the same row should have the same spreading area but different adhesion area. The four columns of the micropatterns had a total TCPS area of 3846, 2826, 1962 and 1256 μm^2, respectively. The circle size of each micrpattern in the same column was different. The cells in micropatterns of the same column should have the same adhesion area but different spreading area.

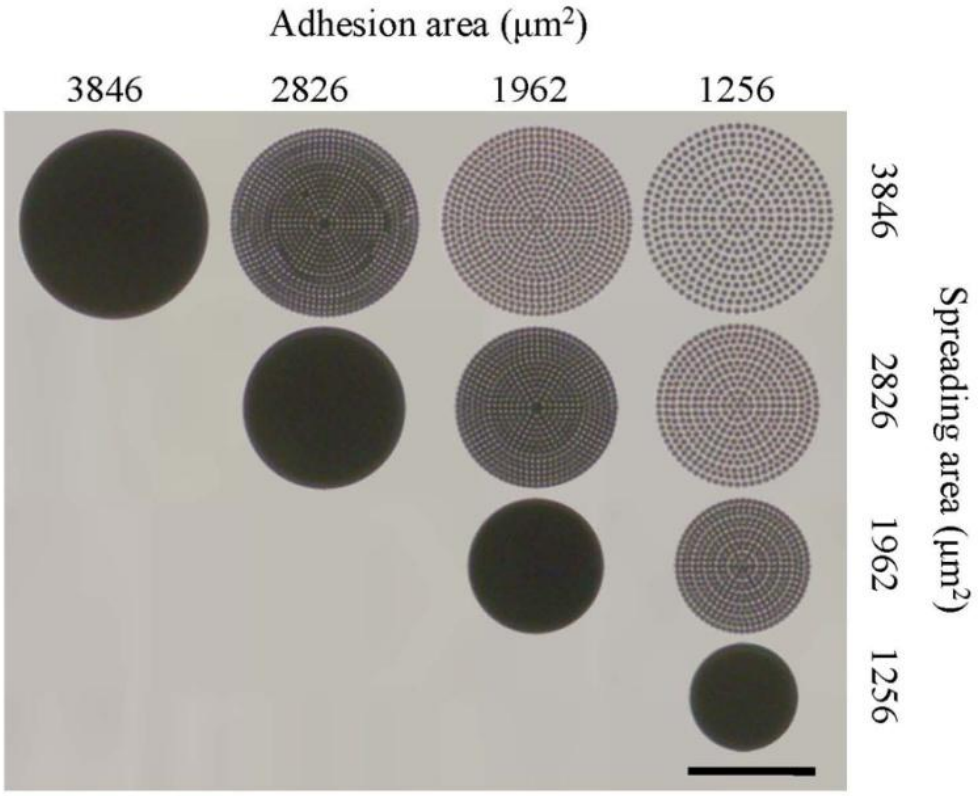

Figure 5.4 Phase-contrast images of the photomasks designed to provide various cell adhesion and spreading areas. Scale bar: 50 μm.

The typical AFM scanning images of a circle with a diameter of 70 μm (an area of 3846 μm^2) and the total TCPS area of 1256 μm^2 are shown in Figure 5.5a and b. The size of both large circle and small microdot were nearly the same as the designed values indicating the good controllability of the micropatterning method. The PVA layer had an average thickness of 57.8 ± 8.9 nm. After preparation of the micropatterns, fibronectin was coated on the TCPS regions. PVA is a hydrophilic polymer that can protect protein adsorption and cell adhesion [32]. Selective adsorption of fibronectin on the TCPS regions was

confirmed by immunological staining of adsorbed fibronectin. The green fluorescence in Figure 5.5c showed the adsorbed fibronectin on the micropatterned TCPS regions. Therefore, the fibronectin coated PVA micropatterned TCPS micropatterns with various adhesion and spreading areas were prepared using UV photolithography.

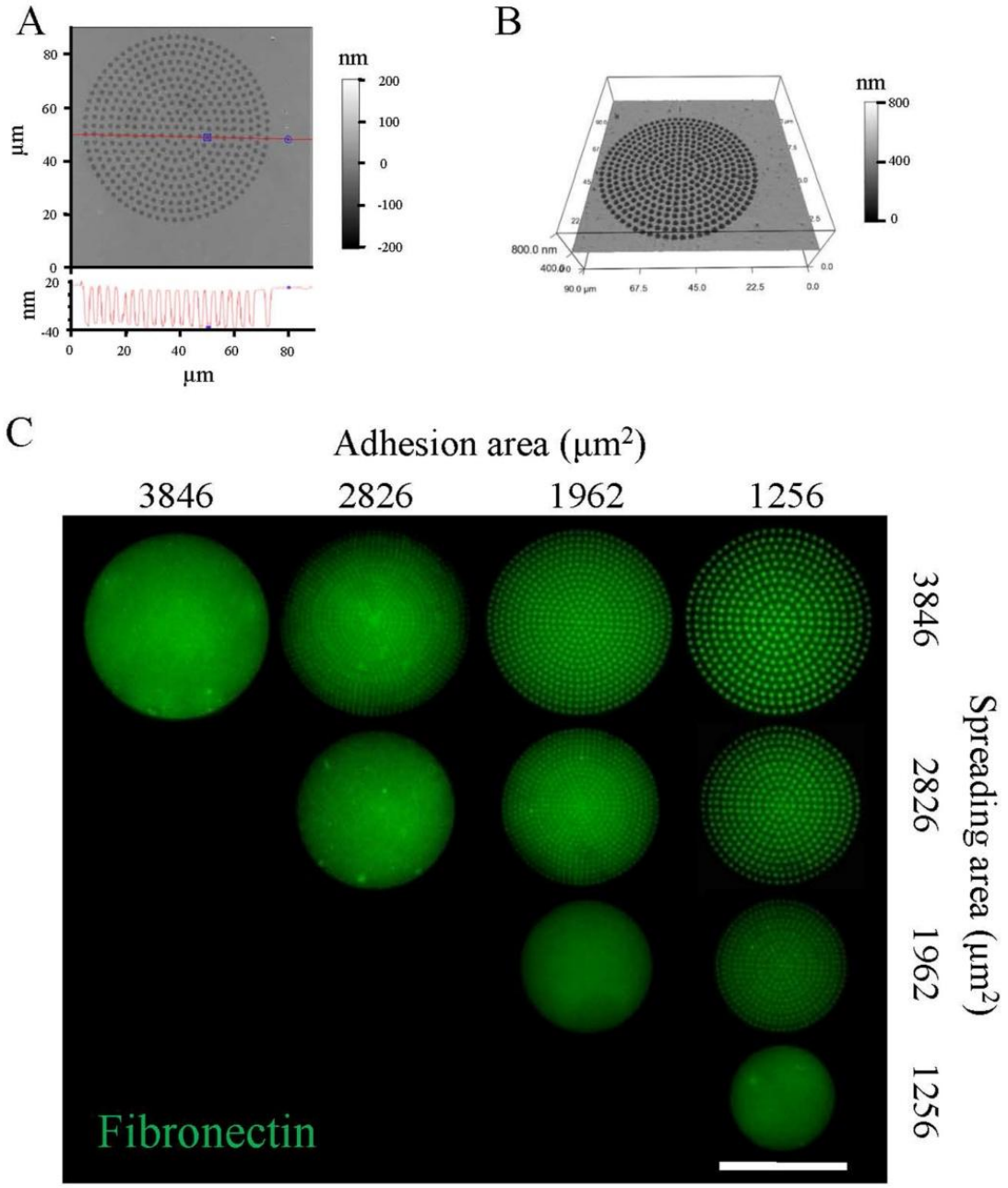

Figure 5.5 Characterization of the micropatterned TCPS surfaces. (a) The height images (up) and section view (down) of a micropattern with a diameter of 70 µm (an area of 3846 µm2) and the total TCPS area of 1256 µm2. The images were scanned by AFM. (b) 3D view of the micropattern shown in b. (c) The immunofluorescence staining images of the fibronectin coated micropatterns. Fibronectin adsorbed onto the TCPS surface but not on the PVA surface. Scale bar: 50 µm.

5.4.2 Cell focal adhesion formation mainly regulated by adhesion area

Human bone marrow-derived MSCs were cultured on the micropatterns. MSCs adhered on the micropatterns and showed round morphology as that of the underlying micropatterns (Figure 5.6). Most of the micropatterns were occupied by single MSCs. The spreading area of MSCs was controlled by the size of each round circle of the micropatterns. The adhesion area of MSCs was controlled by the total area of fibronectin coated TCPS microdots. The MSCs on each row of micropatterns had the same spreading area but different adhesion area. The MSCs on each column of micropatterns had the same adhesion area but different spreading area. The spreading area and adhesion area of MSCs were precisely controlled by the micropatterns.

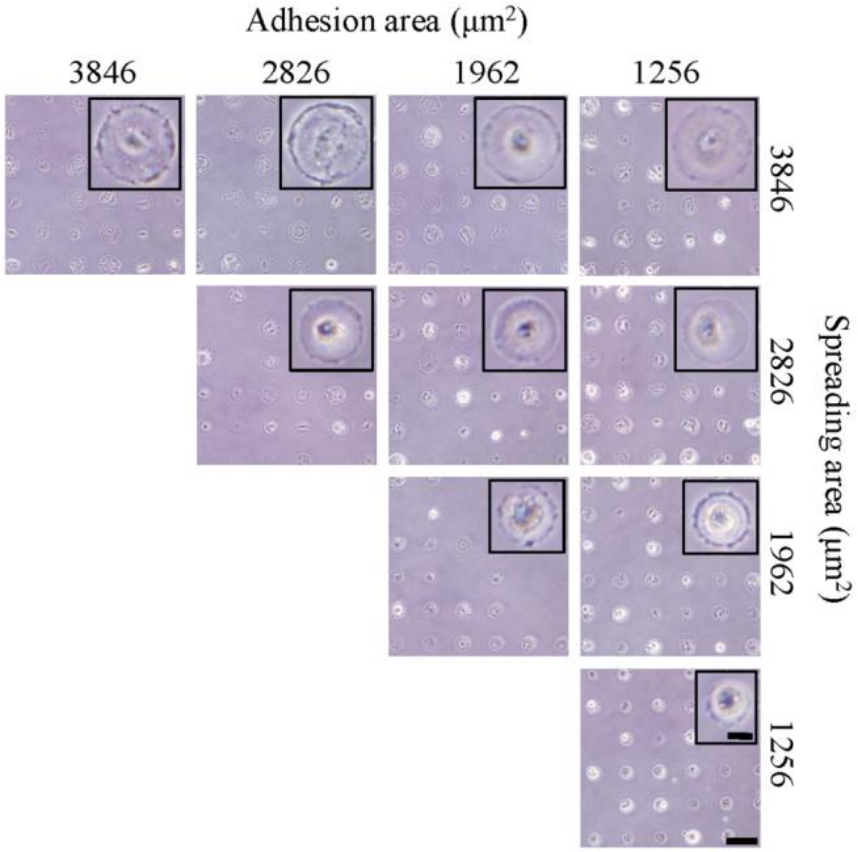

Figure 5.6 Cell attachment after being cultured on micropatterned surfaces in serum-free medium for 6h. Insert is the high magnification of representative image of attached cells. The cell morphology was well controlled by the micropatterns. Scale bar: 100 μm; insert scale bar: 20 μm.

Vinculin was stained to check the focal adhesions (FAs) formation of MSCs on the micropatterns (Figure 5.7).When cell spreading area was the same (each row), MSCs with large adhesion area formed more obvious FAs at the region under main cell body than did the cells with small adhesion area. When cell adhesion area was the same (each column), MSCs with large spreading area formed more obvious FAs at cell periphery region than did the cells with small spreading area. The staining images were further processed using the ImageJ software to identify the FAs level (Figure 5.8). Semi-quantitative analysis of FAs revealed that the average size of FAs increased with increase of spreading areas (Figure 5.9a). However, the total area of FAs slightly but not significantly increased with increase of spreading area (Figure 5.9b). Increasing cell adhesion area caused significant increase of both average size and total area of FAs. The results indicated

that the average size of FAs was influenced by both adhesion and spreading area, but the total area of FAs was determined mainly by the available cell adhesion area rather than the spreading area.

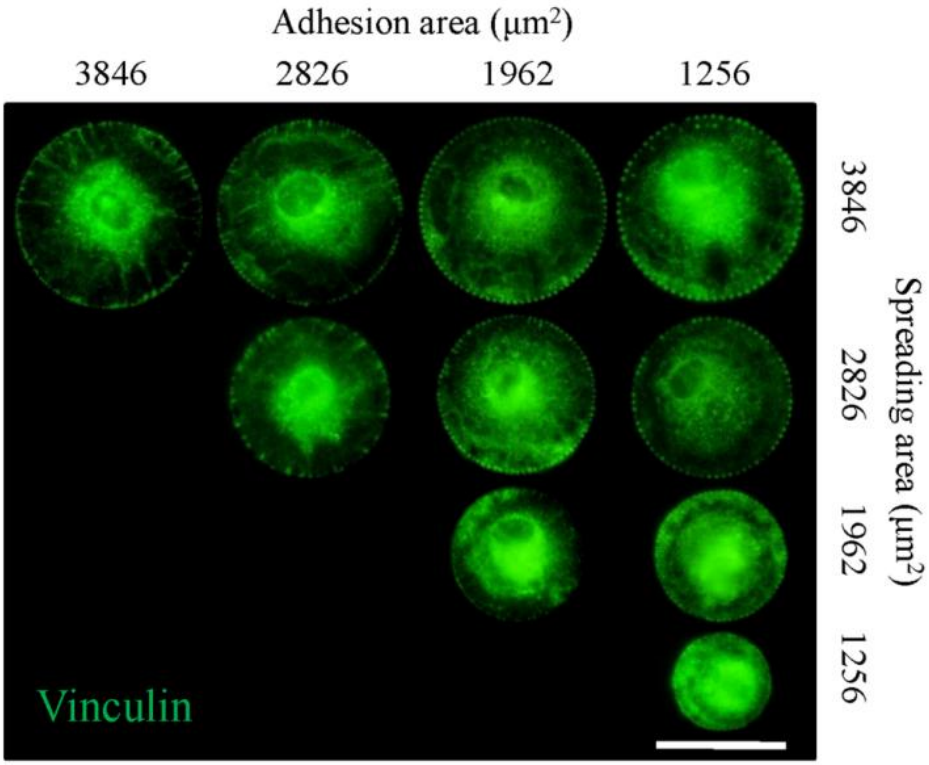

Figure 5.7 Vinculin staining images (green) of micropatterned cells with different adhesion and spreading areas. Scale bar: 50 μm.

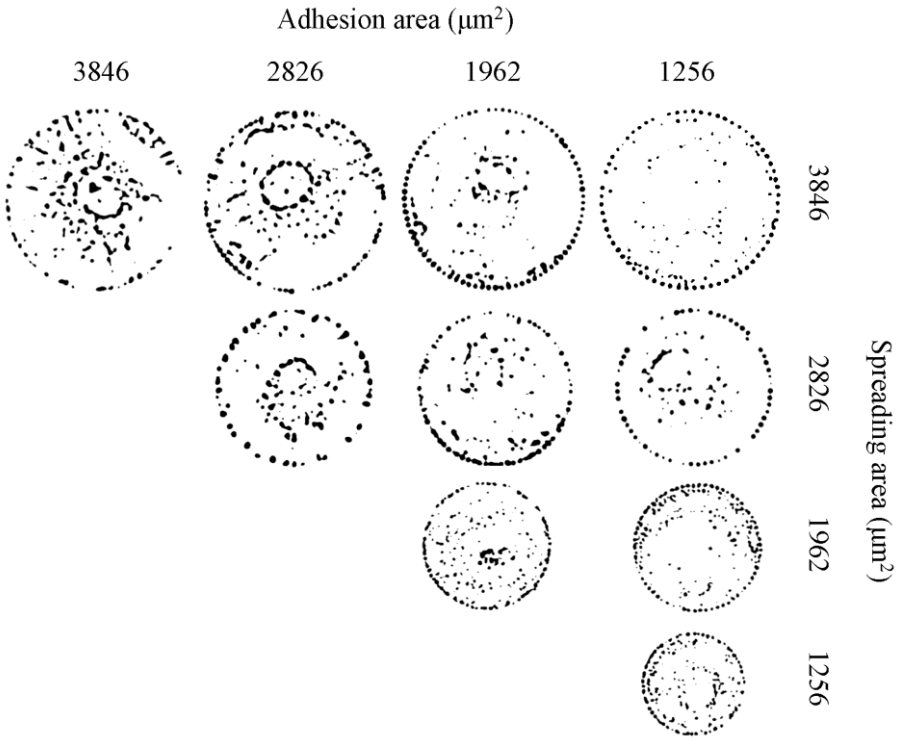

Figure 5.8 The representative vinculin images of micropatterned cells with various adhesion and spreading areas after ImageJ software processing.

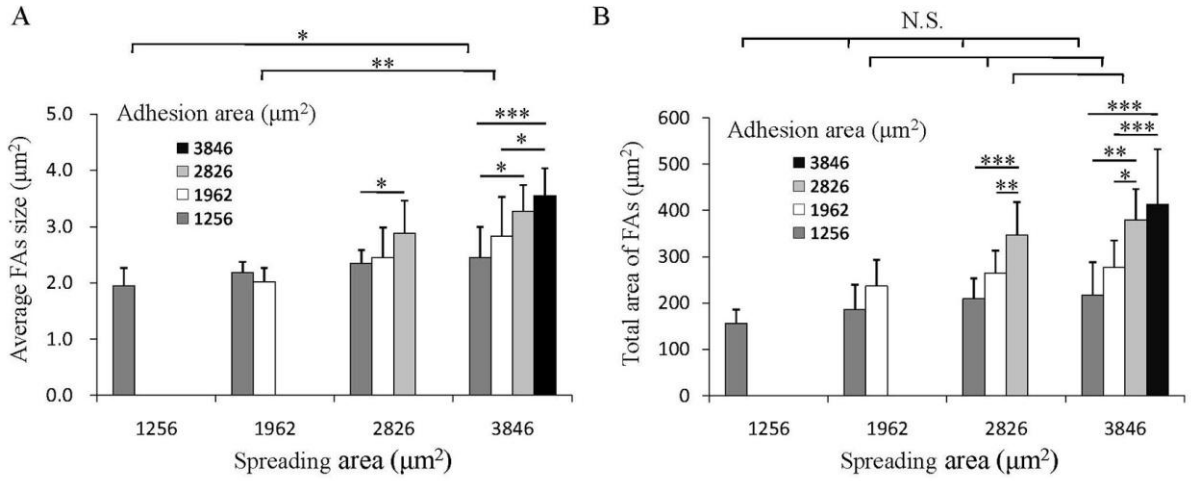

Figure 5.9 Influence of cell adhesion and spreading area on focal adhesion formation. (a) The average size of FAs of micropatterned cells. (b) The total FAs area of the micropatterned cells was acquired by analyzing vinculin staining images. Data are presented as means ± SDs (n = 30). *$p < 0.05$, **$p < 0.01$, ***$p < 0.001$ and N.S. means no significant difference.

5.4.3 Cytoskeletal organization influence by both adhesion and spreading area

F-actin filaments of micropatterned cells were stained to check the influence of adhesion and spreading areas on cytoskeletal organization (Figure 5.10a). According to previous study, the actin stress fibers assembled in mesenchymal cells can be divided into three different subtypes including ventral stress fibers (VSFs), dorsal stress fibers (DSFs) and transverse arcs (TAs) [33]. VSFs are myosin abundant fibers that are highly contractive and are connected to the FAs at both ends. DSFs are non-contractive thin fibers that are connected to the FAs at one end. The other end of DSFs grows toward cell nuclei and weaves into actin cortex around nuclei beneath cell membrane [34]. TAs are contractive fibers that are connected to DSFs rather than to FAs. In a round micropatterned cell, VSFs and DSFs are assembled in radial direction of the circles while TAs are assembled in concentric direction of the circles [35,36]. In this study, the assembly of VSFs, DSFs and TAs of the micropatterned cells was determined by both the cell adhesion area and spreading area. When cell spreading area was the same (each row), cells with large adhesion area formed thicker radial fibers and more concentric fibers than did the cells with small adhesion area. When cell adhesion area was the same (each column), cells with large spreading area formed radial fibers across the whole cell body while cells with small spreading area mainly formed actin network at cell edge. The merged fluorescence images of F-actin and vinculin showed that both ends of the thick radial fibers were connected to FAs, while only one end of the thin radial fibers was connected to FAs. The results confirmed that the increase of spreading area facilitated the formation of DSFs, while the increase of adhesion area contributed to the assembly of VSFs and TAs. The thickness of F-actin fibers was analyzed to evaluate the assembly of the cytoskeleton using the ImageJ software (Figure 5.3). The thickness of F-actin fibers increased significantly with the increase of adhesion area, while did not change significantly when cell spreading area increased (Figure 5.10b). Thickening of stress fibers indicated the reinforcement of the cytoskeleton which usually resulted from the increasing of cytoskeletal tension [37].

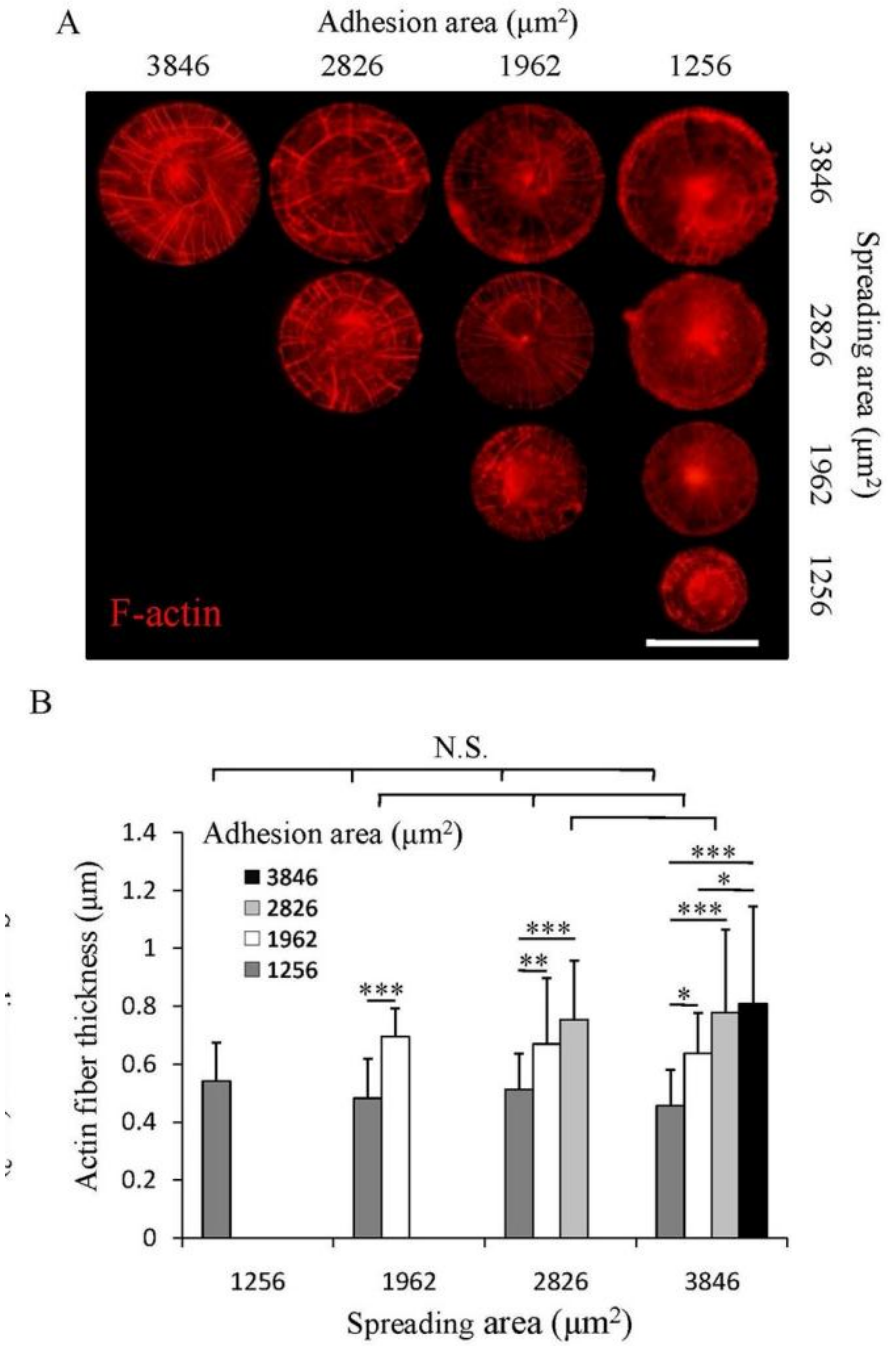

Figure 5.10 Cytoskeletal organization on micropatterns. (a) F-actin staining images (red) of micropatterned cells with different adhesion and spreading areas. Scale bar: 50 μm. (b) Actin fiber thickness of the micropatterned cells. Data are presented as means ± SDs (n = 30). *p < 0.05, **p < 0.01, ***p < 0.001 and N.S. means no significant difference.

5.4.4 Cellular mechanics dominantly regulated by adhesion area

Myosin as the motor protein which binds to F-actin and influences cell contractility was stained to show its distribution in MSCs cultured on the micropatterns (Figure 5.11). Although all the cells showed strong staining of myosin, the assembly of myosin was different in the cells cultured on different

micropatterns. Cells with small adhesion area showed a punctuated pattern of myosin, while those with large adhesion area had filament-like myosin structures assembled in both radial and concentric directions similar to their actin structure. The merged staining images of myosin and F-actin showed a colocalization of the filament-like myosin pattern and F-actin filaments of the cells with large adhesion area. Their colocalization indicated the binding of myosin to the actin filaments. Although the cells with large spreading area and small adhesion area formed DSFs, they were depleted of filament-like myosin pattern. These results demonstrated that the myosin mainly bound to the VSFs and TAs but not to the DSFs which was in accordance with previous report [38].

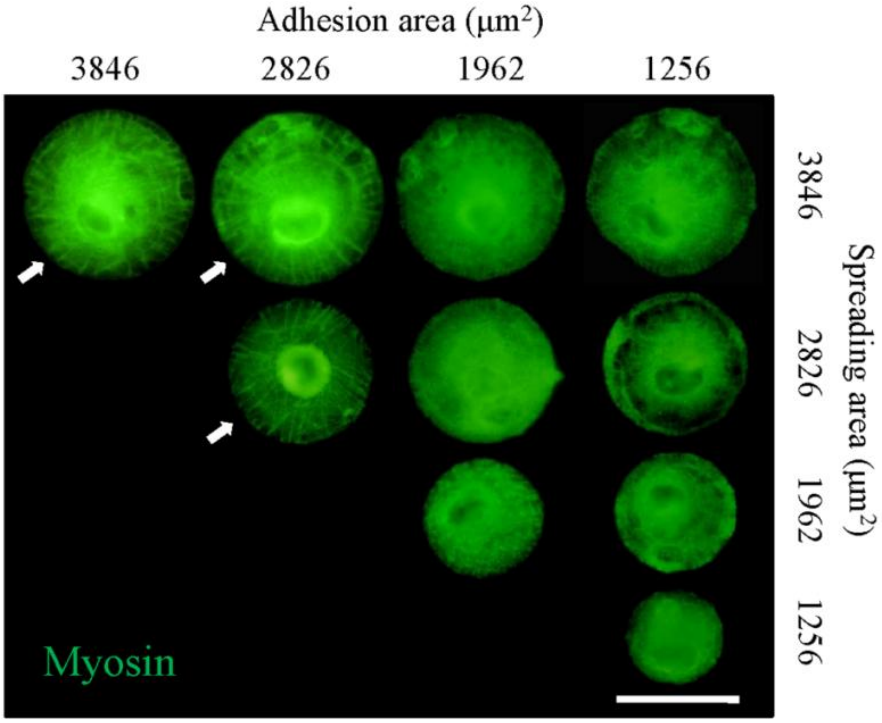

Figure 5.11 Myosin (green) staining images of the micropatterned cells with different adhesion and spreading areas. Arrows indicate the micropatterned cells with a filament-like myosin structure. Scale bar: 50 μm.

The bound myosin can generate traction force along the F-actin filaments and further influence cell mechanical state [39]. To confirm this, AFM was used to evaluate the cytoskeletal tension of MSCs cultured on the micropatterns. The average Young's modulus of MSCs increased with increase of adhesion area (Figure 5.12). The cells with the same adhesion area had similar Young's Modulus even they had different spreading area. The different mechanical properties should be due to the different assembly of myosin and actin filaments. Binding of myosin to the VSFs and TAs which formed in cells with large adhesion area promoted the generation of traction force and resulted in the high cytoskeletal tension of cells. Although MSCs with large spreading area and small adhesion area formed the DSFs, they still had relatively low cytoskeletal tension due to the lack of myosin binding. The results suggest that cellular mechanics was mainly determined by adhesion area rather than spreading area.

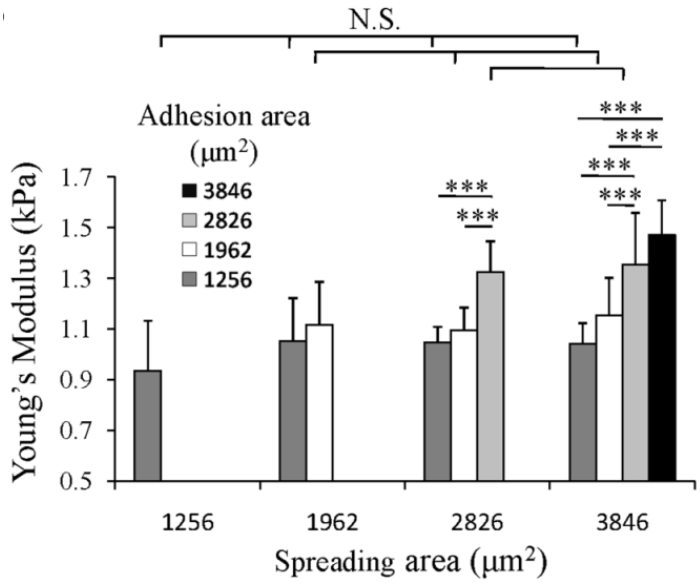

Figure 2.12 The measured Young's modulus of the micropatterned cells. Data are presented as means ± SDs (n = 20). ****p* < 0.001 and N.S. means no significant difference.

5.4.5 Mechanotransduction in MSCs on micropatterns

MSCs changed their cytoskeletal organization and tension depending on their adhesion and spreading areas. Since the cytoskeletal tension can be translated into the nucleus to further influence cell functions, mechanotransduction of the cells cultured on the micropatterns was investgated. Yes-associated protein (YAP) and transcriptional coactivator with PDZ-binding motif (TAZ) have been reported as sensors and mediators of the biophysical stimulus [25]. When cell encounters high cytoskeletal tension, YAP/TAZ will accumulate into cell nucleus and regulate gene transcription to influence cell functions. On the other hand, when cells cannot develop cytoskeletal tension, YAP/TAZ will exclude from nucleus and accumulate into cytoplasm. Therefore, YAP/TAZ was stained to check their localization in cells with various adhesion and spreading areas to confirm the cytoskeletal tension transduction (Figure 2.13a-c). YAP/TAZ was located in the cytoplasm in the majority of cells with small adhesion area. However, increasing adhesion area facilitated the accumulation of YAP/TAZ into nucleus. By counting the number of cells with a clear colocalization of YAP/TAZ and nucleus, we confirmed that cells with the same adhesion area had similar percentage of nuclear YAP/TAZ, while the percentage increased with increase of adhesion area (Figure 2.13d). This result indicated that the mechanical transduction process was mainly affected by cell adhesion area rather than spreading area.

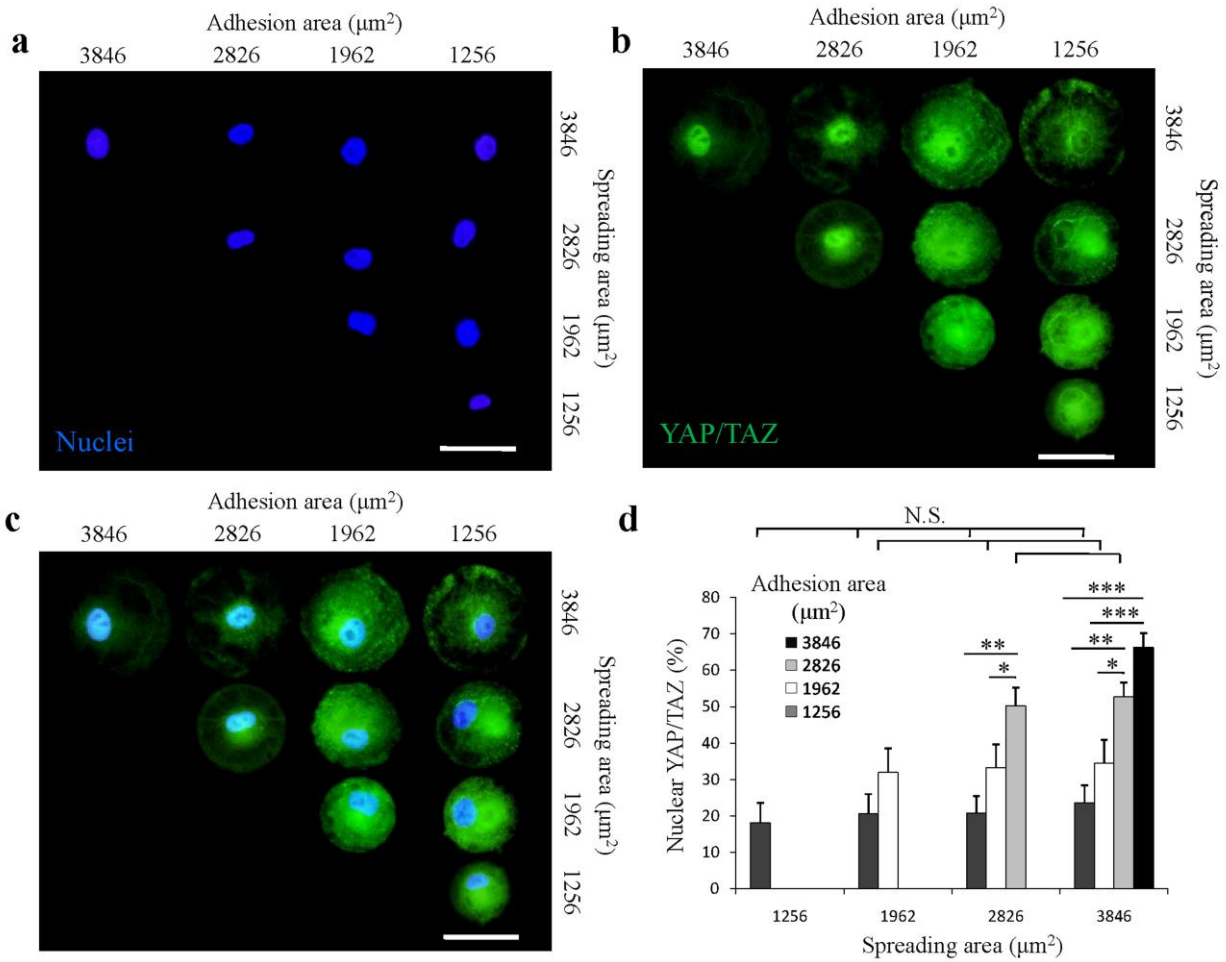

Figure 2.13 Influence of adhesion and spreading areas on mechanotransductin of the micropatterned cells. (**a**) Nuclei (blue) of single micropatterned cells were stained to show their position. Scale bar: 50 μm. (**b**) YAP/TAZ staining images (green) of the micropatterned cells. Scale bar: 50 μm. (**c**) Merged images of (**a**) and (**b**) to show the colocalization of the nuclei and YAP/TAZ. Scale bar: 50 μm. (**d**) The percentage of the micropatterned MSCs with nuclear YAP/TAZ. Data are presented as means ± SDs (n = 3). *$p < 0.05$, **$p < 0.01$, ***$p < 0.001$ and N.S. means no significant difference.

5.4.6 Influence of adhesion and spreading area on differentiation of MSCs

Differentiation as one of the most important functions of stem cells was investigated to elucidate the influence of cell adhesion area and spreading area on stem cell fate determination. After being cultured on the micropatterns for 2 weeks, osteogenic differentiation was investigated by ALP staining and adipogenic differentiation was investigated by Oil Red O staining. Osteogenic differentiation of MSCs was promoted significantly by increasing cell adhesion area (Figure 2.14a and b). However, increase of spreading area did not show significant influence on osteogenic differentiation. On the other hand, the adipogenic differentiation potential decreased significantly with the increase of adhesion area (Figure 2.14c and d). Spreading area showed no influence on adipogenic differentiation. The results should be due to the cytoskeletal tension and activated YAP/TAZ distribution in the cells with different adhesion and spreading areas. The cells with large adhesion area showed high cytoskeletal tension and activated nuclear YAP/TAZ, and therefore had high osteogenic differentiation potential. On the other hand, cells with small adhesion area

lacked cytoskeletal tension, and therefore preferred to adipogenic differentiation. The results indicated that adhesion area could regulate cytoskeletal tension and activation of nuclear YAP/TAZ and had dominant effect on the differentiation of MSCs. Adhesion area was more important than spreading area for manipulation of cell functions.

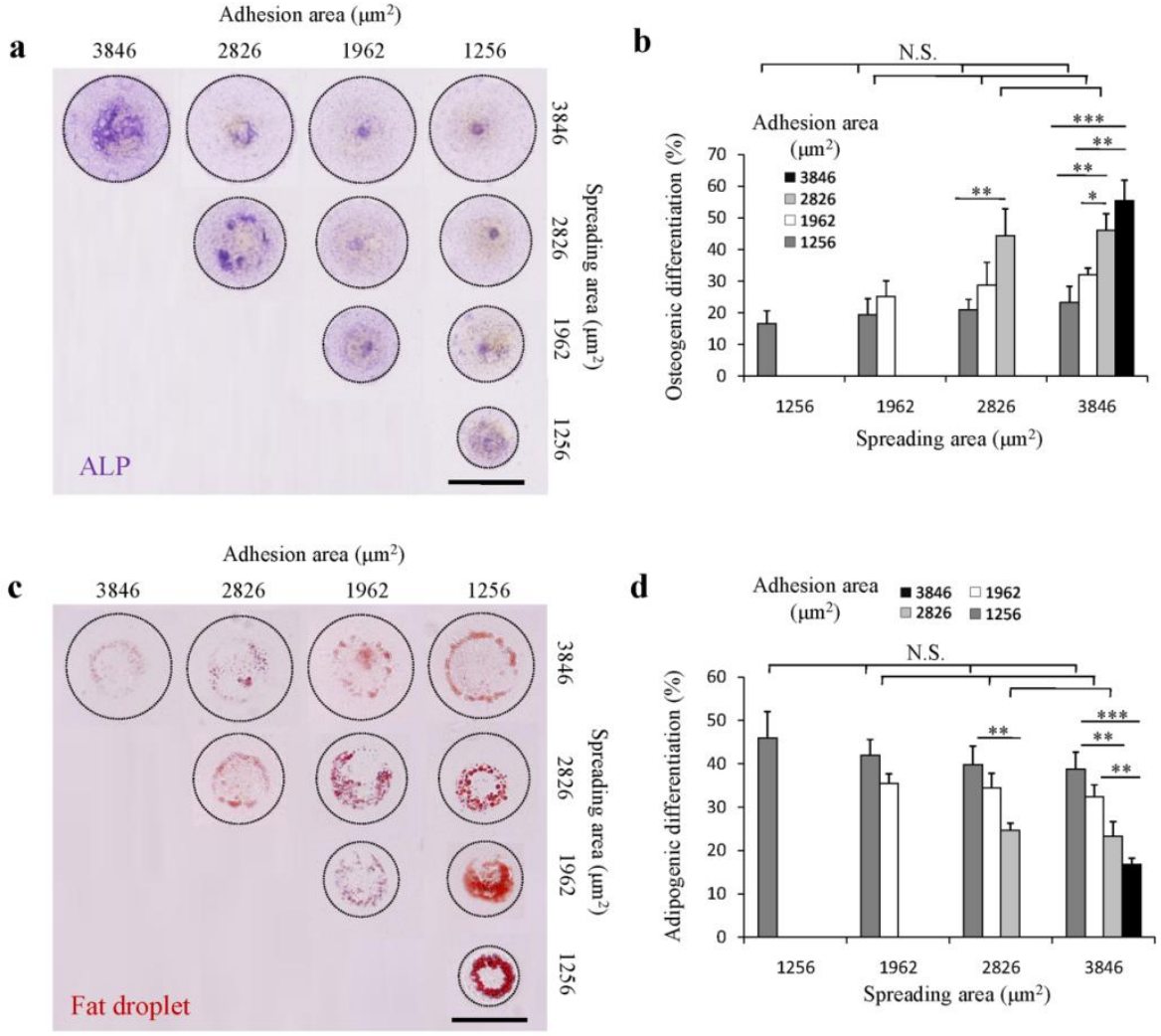

Figure 2.14 Influence of adhesion and spreading areas on osteogenic and adipogenic differentiation of MSCs. (a) Representative micrographs of micropatterned MSCs that are positive for ALP staining. (b) Percentage of ALP positive stained cells indicating the osteogenic differentiation potential of the micropatterned MSCs. (c) Representative micrographs of micropatterned MSCs that are positive for Oil Red O staining. (d) Percentage of Oil Red O positive stained cells indicating the adipogenic differentiation potential of the micropatterned MSCs. The dotted lines indicate the micropattern circles. Data are presented as means ± SDs (n = 3). *p < 0.05, **p < 0.01, ***p < 0.001 and N.S. means no significant difference. Scale bar: 50 μm.

5.5 Discussion

Manipulation of stem cell differentiation is always challenging. Efforts have been paid to elucidate the influence factors. Recently, the influence of biophysical properties of cell microenvironment including elasticity, topography, geometry, wettability, roughness and electricity on stem cell differentiation has

attracted many interests [16-20,40-43]. Changes in most of these stimuli can cause the variation of cell adhesion and spreading which are intimately related to cell functions. Despite of extensive studies, the independent influence of adhesion area and spreading area on cell functions remains elusive. In this study, ten types of micropatterns composed of 2 μm microdots were prepared to investigate the independent influence of adhesion and spreading areas on differentiation of MSCs. The fibronectin coated micropatterns showed good capacity to precisely control the cell adhesion and spreading. Regulation of adhesion and spreading areas influenced the formation of FAs. The average size of FAs increased with increase of both adhesion area and spreading area, while the total area of FAs only increased with the increase of the adhesion area rather than spreading area. Previous studies reported that the total area and average size of FAs can be manipulated with the regulation of adhesion and spreading areas [17,24,26]. The total area and average size of FAs are related with the global cell/material adhesion strength and local maturation of FAs, respectively [44]. Our results indicated that increasing in cell spreading area would facilitate the local maturation of FAs at cell periphery region. And increasing in cell adhesion area not only promoted maturation of FAs but also reinforced the global cell/material adhesion strength.

The assembly of FAs can cause the recruitment of F-actin and direct the cytoskeletal organization [45]. Regulated by the microenvironment, cells assemble complex F-actin networks in various structures including lamellipodia, filopodia, and stress fibers [34]. The stress fibers, which are widely exhibited in micropatterned cells, can be further divided into VSFs, DSFs and TAs depending on their composition and mode of development [35,36]. In this study, these three types of actin stress fibers were abundant in different micropatterned cells depending on their adhesion and spreading areas. Cells with small adhesion and spreading areas had thin actin filaments only at cell edge. Increasing spreading area leaded to the assembly of DSFs and further increase of adhesion area resulted in the assembly of VSFs and TAs. The thickness of stress fibers increased with the increase of adhesion area indicated that large adhesion area facilitated the recruitment of F-actin fibers.

Previous studies classified the VSFs and TAs as myosin abundant fibers while DSFs depleted of myosin [38]. According to the staining results, although all the micropatterned cells showed strong staining intensity of myosin, myosin only associated with the VSFs and TAs and formed filament-like structure in cells with large adhesion area. Movement of myosin along actin filaments generates the traction force to regulate cell mechanical properties. This was confirmed using AFM nanoindentation. When cell spreading area was the same, cells with large adhesion area had higher cytoskeletal tension compared with those having small adhesion area. When cell adhesion area was the same, cells with various spreading areas had similar cytoskeletal tension. Previous study using micropost arrays reported a similar phenomenon that the cytoskeletal tension increased with the increase of adhesion area, and it was identical when the adhesion area was kept at the same degree regardless of their spreading area [26].

The cytoskeletal tension regulated by cell adhesion and spreading areas can be translated into nucleus to affect gene and protein expression through mechanotransduction pathways [46-48]. Recent studies reported the activation of YAP/TAZ which is the transcriptional coactivators of mechanical cues involved in mechanotransduction was regulated by cytoskeletal tension and played crucial roles in stem cell differentiation [22,25,49]. In this study, the YAP/TAZ accumulated into nucleus when cells had large adhesion area, and excluded from the nucleus to cytoplasm when cells had limited adhesion area regardless of the spreading area. This should be attributed to the different degree of cytoskeletal tension influenced by the binding of myosin to F-actin filaments. High cytoskeletal tension facilitated accumulation of YAP/TAZ into nucleus, while low tension facilitated accumulation of YAP/TAZ into cytoplasm.

Although previous studies have reported that parallel increase of adhesion and spreading areas

would enhance osteogenic differentiation while suppresses adipogenic differentiation [50-52], according to our knowledge, there is no report related to the independent influence of adhesion and spreading areas on differentiation of MSCs. Herein, the osteogenic and adipogenic differentiation of micropatterned MSCs with various adhesion and spreading areas was compared to reveal their independent influence. An illustration was proposed to explain the possible mechanism (Figure 2.15). When cell spreading area was the same, cells with small adhesion area formed FAs at cell edge. Their cytoskeletal structure was mainly composed of radically assembled DSFs. The lack of myosin binding to DSFs resulted in low cytoskeletal tension. And the YAP/TAZ mainly distributed in cytoplasm. Therefore, cells with small adhesion area preferred to differentiate into adipocytes. While increasing in cell adhesion area reinforced the cell/material adhesion strength. Cells formed integrated actin network including VSFs, DSFs and TAs. Association of myosin with VSFs and TAs generated high cytoskeletal tension. The cytoskeletal tension stimulated accumulation of YAP/TAZ into nucleus to affect gene expression. Since the osteogenic differentiation was correlated with activation of YAP/TAZ in nucleus, cells with large adhesion area showed high potential to become osteoblasts. When cell adhesion area was the same, changing spreading area did not significantly affected stem cell fate determination. Cells with same adhesion area showed similar potential of osteogenic or adipogenic differentiation.

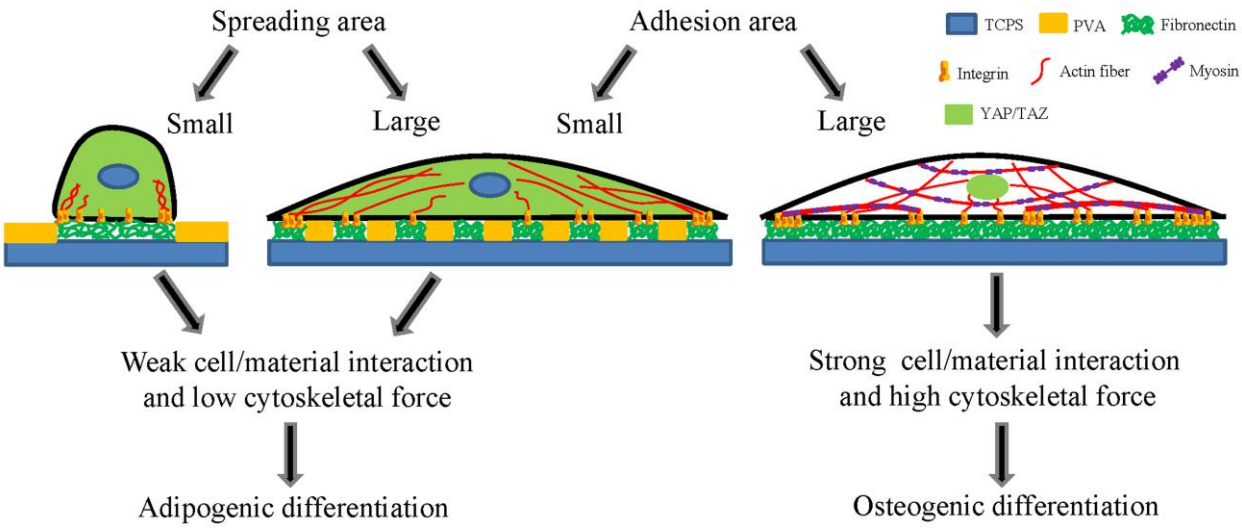

Figure 2.15 Schematic illustration of the influence of adhesion and spreading areas on cell functions. Cell adhesion affected a cascade of events to regulate differentiation of MSCs.

5.6 Conclusions

In conclusion, this study showed that the adhesion area rather than spreading area should play more important roles in manipulating cell functions. The adhesion area regulated the formation of FAs, cytoskeletal assembly, cell mechanical properties and mechanotransduction of micropatterned cells. Altogether, the differentiation of MSCs was determined by the available cell adhesion area rather than spreading area. Large adhesion area facilitated the osteogenic differentiation, while small adhesion area promoted the adipogenic differentiation.

5.7 References

[1] Ridley AJ, Schwartz MA, Burridge K, Firtel RA, Ginsberg MH, Borisy G, et al. Cell migration: integrating signals from front to back. Science. 2003;302:1704-9.
[2] Lauffenburger DA, Horwitz AF. Cell migration: a physically integrated molecular process. Cell. 1996;84:359-69.
[3] Mitra SK, Hanson DA, Schlaepfer DD. Focal adhesion kinase: in command and control of cell motility. Nature reviews Molecular cell biology. 2005;6:56-68.
[4] Slater JH, Boyce PJ, Jancaitis MP, Gaubert HE, Chang AL, Markey MK, et al. Modulation of endothelial cell migration via manipulation of adhesion site growth using nanopatterned surfaces. ACS applied materials & interfaces. 2015;7:4390-400.
[5] Fiorilli P, Partridge D, Staniszewska I, Wang JY, Grabacka M, So K, et al. Integrins mediate adhesion of medulloblastoma cells to tenascin and activate pathways associated with survival and proliferation. Laboratory Investigation. 2008;88:1143-56.
[6] Thakar RG, Cheng Q, Patel S, Chu J, Nasir M, Liepmann D, et al. Cell-shape regulation of smooth muscle cell proliferation. Biophysical journal. 2009;96:3423-32.
[7] McBeath R, Pirone DM, Nelson CM, Bhadriraju K, Chen CS. Cell shape, cytoskeletal tension, and RhoA regulate stem cell lineage commitment. Developmental cell. 2004;6:483-95.
[8] Dalby MJ, Gadegaard N, Oreffo RO. Harnessing nanotopography and integrin-matrix interactions to influence stem cell fate. Nature materials. 2014;13:558-69.
[9] Trappmann B, Gautrot JE, Connelly JT, Strange DG, Li Y, Oyen ML, et al. Extracellular-matrix tethering regulates stem-cell fate. Nature materials. 2012;11:642-9.
[10] Yim EK, Darling EM, Kulangara K, Guilak F, Leong KW. Nanotopography-induced changes in focal adhesions, cytoskeletal organization, and mechanical properties of human mesenchymal stem cells. Biomaterials. 2010;31:1299-306.
[11] Cao B, Peng R, Li Z, Ding J. Effects of spreading areas and aspect ratios of single cells on dedifferentiation of chondrocytes. Biomaterials. 2014;35:6871-81.
[12] Hynes RO. Integrins: versatility, modulation, and signaling in cell adhesion. Cell. 1992;69:11-25.
[13] Miyamoto S, Teramoto H, Coso OA, Gutkind JS, Burbelo PD, Akiyama SK, et al. Integrin function: molecular hierarchies of cytoskeletal and signaling molecules. The Journal of cell biology. 1995;131:791-805.
[14] Geiger B, Spatz JP, Bershadsky AD. Environmental sensing through focal adhesions. Nature reviews Molecular cell biology. 2009;10:21-33.
[15] Lehnert D, Wehrle-Haller B, David C, Weiland U, Ballestrem C, Imhof BA, et al. Cell behaviour on micropatterned substrata: limits of extracellular matrix geometry for spreading and adhesion. Journal of cell science. 2004;117:41-52.
[16] Mandal K, Wang I, Vitiello E, Orellana LAC, Balland M. Cell dipole behaviour revealed by ECM sub-cellular geometry. Nature communications. 2014;5.
[17] Thery M, Pepin A, Dressaire E, Chen Y, Bornens M. Cell distribution of stress fibres in response to the geometry of the adhesive environment. Cell motility and the cytoskeleton. 2006;63:341-55.
[18] Théry M, Racine V, Piel M, Pépin A, Dimitrov A, Chen Y, et al. Anisotropy of cell adhesive microenvironment governs cell internal organization and orientation of polarity. Proceedings of the National Academy of Sciences. 2006;103:19771-6.

[19] Dalby MJ, Gadegaard N, Tare R, Andar A, Riehle MO, Herzyk P, et al. The control of human mesenchymal cell differentiation using nanoscale symmetry and disorder. Nature materials. 2007;6:997-1003.
[20] Schvartzman M, Palma M, Sable J, Abramson J, Hu X, Sheetz MP, et al. Nanolithographic control of the spatial organization of cellular adhesion receptors at the single-molecule level. Nano letters. 2011;11:1306-12.
[21] Engler AJ, Sen S, Sweeney HL, Discher DE. Matrix elasticity directs stem cell lineage specification. Cell. 2006;126:677-89.
[22] Yang C, Tibbitt MW, Basta L, Anseth KS. Mechanical memory and dosing influence stem cell fate. Nature materials. 2014;13:645.
[23] Chen CS, Mrksich M, Huang S, Whitesides GM, Ingber DE. Geometric control of cell life and death. Science. 1997;276:1425-8.
[24] Chen CS, Alonso JL, Ostuni E, Whitesides GM, Ingber DE. Cell shape provides global control of focal adhesion assembly. Biochemical and biophysical research communications. 2003;307:355-61.
[25] Dupont S, Morsut L, Aragona M, Enzo E, Giulitti S, Cordenonsi M, et al. Role of YAP/TAZ in mechanotransduction. Nature. 2011;474:179-83.
[26] Han SJ, Bielawski KS, Ting LH, Rodriguez ML, Sniadecki NJ. Decoupling substrate stiffness, spread area, and micropost density: a close spatial relationship between traction forces and focal adhesions. Biophysical journal. 2012;103:640-8.
[27] Wang X, Song W, Kawazoe N, Chen G. The osteogenic differentiation of mesenchymal stem cells by controlled cell–cell interaction on micropatterned surfaces. Journal of Biomedical Materials Research Part A. 2013;101:3388-95.
[28] Horzum U, Ozdil B, Pesen-Okvur D. Step-by-step quantitative analysis of focal adhesions. MethodsX. 2014;1:56-9.
[29] Wang X, Nakamoto T, Dulińska-Molak I, Kawazoe N, Chen G. Regulating the stemness of mesenchymal stem cells by tuning micropattern features. Journal of Materials Chemistry B. 2016;4:37-45.
[30] Pogoda K, Jaczewska J, Wiltowska-Zuber J, Klymenko O, Zuber K, Fornal M, et al. Depth-sensing analysis of cytoskeleton organization based on AFM data. European Biophysics Journal. 2012;41:79-87.
[31] Nikkhah M, Strobl JS, De Vita R, Agah M. The cytoskeletal organization of breast carcinoma and fibroblast cells inside three dimensional (3-D) isotropic silicon microstructures. Biomaterials. 2010;31:4552-61.
[32] Ito Y, Nogawa M, Takeda M, Shibuya T. Photo-reactive polyvinylalcohol for photo-immobilized microarray. Biomaterials. 2005;26:211-6.
[33] Vallenius T. Actin stress fibre subtypes in mesenchymal-migrating cells. Open biology. 2013;3:130001.
[34] Stricker J, Falzone T, Gardel ML. Mechanics of the F-actin cytoskeleton. Journal of biomechanics. 2010;43:9-14.
[35] Tee YH, Shemesh T, Thiagarajan V, Hariadi RF, Anderson KL, Page C, et al. Cellular chirality arising from the self-organization of the actin cytoskeleton. Nature cell biology. 2015;17:445-57.
[36] Tay CY, Wu Y-L, Cai P, Tan NS, Venkatraman SS, Chen X, et al. Bio-inspired micropatterned hydrogel to direct and deconstruct hierarchical processing of geometry-force signals by human mesenchymal stem cells during smooth muscle cell differentiation. NPG Asia Materials. 2015;7:e199.
[37] Yoshigi M, Hoffman LM, Jensen CC, Yost HJ, Beckerle MC. Mechanical force mobilizes zyxin from focal adhesions to actin filaments and regulates cytoskeletal reinforcement. The Journal of cell biology. 2005;171:209-15.

[38] Hotulainen P, Lappalainen P. Stress fibers are generated by two distinct actin assembly mechanisms in motile cells. The Journal of cell biology. 2006;173:383-94.
[39] Vicente-Manzanares M, Ma X, Adelstein RS, Horwitz AR. Non-muscle myosin II takes centre stage in cell adhesion and migration. Nature reviews Molecular cell biology. 2009;10:778-90.
[40] Abagnale G, Steger M, Nguyen VH, Hersch N, Sechi A, Joussen S, et al. Surface topography enhances differentiation of mesenchymal stem cells towards osteogenic and adipogenic lineages. Biomaterials. 2015;61:316-26.
[41] Hao L, Yang H, Du C, Fu X, Zhao N, Xu S, et al. Directing the fate of human and mouse mesenchymal stem cells by hydroxyl–methyl mixed self-assembled monolayers with varying wettability. Journal of Materials Chemistry B. 2014;2:4794-801.
[42] Kalbacova M, Rezek B, Baresova V, Wolf-Brandstetter C, Kromka A. Nanoscale topography of nanocrystalline diamonds promotes differentiation of osteoblasts. Acta Biomaterialia. 2009;5:3076-85.
[43] Song W, Wang X, Lu H, Kawazoe N, Chen G. Exploring adipogenic differentiation of a single stem cell on poly (acrylic acid) and polystyrene micropatterns. Soft Matter. 2012;8:8429-37.
[44] Seo CH, Jeong H, Feng Y, Montagne K, Ushida T, Suzuki Y, et al. Micropit surfaces designed for accelerating osteogenic differentiation of murine mesenchymal stem cells via enhancing focal adhesion and actin polymerization. Biomaterials. 2014;35:2245-52.
[45] Kuo JC. Mechanotransduction at focal adhesions: integrating cytoskeletal mechanics in migrating cells. Journal of cellular and molecular medicine. 2013;17:704-12.
[46] Vogel V, Sheetz M. Local force and geometry sensing regulate cell functions. Nature reviews molecular cell biology. 2006;7:265-75.
[47] Wang N, Tytell JD, Ingber DE. Mechanotransduction at a distance: mechanically coupling the extracellular matrix with the nucleus. Nature reviews Molecular cell biology. 2009;10:75-82.
[48] Jaalouk DE, Lammerding J. Mechanotransduction gone awry. Nature reviews Molecular cell biology. 2009;10:63-73.
[49] Halder G, Dupont S, Piccolo S. Transduction of mechanical and cytoskeletal cues by YAP and TAZ. Nature reviews Molecular cell biology. 2012;13:591-600.
[50] McBeath R, Pirone DM, Nelson CM., Bhadriraju K, Chen CS. Cell shape, cytoskeletal tension, and RhoA regulate stem cell lineage commitment. Dev. Cell 2004;6:483-495.
[51] Song W, Kawazoe N, Chen G. Dependence of spreading and differentiation of mesenchymal stem cells on micropatterned surface area. Journal of Nanomaterials. 2011;2011:6.
[52] Peng R, Yao X, Cao B, Tang J, Ding J. The effect of culture conditions on the adipogenic and osteogenic inductions of mesenchymal stem cells on micropatterned surfaces. Biomaterials. 2012;33:6008-19.

Chapter 6

Concluding remarks and future prospects

6.1 Concluding remarks

This thesis summarizes the regulation of cell fate determination by cell morphogenesis controlled by the micropatterned surfaces. Diverse micropatterns were prepared on TCPS surfaces using photo-reactive PVA and UV lithography. The influence of cell size, shape, aspect ratio and the independent influence of cell adhesion and spreading area on cell fate determination were systematically investigated.

Chapter 1 introduces the cell sources for tissue engineering and their characteristics. The main components of cell microenvironment and their influences on cell fate determination were summarized. Typical micropatterning techniques were compared and their applications in biological field were exemplified. Designing and preparation of micropatterned surfaces for cell function manipulation is motivated.

Chapter 2 describes the influence of cell morphogenesis on maintenance of multipotency of stem cells. Micropatterns with different sizes, shapes and aspect ratios were prepared and used for culture of MSCs to investigate their influences on the stemness of MSCs at single cell level. With the increase of spreading area and aspect ratio, the percentage of cells that were positively stained by stem cell markers decreased. However, cellular geometry controlled by the geometrical micropatterns showed no significant influence on the expression of stem cell markers. Stemness change of stem cells was accompanied with change of nuclear activity and cytoskeleton. The nuclear activity increased with increase of spreading area and aspect ratio. The actin filament structure was significantly influenced by spreading area and aspect ratio. Cells became stiffer when they had sufficient area to spread or were elongated.

Chapter 3 describes the nanomechanical properties of MSCs, NHOst and MG-63 cells on micropatterns with various sizes. Stiffness of normal cells increased with increase of spreading area due to the ordering of cytoskeleton. Disrupting F-actin assembly reduced cell stiffness. Meanwhile, cell size influenced the expression of phosphoezrin that affected cell surface roughness. Rough membrane was accompanied with high non-specific adhesion force and migration rate. However, cancer cells behaved less dependently on their microenvironment as their cytoskeleton did not change much by manipulating cell size.

Chapter 4 describes the cellular uptake of AuNPs influenced by cell morphogenesis. Photo-reactive PVA micropatterned TCPS surfaces were used to control the cell size and investigated how the cell size affected the cellular uptake of PEG-AuNPs. Cells with large size had a high total cellular uptake, but showed a low average uptake per unit membrane area. While cells with small size showed opposite behaviors. This is the contribution of both cell/NPs contacting area and membrane tension that depends on cell size. Large size always leaded to a high total cellular uptake due to the large contact area with the NPs. However, high membrane tension resulted from large cell size would require high wrapping energy for engulfing of NPs and thus reducing the uptake. This study would shed light on the influence of microenvironment of cells on cellular uptake behaviors.

Chapter 5 describes the independent influence of cell adhesion area and spreading area on osteogenic and adipogenic differentiation of MSCs. Ten types of isotropical micropatterns that were composed of 2 μm microdots were prepared to precisely control the adhesion area and spreading area of MSCs. The respective influence of adhesion and spreading areas on stem cell functions was investigated. Adhesion area showed more significant influences on the focal adhesion formation, binding of myosin to actin fibers, cytoskeletal organization, cellular Young's modulus, accumulation of YAP/TAZ in nuclei, osteogenic and adipogenic differentiation of MSCs than did the spreading area. The results indicated that adhesion area rather than spreading area played more important roles in regulating cell functions.

In summary, photo-reactive PVA was synthesized and used to prepare the micropatterns on TCPS using UV photolithography. This simple and robust method provided a suitable strategy to fabricate the micropatterns on prevalent cell-culture substrates. Investigation of single cell behaviors could be directly and systematically achieved using the prepared micropatterns without external interferences resulting from separate cell culture. The micropatterns were designed to control cell size, shape and aspect ratio to investigate their influence on cell functions. The stemness, nanomechanical properties, cell/nanomaterials interaction and cell differentiation were investigated using the ingeniously designed micropatterns. The micropatterned cells showed different behaviors indicating that the cell morphogenesis regulated by micropatterns played critical roles in cell fate determination. All these results proved that the micropatterning technology is useful for manipulation of cell behaviors. And the insights of this study should inspire the design of biomaterials for manipulation of diverse cell functions.

6.2 Future prospects

In this thesis, the photo-reactive PVA micropatterned TCPS surfaces were prepared using UV lithography for manipulation of cell functions. The individual influences of cell morphogenesis on stem cell fate determination controlled by micropatterned structures have been systematically investigated. Little is known about the interplay of multiple stimuli on regulation of cell behaviors. Further researches are required to advance the integration of micropatterning techniques with other technologies to investigate the synergistic effects of various microenvironment cues on cell fate determination.

Preparation of hybrid micro-/nano-structured biointerfaces: Nano-engineering enabled the fabrication of surfaces with diverse nanofeatures (nanoarrangement, nanospacing, nanoroughness,

nanotopography, etc.) mimicking the *in vivo* nanostructures. And these surfaces have been applied in biomedical application and shown great influence on cell functions. But the cell morphogenesis was still lack of control on the nanopatterns. Therefore, integration of micropatterning and nanopatterning for fabrication of the hybrid micro-/nano-patterns would provide novel platform for cell function manipulation. Nanostructures can be firstly prepared on the organic substrate using conventional methods. Followed by the micropatterning using photo-reactive polymer and UV lithography, the hybrid micro-/nano-patterned surfaces can be achieved. The hybrid surface will combine the merits of both micropatterns and nanopatterns and is suitable to investigate the cell response to their niche in both micro- and nano-scale.

Fabrication of dynamic micropatterns: *In vivo*, cells are living in a dynamic microenvironment. The dynamic cellular response to the changes in microenvironment is critical for cells to tune their functions. However, most of the currently developed micropatterned surfaces are studied in a static mode. Therefore, development of the dynamic micropatterns should become urgently needed in the near future. Some materials have been found to be thermo-responsive, light-responsive or voltage-responsive. Fabricating micropattens on such kind of substrates would provide the dynamically tunable micropatterns for cell function manipulation.

Construction of the three dimensional micropatterned structures: Three dimensional cell culture is supposed to be an advantage strategy for cell function manipulation. By using the UV lithography and a stamp (used in soft lithography), the three dimensional micropatterned structures could be acquired. High concentrate of cell adhesive photo-reactive polymer would be poured in a container, then press the stamp into the photo-reactive solution to create the microfeatures. After UV irradiation, the three dimensional micropatterns could be obtained. Depending on the stamp geometry and volume of the photo-reactive polymer, the three dimensional structures of the micropatterns could be controlled. And these micropatterns would be useful to investigate the cytoskeleton assembly in three dimensional structures and cell response to the microenvironment in three dimensional scales at single cell level.

List of publications and awards

Publications:

1. Xinlong Wang, Xiaohong Hu, Naoki Kawazoe, Yingnan Yang and Guoping Chen. Manipulating Cell Nanomechanics Using Micropatterns. *Advanced Functional Materials* 2016, DOI: 10.1002/adfm.201601585.

2. Xinlong Wang, Xiaohong Hu, Ida Dulinska-Molak, Naoki Kawazoe, Yingnan Yang and Guoping Chen. Discriminating the Independent Influence of Cell Adhesion and Spreading Area on Stem Cell Fate Determination Using Micropatterned Surfaces. *Scientific Reports* 2016, 6, 28708.

3. Xinlong Wang, Tomoko Nakamoto, Ida Dulinska-Molak, Naoki Kawazoe and Guoping Chen. Regulating the Stemness of Mesenchymal Stem Cells by Tuning Micropattern Features. *Journal of Material Chemistry B* 2016, 4: 37-45.

4. Xinlong Wang, Xiaohong Hu, Jingchao Li, Adriana C. Mulero Russe, Naoki Kawazoe, Yingnan Yang and Guoping Chen. Influence of Cell Size on Cellular Uptake of Gold Nanoparticles. *Biomaterials Science* 2016, 4: 970-978.

5. Xinlong Wang, Yingjun Yang, Xiaohong Hu, Naoki Kawazoe, Yingnan Yang and Guoping Chen. Morphological and mechanical properties of osteosarcoma microenvironment cells explored by atomic force microscopy. *Analytical Sciences* 2016, In press.

6. Xinlong Wang, Wei Song, Naoki Kawazoe and Guoping Chen. The Osteogenic Differentiation of Mesenchymal Stem Cells by Controlled Cell-cell Interaction on Micropatterned Surfaces. *Journal of Biomedical Materials Research A* 2013, 101A: 3388-3395.

7. Jingchao Li, Jia'En Jasmine Li, Jing Zhang, Xinlong Wang, Naoki Kawazoe and Guoping Chen. Gold Nanoparticle Size and Shape Influence on Osteogenesis of Mesenchymal Stem Cells. *Nanoscale* 2016, 8: 7992-8007.

8. Xiaomeng Li, Shangwu Chen, Jingchao Li, Xinlong Wang, Jing Zhang, Naoki Kawazoe and Guoping Chen. 3D culture of chondrocytes in gelatin hydrogels with different stiffness. *Polymers*, 2016, 8, 269.

9. Tomoko Nakamoto, Xinlong Wang, Naoki Kawazoe and Guoping Chen. Influence of Micropattern Width on Differentiation of Human Mesenchymal Stem Cells to Vascular Smooth Muscle Cells. *Colloids and Surfaces B: Biointerfaces* 2014, 122: 316-323

Awards:

1. **Merit Award**, The 10th World Biomaterials Congress (WBC 2016), Montreal, Canada, 2016.

2. **Best Presentation Award**, Nanotechnology Students' Summer School 2015, Tsukuba, Japan, 2015

3. **Excellent Presentation Award,** Student Seminar in the Doctoral Program in Materials and Engineering, Tsukuba, Japan, 2015.

4. **Student Presentation Award**, The 43rd Biomedical Polymers symposium, Tokyo, Japan, 2014.

5. **Excellent in YIA Award**, The 2014 International Symposium of Materials on Regenerative Medicine, Taipei, 2014.

6. **The SYIS Oral Presentation Award**, The 2014 Tissue Engineering and Regenerative Medicine International Society-Asia Pacific Meeting (2014 TERMIS-AP), Daegu, Korea, 2014.

7. **The Award for Encouragement of Research**, the International Union of Materials Research Societies-International Conference in Asia (IUMRS-ICA) 2014, Fukuoka, Japan, 2014.

8. **Gold Poster Award**, The 7th International Conference on the Science and Technology for Advance Ceramics (STAC-7), Yokohama, Japan, 2013.

Acknowledgements

This PhD thesis was accomplished with the supervision of my supervisor Professor Guoping Chen. During my PhD study, Professor Chen has devoted to supervising my research from selecting research topics and suggesting solutions of problems encountered in my experiments and revising research papers and thesis. His expertise, innovation, passion and seriousness in scientific research have deeply affected me and greatly encouraged me during my PhD study. In addition, Professor Chen has always been generous in offering tips on effective communication and building interpersonal relationships. His advice in scientific research and life will continue guiding me in my future career and life. It is my great honor to be able to do research in Professor Chen's group. Therefore, I am taking this opportunity to give my sincere great gratitude to him.

Special thanks also go to Dr. Naoki Kawazoe for his warm support and encouragement during my 5 years of research in NIMS. His immense knowledge, professional skill, and modest character have deeply impressed me. It is my great pleasure to work and learn from him.

I really appreciate the valuable suggestion and assistance from Dr. Tomoko Nakamoto, Dr. Wei Song, Dr. Ida Dulinska-Molak, Ms. Xiaohong Hu and Mrs. Harue Nagata, Mrs. Kobayashi, Mrs. Tateno and Mrs. Hidaka. Dr. Tomoko Nakamoto, Dr. Wei Song, Dr. Ida Dulinska-Molak and Ms. Xiaohong Hu have always been supporting me in my research and daily life. Mrs. Harue Nagata, Mrs. Kobayashi, Mrs. Tateno and Mrs. Hidaka have helped me a lot for the procedures of university enrollment and daily life in Tsukuba. And I would like to give my thanks to current members in Tissue Regeneration Materials Unit and former members in Polymeric Biomaterials Group for their teaching of experiments and cooperation in managing of our lab. They are Dr. Hongxu Lu, Dr. Qin Zhang, Dr. Jasmine Lee, Dr. Koki Hagiwara, Dr. Himansu Nandasekhar, Dr. Hongli Mao, Dr. Cai Rong, Dr. Jianming Yang, Dr. Shangwu Chen, Professor Yingnan Yang, Professor Gang Wu, Professor Shujun Dong, Professor Kaili Lin, Mr. Yuichi Hirayama, Mr. Radyum Ikono, Mr. Jingchao Li, Mr. Xiaomeng Li, Ms. Jing Zhang, Ms. Ying Chen, Mr. Yingjun Yang, Ms. Xiuhui Wang, Ms. Jiahui Ng, Ms. Nur Rofiqoh Eviana Putri and Ms. Adriana.

Beside my supervisor, I would like to give my sincere thanks to the rest of my thesis committee, Professor Heeyoung Kim, Professor Tetsushi Taguchi and Professor Mitsuhiro Ebara for their insightful comments, encouragement and kind suggestions during my PhD defense and my presentations in NIMS student seminars.

I would like to give my most sincere thanks to my parents and all my friends who have been supporting me during my PhD study.

This work was performed at Tissue Regeneration Materials Unit, International Center for Materials Nanoarchitectonics (MANA), National Institute for Materials Science and Graduate School of Pure and Applied Science of University of Tsukuba. I appreciate the financial support from NIMS (Junior Research Assistantship) and JSPS (Research Fellowship for Young Scientists; KAKENHI Grant No.15J01781) during my 5-year research in NIMS.